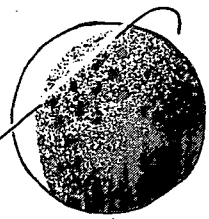

NAVIGATION STRATEGY AND FILTER DESIGN FOR SOLAR ELECTRIC MISSIONS

BY

B. D. TAPLEY AND HAMILTON HAGAR, JR.

AMRL 1040 MAY, 1972

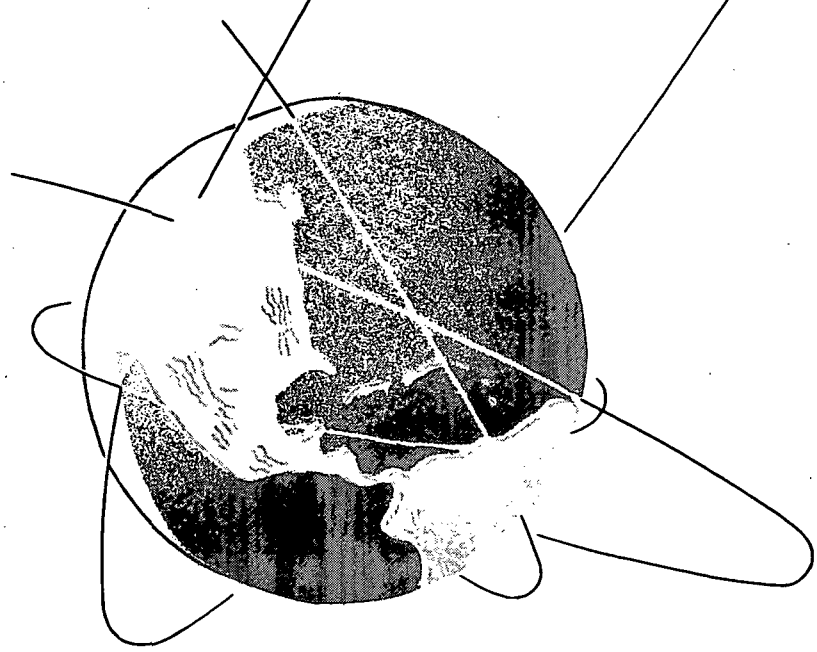

APPLIED MECHANICS RESEARCH LABORATORY

THE UNIVERSITY OF TEXAS AT AUSTIN AUSTIN, TEXAS

This report contains information prepared by

Applied Mechanics Research Laboratory
The University of Texas at Austin
Austin, Texas

for the
California Institute of Technology
Jet Propulsion Laboratory
under

JPL Subcontract 953147

This work was performed for the Jet Propulsion Laboratory, California Institute of Technology, sponsored by the National Aeronautics and Space Administration under Contract NAS7-100.

LIST OF SYMBOLS

A	$\partial F(\bar{X}, t)/\partial X$
a	Total thrust acceleration magnitude
a_o	Nonimal thrust acceleration magnitude
B	Diagonal matrix of model parameters, β_1, β_2, β_3
E	Expected value operator
$F(X, t)$	Right side of state differential equation in canonical form
$G(X_k, t_k)$	Observation function
H_k	$\partial G(X_k, t_k)/\partial X_k$
I	Identity matrix
K_k	Value of filter gain at time, t_k
k_o	Accelerometer random bias
k_3	Maximum accelerometer aging error
$m(t)$	Unmodeled acceleration
P_k	State error covariance matrix at time, t_k
$\bar{P}_k$	Predicted state error covariance at time, t_k
Q	State noise covariance matrix
q	Submatrix of state noise covariance corresponding to unmodeled effects
R_k	Observation covariance matrix at time, t_k
r	3-vector of position components
T	3-vector of thrust acceleration components
T^*	3-vector of nominal thrust acceleration components
T_m	3-vector of thrust acceleration components as measured by the IMU
t, τ	Time
u	3-vector of white noise components
u_a	3-vector of white noise acceleration components

v	3-vector of velocity components
$X(t)$	State Vector
$\bar{X}_k$	Predicted state vector at time, t_k
$\hat{X}_k$	Best estimate of state vector at time, t_k
X, Y, Z	Heliocentric Cartesian coordinates
x, y, z	Vehicle-centered Cartesian coordinates
Y_k	Observation at time, t_k
$\beta_1, \beta_2, \beta_3$	First and second error compensation model parameters
γ	Normally distributed random angle controlling thrust vector deviation from the nominal
$\delta(t - \tau)$	Dirac delta
$\delta_1, \delta_2, \delta_3$	Platform misalignment angles (also the damping coefficients in the second order error compensation model)
$\varepsilon(t)$	Approximation to the unmodeled acceleration, $m(t)$
ε_a	Accelerometer error
ε_g	Gyro error
$\varepsilon_m(t)$	Accelerometer output
$\hat{\varepsilon}(t)$	Best estimate of unmodeled acceleration
θ	Uniformly distributed random angle used in controlling thrust vector deviation from the nominal
μ	Gravitational parameter of the Sun
ν_i	Zero mean white noise in observations
ξ	Accelerometer aging constant
σ_a^2	Variance of the magnitude of the simulated thrust acceleration random component
σ_{ax}^2	Variance of the accelerometer error random component
σ_{pl}^2	Variance of platform misalignment random component
σ_γ^2	Variance of the thrust vector angle, γ

σ_θ^2	Variance of the thrust vector angle, θ
ψ	Angle between the vehicle position vector and the Heliocentric X-axis
ω	Frequency of the sinusoidal component of the simulated thrust acceleration error magnitude

ABSTRACT

For the low-thrust interplanetary space vehicle, errors due to unmodeled forces acting on the spacecraft present one of the fundamental limitations on the navigation accuracy. Methods which have been proposed to improve the navigation accuracy for the low-thrust space vehicle include modifications to the standard Sequential- and Batch-type orbit determination procedures and the use of Inertial Measuring Units (IMU) which measures directly the acceleration applied to the vehicle. This investigation compares the navigation accuracy obtained using one of the more promising modifications to the orbit determination procedures with a combined IMU-Standard orbit determination procedure for the low-thrust space vehicle.

In the modified orbit determination procedure, referred to as the Dynamic Model Compensation (DMC) algorithm, the components of the unmodeled acceleration are interpreted as additional state variables and their values estimated, sequentially, along with the components of the position and velocity. In the study, the unknown accelerations are approximated as both first-order and second-order Gauss-Markov processes. The comparison is based on numerical results obtained in a study of the navigation requirements of a numerically simulated 152-day low-thrust mission to the asteroid Eros.

The results obtained in the simulation indicate that the DMC algorithm will yield a significant improvement over the navigation accuracies achieved with previous estimation algorithms. In addition, the DMC algorithms will yield better navigation accuracies than the IMU-Standard Orbit Determination algorithm, except for extremely precise IMU measurements, i.e., gyro-platform alignment $< .01^{\circ}$ and accelerometer signal-to-noise ratio $> .07$.

Furthermore, unless these accuracies are achieved, the IMU navigation accuracies are generally unacceptable.

TABLE OF CONTENTS

		Page
	ABSTRACT	vi
	TABLE OF CONTENTS	viii
I.	INTRODUCTION	1
II.	ESTIMATION IN THE PRESENCE OF UNMODELED ACCELERATIONS	5
III.	ESTIMATION ALGORITHM	16
IV.	MATHEMATICAL MODEL FOR SOLAR ELECTRIC NAVIGATION STUDY	21
V.	NUMERICAL SIMULATIONS AND DATA PRESENTATION	37
VI.	DATA ANALYSIS AND COMPARISON	41
VII.	CONCLUSIONS AND RECOMMENDATIONS	49
	REFERENCES	52

I. INTRODUCTION

For the low-thrust interplanetary space vehicle, errors due to unmodeled forces acting on the spacecraft present one of the fundamental limitations on the navigation accuracy. The effects of errors in both the dynamical equations and in the observation equations are discussed in Ref. (1). The fundamental error source for the low-thrust space vehicle will be the error due to anomalies in the thrust. Since the thrust is applied throughout the mission, small anomalies have time to cause significant terminal errors. Ref. (2) points out the need for alternate orbit determination procedures to the conventional least squares methods used in most interplanetary missions if acceptable navigation accuracy is to be obtained during a low-thrust mission.

Two approaches to reducing the effects of errors due to inaccuracies in the dynamical model are possible. In the first, the actual acceleration which the vehicle is undergoing can be measured using "on-board" accelerometers to determine the error in the thrust. Provided that the signal-to-noise ratio is sufficiently high, this information could be used to improve the orbit determination characteristics by reducing the uncertainty in the errors in the mathematical model. In the second approach, the observation data is used to estimate directly the effect of the unmodeled accelerations during the process of estimating the state of the vehicle. In both approaches, other observations such as range-rate observations from Earth-fixed tracking stations and/or on-board angle measurements must be processed to obtain estimates of the state of the vehicle. As a consequence, the characteristics of the methods for estimating the state will be an important factor in determining

the ultimate accuracy of the navigation procedure.

The problem of estimating the state of any nonlinear dynamical system influenced by random forces using discrete observations which are subject to random error has received considerable attention during the last decade. The conventional solution to the problem involves linearizing the nonlinear equations about a reference solution and, then, applying linear estimation techniques. The estimate of the deviation from the reference solution can be obtained, then, by either a batch data processing algorithm in which a large batch of observations are used to obtain the estimate of the state at some reference epoch or the state may be estimated sequentially by processing each observation as it is made.

Errors of four basic types influence the accuracy of the linear estimates:

1. errors due to the linearization assumptions;
2. errors introduced in the computational procedures;
3. errors which occur in the observation process; and
4. errors due to inaccuracies in the mathematical model used to describe the dynamical process.

In most orbit determination problems the errors due to the first two effects can be controlled to an acceptably small value. The effects of the last two error sources will be the primary factors influencing the navigation accuracy for the low-thrust space vehicle. While the effects of observation errors play an important role in limiting the ultimate navigation accuracy, procedures for compensating for the effects of these errors will not be of primary consideration in this investigation. The primary consideration will be directed towards methods for reducing navigation errors due to inaccuracies in the dynamic model.

There have been a comparatively few studies related to the problem of orbit determination in the presence of unmodeled dynamic errors (as contrasted with a considerable bibliography of literature which considers the effects of the first three error sources). Since the unmodeled accelerations will vary, generally, with time, the effect of the unmodeled accelerations can be compensated for most easily by using a sequential or Kalman-Bucy type of filter (3). Furthermore, if the extended form of the sequential estimation procedure (4) is used, where the estimate at a time, t_i , is used to define the reference trajectory for propagating the estimate to the next observation epoch, t_j , then the errors due to the linearization assumptions will be minimized. In view of these comments, only sequential estimation algorithms and the errors which influence the application of these algorithms to the orbit determination problem for the low-thrust space vehicle will be considered in this investigation.

Primary attention will be given to the effects of errors due to an incomplete or inaccurate dynamical model. The effects of errors in the mathematical model on the accuracy and stability of the navigation procedures will be considered. Methods for improving the navigation accuracy by the use of accelerometers to compensate for the unmodeled accelerations as well as methods for directly estimating the unmodeled accelerations during the orbit determination process will be investigated. The objective of the investigation will be to determine the feasibility and to compare the effectiveness of each of these approaches as a means of improving the navigation accuracy for the low-thrust space vehicle. In the latter approach, the components of the unmodeled acceleration are interpreted as additional state variables and their values are estimated, sequentially, along with the components of the position and velocity. The estimates of the unmodeled

acceleration are described in Section II. Section III discusses the estimation procedure used in the study of the application to the low-thrust space vehicle. Section IV describes the mathematical model used in the simulated navigation study. Section V discusses the simulation procedure and presents the numerical results obtained in a simulated study of the navigation requirements of a 152-day low-thrust mission to the asteroid Eros and Section VI presents the data analysis and comparison of the results. Finally, the conclusions and recommendations for further study are summarized in Section VII.

II. ESTIMATION IN THE PRESENCE OF UNMODELED ACCELERATIONS

Mathematical Model

The equations which describe the motion of a nonlinear dynamical system can be expressed as

$$\dot{r} = v \quad , \quad \dot{v} = a_m(r,v,t) + m(t) \tag{2.1}$$

where r is a 3-vector of position components, v is a 3-vector of velocity components, and $a_m(r,v,t)$ is a 3-vector of modeled acceleration components. The three-vector $m(t)$ designates the unmodeled acceleration components and it represents the effects of all accelerations which are not accounted for in the mathematical model used to describe the physical process. Some of these effects, such as those due to parametric uncertainties, can be handled by treating certain parameters in the modeled accelerations in Eqs. (2.1) as unknown, but constant, parameters and estimating their value during the orbit determination process. However, in situations where a large number of such parameters are required, as in the description of the Earth or Lunar gravitational fields, this approach will lead to difficulties. See, for example, Refs. (5), (6), (7), and (8). Other effects such as radiation pressure, translational forces due to unbalanced attitude jets, fluctuations in atmospheric drag, anomalies in propulsion systems, etc. depend on such a large number of parameters that they can be approximated best as a continuous dynamic process.

There have been a number of investigations which have considered the problem of state estimation in the presence of such unmodeled forces. In particular, the effects of errors in the mathematical model on the accuracy

and stability of the linear sequential estimation procedures are discussed in Refs. (9), (10), and (11). In Ref. (9), the question of divergence of the estimation procedure due to errors in the dynamic model is considered.

There have been a number of methods proposed for alleviating the problem of estimation divergence. These methods include the addition of a constant matrix to the state error covariance matrix to account for noise in the differential equations which govern the state process (11), specification of a minimum bound on the estimation error covariance matrix (12) and the techniques of using a finite (4) or exponentially time-decaying (13) data set. Ref. (14) describes the application of a number of these methods to the problem of estimation of the trajectory of a re-entering space vehicle. While such methods will lead to a more stable estimation algorithm, they suffer from several disadvantages. First, the accuracy and stability of the estimate is determined by certain emperical parameters which must be determined "a priori". It is well known that the technique of adding an arbitrary matrix to the relation for propagating the state error covariance matrix will delay divergence at the expense of estimation accuracy. That is, in the presence of unmodeled accelerations, an accurate estimate may be obtained over a short time period or a less accurate estimate may be obtained over a longer time period, depending on the magnitude of the term added to the differential equation for the state error covariance matrix. The justification for using the finite or decaying data set lies in the fact that, due to dynamic model errors, the solution to the differential equations will fit a perfect data set over only a finite time interval. In each of these methods, the primary effect is to specify a lower bound on the state estimation error covariance matrix. However, the fundamental problem of attempting to use the observations to determine the nature of the unmodeled accelerations and to use this information to

improve the model is not considered. Based on previous studies of the error-growth during low-thrust missions due to errors in the thrust acceleration, it would appear that an estimation procedure which attempts to compensate for the effects of the unmodeled acceleration by estimating the value of the unmodeled accelerations during the estimation process should be used.

There have been a number of approaches proposed in the literature for compensating for the unmodeled acceleration in a continuous dynamic system. The simplest approach is to select $\varepsilon(t)$ to approximate $m(t)$ and let $\varepsilon(t)$ be assumed to be a constant (3×1)-vector. Eqs. (2.1) can be approximated then by the following systems:

$$\begin{aligned} \dot{r} &= v && , \quad r(t_o) = r_o \\ \dot{v} &= a_m(r,v,t) + \varepsilon && , \quad v(t_o) = v_o \\ \dot{\varepsilon} &= 0 && , \quad \varepsilon(t_o) = \varepsilon_o \end{aligned} \tag{2.2}$$

For most unmodeled accelerations, $m(t)$ can be approximated by a constant value, ε_o, over only a short time interval. This representation is used to estimate the unmodeled accelerations due to a constant bias in the dynamical equations in Ref. (15). In Ref. (16), the constant bias representation is used to approximate a continuous time-dependent acceleration by a piecewise constant function. The constant bias approximation has the advantage of simplicity and a low number of parameters, i.e., ε_o, which must be estimated to describe the unmodeled acceleration. The values are estimated in the same manner as a constant parameter in the modeled portion of the equations of motion. The approach has the disadvantage that, as the number of observations increase, the estimate of the values of ε will approach a constant value. If a sequential estimation procedure is used, the value will

be determined by the initial values of the unmodeled accelerations and the estimation procedure will be insensitive to the values of later observations. Russell and Curkendall (16) overcome this disadvantage by using piece-wise constant functions to approximate various regions of the unmodeled acceleration. This approach will allow a more complex function to be represented, but will require the estimation of a larger number of unknown parameters.

The most serious disadvantage of the constant approximation for time-varying phenomena lies in the fact that once a reasonable value of the constant parameters have been obtained, the representation will be insensitive to further changes in the unknown acceleration.

In addition, with a deterministic approximation to the unmodeled accelerations, the state error covariance matrix will be governed by the solution to a homogeneous Ricatti equation, i.e., Eq. (3.13) with Q set equal to zero, whose solution will asymptotically approach zero. As this occurs, the filter estimate will diverge due to the modeling errors, computational errors, etc. As a consequence, a more flexible method of approximating the unknown acceleration is required.

The logical extension of the constant bias approximation would be to approximate $m(t)$ with a time-varying function. Two approaches are possible. The functional form for $\varepsilon(t)$ could be chosen so as to approximate $m(t)$ by a Fourier or Chebyshev series or $\varepsilon(t)$ could be specified to be the solution to an ordinary differential equation. If $m(t)$ is a continuous and a sufficiently smooth function of time, then the approximation of $m(t)$ may be made by some ordinary differential equation. For the sequential estimation algorithms, the differential equation for $\varepsilon(t)$ will have to approximate the behavior of $m(t)$ only over time intervals between observations

and, hence, it is reasonable to approximate $m(t)$ by a set of functions which are solutions to ordinary linear differential equations, i.e., exponential, polynomial and trigonometric functions. With this assumption $m(t)$ can be approximated by the solution to a k^{th} order linear ordinary differential equation, i.e.,

$$\frac{d^k\varepsilon_i}{dt^k} + \sum_{j=1}^{k-1} \alpha_{ij} \frac{d^j\varepsilon_i}{dt^j} = 0 \quad , \quad i = 1,2,3 \quad . \tag{2.3}$$

If the initial parameters $\frac{d^j\varepsilon_i}{dt^j} = c_j$, $j = 1,\ldots,k-1$ and $i = 1,2,3$ are specified correctly, the solution $\varepsilon^T = [\varepsilon_1\varepsilon_2\varepsilon_3]$, determined by Eqs. (2.3), can be used to approximate $m(t)$ over some finite time interval. Eqs. (2.3) can be expressed in normal form and adjoined to Eqs. (2.1) with $m(t)$ replaced by $\varepsilon(t)$ to obtain the differential equations governing the dynamic process. The values of $r(t)$, $v(t)$ and $c_j(t)$, $j = 1,2,\ldots,k-1$, are estimated at each observation epoch. Eqs. (2.3) have the disadvantage of requiring that the coefficients, α_{ij} , must be specified. One procedure for avoiding this specification would be to interpret the constants α_{ij} as unknown parameters and estimate their values. For this case, Eqs. (2.3) would be expressed as

$$\begin{aligned} \frac{d^k\varepsilon}{dt^k} + \sum_{j=1}^{k-1} \alpha_j \frac{d^j\varepsilon}{dt^j} &= 0 \\ \dot{\alpha}_j &= 0; \; j = 1, \ldots, k-1 \end{aligned} \tag{2.4}$$

where $\frac{d^j\varepsilon}{dt^j}(t_o) = c_j(t_o)$ and $\alpha_j(t_o) = \alpha_j$, $j = 1,\ldots,k-1$ for any reference epoch t_o . The (3×3) matrix α_j is defined as

$$\alpha_j = \begin{bmatrix} \alpha_{1j} & 0 & 0 \\ 0 & \alpha_{2j} & 0 \\ 0 & 0 & \alpha_{3j} \end{bmatrix} , \quad j = 1,\ldots,k-1 \qquad (2.5)$$

The constants c_j and α_j completely specify the solution to Eq. (2.4) and their values can be estimated during the estimation process to obtain an approximate solution to the unmodeled accelerations. This procedure is used in Ref. (17) to describe a method for estimating the complete thrust force acting on a space vehicle by breaking the thrust history up into a number of regions and specifying the thrust history in each region by a differential equation of the form of Eq. (2.4). By this procedure, a piece-wise continuous analogue to the piece-wise constant approximation in Ref. (16) is obtained. This approach suffers from the disadvantage of requiring a very large number of coefficients to specify the approximation to the unknown acceleration. However, the representation can be used to obtain a good approximation of a time-varying function over some finite time period. But, once the estimates of the values of the coefficients have converged, the method will not adapt to additional changes in the nature of the unmodeled accelerations. Furthermore, since the approximation is deterministic, the state-error covariance matrix, Eq. (3.13) with Q set equal to zero, will approach zero asymptotically and the estimate will diverge due to either model errors or computation errors (9).

In order to prevent this divergence, the inclusion of terms to account for noise in the equations of state which will convert the covariance matrix to a nonhomogeneous differential equation is a desirable additional feature. This can be accomplished by assuming that the constant parameters are corrupted by a random driving noise, i.e., let $\varepsilon(t)$ approximate

$m(t)$ where $\varepsilon(t)$ is a random parameter which satisfies the equation

$$\dot{\varepsilon}(t) = u(t) \tag{2.6}$$

and where the apriori statistics on $\varepsilon(t)$, $E[\varepsilon(t_o)] = \bar{\varepsilon}_o$ and $E[\varepsilon(t_o)\varepsilon^T(t_o)] = P_{\varepsilon_o\varepsilon_o}$ are assumed to be given. The driving noise $u(t)$ is assumed to be characterized by the specified statistics

$$E[u(t)] = 0 \qquad E[u(t)u^T(\tau)] = q(t)\delta(t - \tau) \tag{2.7}$$

where $q(t)$ is a 3×3 matrix and $\delta(t - \tau)$ is the dirac delta function. The value of $q(t)$ is selected to account for the modelling errors. This procedure is used in Ref. (10) to compensate for errors in the atmospheric drag on a re-entering space vehicle and in Ref. (18) to model inertial gyroscope drift. The method has the advantage that it is characterized by a few parameters, $\bar{\varepsilon}(t_o)$, $P_{\varepsilon_o\varepsilon_o}$ and $q(t)$, and the effects of the driving noise will lead to a non-homogeneous Ricatti-type differential equation for the behavior of the state error covariance matrix, i.e., Eq. (3.13). In this way, the addition of the so-called Q-matrix in Eq. (3.13) occurs in a natural manner. The method suffers from the disadvantage that a time-varying function is being approximated by piece-wise constant functions whose values form a random sequence. As a consequence, the estimated value of the constant parameter may not follow the time-varying function precisely.

In order to obtain a more flexible approximation for the unmodeled accelerations, a differential equation forced by a random noise has been used in a number of studies. It is desirable to have a method for approximating $m(t)$ which is characterized by a minimum number of parameters. One possible approximation which has been used in a number of studies is the following

equation

$$\dot{\varepsilon}(t) = B\varepsilon(t) + u(t) \tag{2.8}$$

where B is a 3×3 matrix of correlation coefficients and $u(t)$ is a random driving noise whose statistics are

$$E[u(t)] = 0 \qquad E[u(t)u^T(\tau)] = q(t)\delta(t - \tau) \tag{2.9}$$

In most applications, the matrix $B(t)$ is a diagonal matrix, i.e.

$$B = \begin{bmatrix} \beta_1 & 0 & 0 \\ 0 & \beta_2 & 0 \\ 0 & 0 & \beta_3 \end{bmatrix} \tag{2.10}$$

The random process generated by the solution to Eqs. (2.8) is referred to as a first-order Gauss-Markov process. The solution can be shown to consist of the superposition of a purely random component and an exponentially correlated component. This model has been used in a large number of studies as a model for the errors in an inertial guidance system. It has been used, in particular, as a model for gyro error which has a drift component, which can be approximated by the exponential component in the solution, and a random component. See, for example, Refs. (19), (20) and (21). In further studies, this model has been used to compensate for the effects of random fluctuations in atmospheric drag (22) and to estimate the state of a vehicle in the presence of propulsion thrust anomalies (23). It has been used to model instrument pointing errors in the optical navigation systems in Ref. (24) and the accelerations acting on a low-thrust space vehicle in Refs. (25) and (26). Finally, Ref. (27) uses this model in a study of the problem of sequential estimation in the presence of correlated observation noise. The model is used to reduce the correlated observation noise-case to the usual uncorrelated

case described in Section III.

Ref. (25), also, discusses the integral form of Eq. (2.8) which can be expressed as follows:

$$\varepsilon(t) = E\varepsilon_i + \ell_i \quad ; \tag{2.11}$$

where

$$E = \begin{bmatrix} \alpha_1 & 0 & 0 \\ 0 & \alpha_2 & 0 \\ 0 & 0 & \alpha_3 \end{bmatrix} \quad , \quad \ell_i = \begin{bmatrix} \sigma_1\sqrt{1-\alpha_1^2}\, u_1 \\ \sigma_2\sqrt{1-\alpha_2^2}\, u_2 \\ \sigma_3\sqrt{1-\alpha_3^2}\, u_3 \end{bmatrix} \tag{2.12}$$

for

$$\alpha_j = \exp[-\beta_j(t - t_j)] \quad , \quad j = 1,2,3$$

In addition, $E[u_j] = 0$, $E[u_j u_k^T] = q_j \delta_{jk}$. This form of Eq. (2.8) is particularly useful for discrete observation estimation problems where the time interval $\Delta t = t - t_j$ is on the order of the observation interval. Note that a given component in Eq. (2.11), i.e.,

$$\varepsilon_1(t_j) = \alpha_1 \varepsilon_1(t_i) + \ell_1(t_j) \tag{2.14}$$

can be completely specified by four parameters: ε_i , $\Delta t = t_j - t_i$, β_i and σ_i . Since Δt will be specified by the observation interval and ε_i will be estimated as a state variable if Eq. (2.14) is used to compensate for $m_1(t)$, the parameters β_i and σ_i must be specified apriori. By appropriate choice of the correlation coefficient, β_i , a wide range of random processes can be represented. For example, if

$$\beta_1 = 0 \quad ; \quad \varepsilon_1(t_j) = \varepsilon(t_i) \tag{2.15}$$

and Eq. (2.14) represents a constant bias. On the other hand,

$$\beta_1 \to \infty \quad ; \quad \varepsilon_1(t_j) = \sigma_1 u_i \tag{2.16}$$

or a purely random process. For $0 < \beta < \infty$ some random process between a constant bias and a purely random process can be obtained. Hence, Eq. (2.14) has the advantage that it can represent a wide range of random processes with a function which has only two parameters. However, this fact can be regarded with certain measure as a disadvantage since the correct functional form of the solution will depend on the apriori value assigned to β_1 .

As a consequence of this fact, a modified form of Eq. (2.8) is proposed in Refs. (27), (28) and (29) in which the correlation coefficients, β_i , $i = 1,2,3$, are treated as unknown parameters whose values are to be estimated during the estimation process. This is accomplished by adjoining to Eq. (2.11) the additional differential equation

$$\dot{\beta} = 0 \tag{2.17}$$

where $\beta^T = [\beta_1 \beta_2 \beta_3]$. By this procedure an adaptive first-order Gauss-Markov process is used to approximate the unmodeled acceleration, $m(t)$ and the correct values of the correlation coefficients, β , are determined during the early portion of the estimation period. It should be noted that the solution obtained either by Eq. (2.8) or Eq. (2.9) will be quite sensitive to the values of the apriori noise covariance $q(t)$. A completely adaptive estimation algorithm should attempt to estimate the parameters, $q(t)$, also.

An additional model which is considered in the following investigation is an adaptive second-order Gauss-Markov process described by the following set of equations:

$$\begin{aligned} \dot{\varepsilon} &= \eta \\ \dot{\eta} &= -D\eta - B\varepsilon + u(t) \\ \dot{\beta} &= 0 \\ \dot{\delta} &= 0 \end{aligned} \tag{2.18}$$

where $u(t)$ is a random process characterized by the following apriori statistics

$$E[u(t)] = 0 \qquad E[u(t)u^T(\tau)] = q(t)\delta(t - \tau) \tag{2.19}$$

The matrices D and B are defined as

$$D = \begin{bmatrix} \delta_1 & 0 & 0 \\ 0 & \delta_2 & 0 \\ 0 & 0 & \delta_3 \end{bmatrix} \qquad B = \begin{bmatrix} \beta_1 & 0 & 0 \\ 0 & \beta_2 & 0 \\ 0 & 0 & \beta_3 \end{bmatrix} \tag{2.20}$$

Eqs. (2.18) can represent both decaying as well as oscillatory phenomena perturbed by the random noise, $u(t)$.

In the following investigation, primary attention will be given to a study of the effectiveness of both the first-order adaptive Gauss-Markov process described by Eq. (2.8) combined with Eq. (2.17) and the second-order model, described by Eq. (2.18). The primary question in the study will be the ability of two representations to estimate the unmodeled accelerations on a low-thrust space vehicle due to anomalies in the thrust. The accuracy of the estimate is compared with the estimate obtained when the thrust errors are determined by using on-board accelerometer measurements of the thrust. The estimation algorithm and the simulation program used in the study are discussed in the following sections.

III. ESTIMATION ALGORITHM

In the following discussion, a sequential estimation method, which compensates for unmodeled effects in the differential equations which describe the motion of a continuously thrusting solar electric space vehicle, is described. The method has two advantages: (1) the compensation for the effects of the unmodeled accelerations will yield an improved estimate of the vehicle state in real time estimation problems and (2) the method will yield information which can be used in post-flight data analysis to improve the mathematical model. The "unmodeled" accelerations are assumed to consist of the superposition of a time correlated component and a purely random component and are approximated as either a first-order or second-order Gauss-Markov process.

The equations which describe the motion of the low-thrust space vehicle can be expressed as

$$\dot{r} = v \quad , \quad \dot{v} = a_m(r,v,t) + m(t) \tag{3.1}$$

where r is a 3-vector of position components, v is a 3-vector of velocity components, and $a_m(r,v,t)$ is a 3-vector of modeled accelerations. The three-vector $m(t)$ is referred to as the unmodeled accelerations and it represents the effects of all accelerations not accounted for in the mathematical model used to describe the motion of the low-thrust vehicle. In the following discussion of the estimation procedure, the unmodeled acceleration, $m(t)$ is approximated as an adaptive first order Gauss-Markov process, $\varepsilon(t)$, which satisfies the following vector differential equation

$$\dot{\varepsilon}(t) = B\varepsilon(t) + u(t) \tag{3.2}$$

where $\varepsilon(t)$ is a three-vector and $u(t)$ is a 3-vector of Gaussian noise whose components are assumed to be described by the apriori statistics:

$$E[u(t)] = 0 \qquad E[u(t)u^T(\tau)] = q(t)\delta(t - \tau) \tag{3.3}$$

The coefficient matrix, B, is defined by the components $B_{ij} = \beta_i \delta_{ij}$ $(i,j = 1,2,3)$ where the β_i are assumed to be unknown parameters whose values are to be determined during the estimation process by the addition to Eq. (3.2) of the equation $\dot{\beta} = 0$ where $\beta^T = [\beta_1 \beta_2 \beta_3]$. If $\varepsilon(t)$ is substituted for $m(t)$ in Eq. (3.1) and if the state vector $X(t)$ is defined as

$$X^T = [r^T : v^T : \varepsilon^T : \beta^T] \tag{3.4}$$

then Eqs. (3.1), (3.2) and the relations $\dot{\beta} = 0$ can be combined to obtain the following differential equations for the state:

$$\dot{X} = F(X,u,t) \quad , \quad X(t_o) = X_o \tag{3.5}$$

where $F^T = [v^T : (a + \varepsilon)^T : (B\varepsilon + u)^T : 0]$ and where the initial conditions, X_o, are unknown.

The relationship between the p-dimensional observation vector Y_i, the p-vector of observation noise, ν_i, and the state at the time, t_i, is

$$Y_i = G(X_i,t_i) + \nu_i \tag{3.6}$$

where it is assumed that the observation noise ν_i, satisfies the following statistics:

$$E[\nu_i] = 0 \quad , \quad E[\nu_i \nu_j^T] = R_i \delta_{ij} \quad , \quad E[\nu_i X_j^T] = 0 \quad , \tag{3.7}$$

for all i,j.

The problem to be considered, then, is posed as follows: Given the

relation which governs the state history, Eq. (3.5), the initial state estimate $\hat{X}_{k-1}$ and P_{k-1}, the statistical properties of the state noise, Eq. (3.3), the observation-state relationship, Eq. (3.6), the statistical properties of the observation noise, and the observation sequence Y_i, $i = 1, \ldots, p (p > n)$; find the best estimate in the minimum variance sense, of the state, $\hat{X}_k$, at the time t_k, $k \geq p$.

Under the conditions in the previous problem statement, the extended sequential estimation algorithm (4) can be implemented by the following recursive sequence:

1) Given the estimate $\hat{X}_{k-1}$, P_{k-1}, integrate

$$\begin{aligned} \dot{\bar{X}} &= F(\bar{X},t) \quad , \quad \bar{X}(t_{k-1}) = \hat{X}_{k-1} \\ \dot{\bar{P}} &= A(t)\bar{P} + \bar{P}A^T(t) + Q \quad , \quad \bar{P}(t_{k-1}) = P_{k-1} \end{aligned} \tag{3.8}$$

from the time epoch t_{k-1} to the next observation epoch t_k to obtain the apriori estimate $\bar{X}_k$ and the apriori state estimate covariance matrix $\bar{P}_k$.

(2) Obtain the p×1 observation vector Y_k and evaluate the p×n matrix H_k and the n×p matrix K_k where:

$$\begin{aligned} H_k &= [\partial G(\bar{X}_k,t_k)/\partial X_k] \\ K_k &= \bar{P}_k H_k^T [H_k \bar{P}_k H_k^T + R_k]^{-1} \end{aligned} \tag{3.9}$$

(3) Form the new estimate of the state $\hat{X}_k$ and the state error covariance P_k as follows:

$$\begin{aligned} \hat{X}_k &= \bar{X}_k + K_k[Y_k - G(\bar{X}_k,t_k)] \\ P_k &= [I - K_k H_k]\bar{P}_k \end{aligned} \tag{3.10}$$

(4) Return to Step (1) and replace t_{k-1} with t_k and repeat the sequence.

The n×n matrix $A(t)$ is defined as

$$A(t) = [\partial F(\bar{X},t)/\partial X] \tag{3.11}$$

and it must be evaluated at each integration step associated with the first of Eqs. (3.8) in order to integrate the second of Eqs. (3.8).

The solution to the second of Eqs. (3.8) can be expressed as

$$\bar{P}(t) = \Phi(t,t_{k-1})P_{k-1}\Phi^T(t,t_{k-1}) + \int_{t_k}^{t} \Phi(t,\tau)Q\Phi^T(t,\tau)d\tau \tag{3.12}$$

Hence, the n×n coupled system of equations

$$\dot{\bar{P}} = A(t)\bar{P} + \bar{P}A^T(t) + Q(t) \quad , \quad \bar{P}(t_k) = P_k \tag{3.13}$$

can be replaced by the integration of the 2n×n system of uncoupled differential equations

$$\begin{aligned} \dot{\Phi}(t,t_k) &= A(t)\Phi(t,t_k) \quad , \quad \Phi(t_k,t_k) = I \\ \dot{\Gamma}(t,t_k) &= \Phi(t,t_k)Q\Phi^T(t,t_k) \quad , \quad \Gamma(t_k,t_k) = 0 \end{aligned} \tag{3.14}$$

Then, the solution given by Eq. (3.12) can be expressed as

$$\bar{P}(t) = \Phi(t,t_k)P_k\Phi^T(t,t_k) + \Gamma(t) \quad . \tag{3.15}$$

However, since $\bar{P}(t)$ is a symmetric matrix only $[n\times(n+1)]/2$ of the n×n coupled equations in Eq. (3.13) have to be integrated. The choice, then, is one of integrating the 2n×n uncoupled equations given by Eqs. (3.14) or integrating $(n^2 + n)/2$ of the n×n equations given by Eq. (3.13). In this study, the latter alternative is used.

The estimation algorithm for the adaptive second-order Gauss-Markov approximation is implemented in the same way as the first order algorithm

except that Eqs. (2.18) are combined with Eqs. (3.1) to form the equations of state, Eqs. (3.5). The state vector for this case will be expressed as

$$X^T = [r^T : v^T : \varepsilon^T : \eta^T : \beta^T : \delta^T]$$

The remaining steps in the algorithm will be the same as in the algorithm for the first-order model.

In the following section, the simulation procedure and the results obtained with the simulation procedure are described for an application to the orbit determination problem for a low-thrust space vehicle.

IV. MATHEMATICAL MODEL FOR SOLAR ELECTRIC NAVIGATION STUDY

Introduction

This section describes the mathematical model used for the simulation study of the navigation performance of a solar electric, continuous low-thrust space vehicle subject to uncertainties in the knowledge of the thrust acceleration vector. The orbit determination process is carried out using the Extended Sequential Estimation Algorithm equations (i.e., the Extended Kalman-Bucy Filter). The uncertainties in the applied thrust are estimated using the Dynamic Model Compensation (DMC) estimation procedure described in Section III. Two basic navigation procedures are considered. In the first, the DMC estimation algorithm is used to obtain an estimate of the unmodeled accelerations directly. In the second procedure, on-board accelerometers are used to measure the actual acceleration. With perfect measurements, the uncertainties in the acceleration will be those caused by errors in the mechanization and performance of the IMU equipment. While it is possible that these unmodeled errors can be estimated by the dynamic model compensation technique described in the previous section, this approach is not considered in this investigation.

Using both procedures, Earth-based range rate measurements and "on-board" celestial observations are used as data types in the state estimation process.

Solar Electric Propulsion

The electric propulsion systems are characterized by thrust levels in the range of 10^{-5} to 10^{-3} g. In general, the electric propulsion system

consists of a power supply and conditioning system, and a bank of thrusters. The thruster modes may be conceived as being either variable or constant level. Constant thrust systems are easiest to mechanize, but constrain the trajectory design process. Variable thrust systems offer more flexibility and navigation efficiency but are more difficult to implement. Employing a bank of constant level thrusters which may be turned on or off individually may approximate the advantages of variable thrust systems (31).

In solar electric propulsion (SEP) systems thruster power is obtained from solar cell panels. Thus, the power, and, hence, the thrust are generally trajectory dependent. The available power on out-bound missions varies approximately as $r^{-1.7}$ instead of r^{-2}; this is due to higher solar cell efficiencies at lower temperatures. On in-bound missions the available power is limited to about 1.2 to 1.3 times the power at 1 a.u. (to avoid burning out the cells, the panels may have to be tilted). A typical curve of the relative power versus heliocentric distances is given in Figure 1a. In general, since the power, and hence the acceleration, is a function of vehicle position, errors in the state estimate may be compounded by the corresponding errors in the power level. This particular coupling can be eliminated essentially through mechanization of the SEP system in a constant thrust level mode of operation. In fact, thruster design can be such as to allow operation at a power consumption level well below the nominally available power (2); and for out-bound missions within at least a 1.5 a.u. radius, thrust acceleration may be assumed independent of the power versus the heliocentric distance relationship. Although optimally guided missions require a time-varying thrust acceleration history (2), in this investigation a constant level thrust acceleration is assumed unless otherwise noted.

Data Types

The types of observations considered are Earth-based range-rate observations and vehicle on-board celestial star angle and accelerometer measurements of the thrust accelerations. As indicated previously, one objective of this study is to compare the method of estimating the unmodeled accelerations with that of utilizing on-board acceleration measurements in the navigation process. For a meaningful comparison, allowance is made for omitting and combining various observation types.

The techniques of radar range and range-rate observations are well-known and will not be discussed further. Of the two types, only range-rate measurements are employed in this investigation.

Several choices are available for the implementation of celestial and inertial measurement systems. A purely inertial system furnishing acceleration measurements supplemented by celestial fixes is one possibility. One configuration is a strapdown system. This approach involves additional complexity since it involves vehicle attitude dynamics and, hence, knowledge of the vehicle design. A purely inertial reference system provided by a gyro-stabilized platform is another alternative; however, platform misaglinment and gyro drift can produce errors which become unacceptable.

A celestially-aided inertial system is a more reasonable alternative (31), and basically, this is the approach adopted here. The system is configured by having appropriate accelerometers mounted on an inertial platform which is assumed to be continually aligned by information from a stellar monitoring device (star tracker).

Celestial Observations

Basically there are two measurement configurations for celestial

sensors: Theodolite-type and sextant-type. Theodolite-type sensors employ an altitude-azimuth configuration measuring longitude (λ) and latitude (ϕ) of a celestial object (Figure 1b). Sextant-type sensors furnish the direct angle between two points (Figure 1c). In this study, theodolite measurements are assumed to be employed by the star tracker. Celestial fixes are furnished by sextant observations of the star-vehicle-planet, and sun-vehicle-star angles.

Stellar Monitor and Platform Alginment

During flight, errors such as gyro drift cause platform misalignment. The theodolite-type measurements continually provide realignment information for the platform. Thus, a star tracker accurately referenced to the platform continually provides values through which the platform may be torqued to null the misalignment. In Figure 1d let (x,y,z) be the true (misaligned) orientation of the platform axes and let (X,Y,Z) be the nominal or aligned orientation. Nominal values for the observed star are λ and ϕ. Because of system errors, the true star position is $\Delta\lambda$ and $\Delta\phi$ away from the nominal. These angular deviations then may be related to the platform misalignment angles, $\delta^T = (\delta_x, \delta_y, \delta_z)$. An additional star position must be found to uniquely determine δ, one of the four measurements being used redundantly.

It should be noted that during this continuous realignment process, errors in the stellar monitor map into a residual platform misalignment. In fact, Friedlander (31) has shown that the majority of the platform misalignment may reasonably be attributed to errors in the star tracker. Basically, since the star tracker information is used to null platform-associated errors

(drift, etc.), the residual errors may reasonably be considered to be those caused by tracker errors.

Vehicle Equations of Motion

Having discussed the basic navigation concepts for a continuous low-thrust mission, the vehicle equations of motion are modeled as:

$$\begin{aligned} \dot{r}(t) &= v(t) \\ \dot{v}(t) &= \frac{\mu}{|r|^3} r + T(t) \end{aligned} \tag{4.1}$$

where $r(t)$ and $v(t)$ are the heliocentric position and velocity vectors, and $T(t)$, the thrust to mass ratio, is some thrust acceleration history. Usually $T^*(t)$, the nominal or design thrust acceleration history, will be specified to optimize the transfer trajectory in some sense. The optimal transfer trajectory will satisfy initial and terminal conditions, such as:

$$\begin{aligned} &\text{at } t_o: \quad r(t_o) = r_o \quad , \quad v(t_o) = v_o \\ &\text{at } t_f: \quad r(t_f) = r_f \quad , \quad v(t_f) = v_f \end{aligned} \tag{4.2}$$

Under the influence of the true thrust acceleration, the low-thrust vehicle will not follow the design trajectory and the deviation from the design trajectory must be estimated by the navigation procedure.

Acceleration Error

Consider the thrust acceleration error, $m(t) = T(t) - T^*(t)$. $T(t)$ is the true thrust acceleration, and $T^*(t)$ is some nominal thrust acceleration. Let $\varepsilon(t)$ be the approximation to the thrust acceleration error, $m(t)$. When inertial measurements are not simulated, the components of $\varepsilon(t)$, the approximation to the acceleration error, are estimated as $\hat{\varepsilon}(t)$, i.e.,

part of an augmented state vector. The true acceleration, $T(t)$, is estimated then as $\hat{T} = T^* + \hat{\varepsilon}$. When the inertial navigation configuration is simulated, $\varepsilon(t)$ represents the inertially-sensed acceleration (IMU output). This includes not only the deviation of the thrust acceleration from the design value due to errors in the thruster mechanization and control, but the inertial measuring unit (IMU) errors as well. In this case, we define $\varepsilon_m(t) \triangleq \varepsilon(t)$ and $T_m \triangleq T^* + \varepsilon_m(t)$. Thus, $\hat{\varepsilon}(t)$ is the direct estimate of $m(t)$, while $\varepsilon_m(t)$ is the inertial measurement of $m(t)$, including the IMU errors.

Outline of the Study

As indicated in the introduction, two navigation configurations are considered which attempt to account for uncertainties in the thruster operation; direct estimation of the acceleration errors, and the use of an IMU (also subject to errors) to measure the acceleration. Two fundamental questions investigated are:

1. What navigation accuracies may be obtained using IMU equipment, and what are the associated IMU characteristics?

2. Can thrust acceleration errors be directly estimated with accuracy comparable to that achieved by appropriate IMU equipment?

The following outline summarizes the assumption used for the study:

1. Nominal mission definition:
   a. Asteroid Eros flyby
   b. Heliocentric two-body motion

2. Thrust acceleration error simulation:
   a. Low frequency component in thrust magnitude
   b. High frequency errors in magnitude and direction of thrust vector modeled as white noise

3. IMU configuration:

   a. Accelerometer errors: the null uncertainty is modeled as white noise; aging is modeled as exponential change in the accelerometer output
   b. Gyro (Platform) errors: the null uncertainties are modeled as white noise; constant drift rates are assumed.

4. Estimation of unmodeled acceleration errors:

   a. Model 1 - Modeling of acceleration error components by exponentially autocorrelated process (first-order Gauss-Markov process); heliocentric reference frame
   b. Model 2 - Modeling of control parameters (thrust acceleration magnitude and pointing angles) by exponentially autocorrelated process; vehicle fixed reference frame
   c. Model 3 - Modeling of control parameters by second-order Gauss-Markov process; vehicle fixed reference frame

5. Numerical simulations and data:

   a. The standard orbit determination (o.d.) was simulated with:

      (1) No model error compensation and
      (2) Model uncertainties represented by uncorrelated, zero mean random process (purely white noise).

   b. The orbit determination using IMU measurements was simulated:

      (1) Using several IMU error characteristics and continuous platform realignment using stellar monitor and
      (2) Using the most accurate IMU specifications but with no platform realignment or celestial observations.

   c. The orbit determination estimating the unmodeled acceleration components was performed:

      (1) With the unknown acceleration approximated by first-order Gauss-Markov process in heliocentric reference system (direct estimation of acceleration components)
      (2) With first-order Gauss-Markov process in vehicle fixed reference system (direct estimation of control parameters)
      (3) With second-order Gauss-Markov process in vehicle fixed reference system (direct estimation of control parameters).

Further discussion of these assumptions is given in the following section.

Nominal Mission Definition

The nominal mission selected for the study is a continuous low-thrust vehicle flyby of the asteroid, Eros. Certain simplifying assumptions were made in the interests of economy; at this level of investigation they are not unreasonable. The initial heliocentric position and velocity are near the

Earth's sphere of influence. The Earth's orbit is assumed circular; the Sun is the central body with all perturbing gravitational forces ignored. The nominal thrust acceleration vector is assumed parallel to the ecliptic (the X-Y plane), and perpendicular to the vehicle position vector. The nominal value of thrust acceleration magnitude is assumed as a constant 4 meters/sec^2 (except as noted later). At an initial heliocentric velocity (perpendicular to the initial position vector) of 31,743 meters/sec, nominal flight time to encounter with Eros is 152 days. The encounter point is assumed to occur at Eros' mean heliocentric distance, 1.45 a.u. Computation of the simulated trajectory is performed by numerically integrating the dynamic equations using a 4th-order Runge-Kutta-Gill integration scheme. All computations have been performed on the CDC 6400-6600, UT-2 Operating System, at The University of Texas at Austin.

Thrust Acceleration Error Simulation

Consider the local vehicle reference frame, xyz , shown in Figure 1e and related to the heliocentric frame, XYZ , by the transformation

$$\begin{bmatrix} X \\ Y \\ Z \end{bmatrix} = R \begin{bmatrix} x \\ y \\ z \end{bmatrix} \tag{4.3}$$

where

$$R = \begin{bmatrix} \cos\psi & -\sin\psi & 0 \\ \sin\psi & \cos\psi & 0 \\ 0 & 0 & 1 \end{bmatrix} \tag{4.4}$$

Let a be the magnitude of the thrust acceleration, and let γ and θ be control angles with nominal values of zero. Thus, the nominal thrust vector

control history is such that the nominal thrust acceleration vector is directed along the y-axis. Motivated by Rourke and Jordan (2), the following 1σ error values are assumed for the simulation:

1. A value of 6% is used for the low frequency variation in thrust acceleration magnitude due to beam current, beam voltage and mass flow rate variations.
2. A value of 1% is adopted for the high frequency variation in thrust acceleration magnitude due to beam current and beam voltage where the variation is modeled as white noise.
3. A value of 1% is adopted for the high frequency variation in the thrust acceleration direction where the variation is modeled as white noise.

Since the thrust acceleration direction is determined by the angles γ and θ (nominally zero), in accordance with item 3 above, these angles are simulated as random variables where γ is assumed to be distributed normally and θ is assumed to be distributed uniformly with the statistics.

$$\begin{aligned} E[\gamma] &= 0 \quad , \quad \sigma_\gamma^2 = 3.045\times10^{-4} \text{ rad}^2 \\ E[\theta] &= 0 \quad , \quad \sigma_\theta^2 = 3.3 \text{ rad}^2 \end{aligned} \tag{4.5}$$

The low frequency variation, δa, of the thrust acceleration magnitude is simulated as a sinusoidal error with amplitude, δa_o, equal to 6% of nominal thrust, and period equal to 10 days. White noise, u_a, representing the 1% high frequency variations is combined linearly to obtain the following relation:

$$\delta a = \delta a_o \sin \omega t + u_a \quad , \quad E[u_a] = 0 \quad , \quad E[u_a^2] = \sigma_a^2 \tag{4.6}$$

An important characteristic of the simulation is the relationship of the integration stepsize and the simulation of the white noise components of the thrust acceleration errors. The numerical integration scheme requires that the integrand be continuous over the integration step. The simulated

noise components are selected at random from normal distributions and are assumed constant over the integration interval. Thus, the fidelity with which the white noise is simulated will depend on the length of the integration step. If the step is too large, the "random" acceleration errors are constant over an unrealistically long period of time. On the other hand, the problem of computing economy is exposed as the step is decreased to more accurately model white noise. For the majority of the simulations in this investigation, a stepsize of 100 minutes was selected as a realistic compromise.

The control parameters a, γ and θ have components in the xyz frame of

$$\begin{bmatrix} T_x \\ T_y \\ T_z \end{bmatrix} = \begin{bmatrix} a \sin\gamma \cos\theta \\ a \cos\gamma \\ a \sin\gamma \sin\theta \end{bmatrix} \tag{4.7}$$

where a is the total thrust acceleration magnitude. In the XYZ frame, the components of the thrust acceleration become

$$\begin{bmatrix} T_X \\ T_Y \\ T_Z \end{bmatrix} = a \begin{bmatrix} X/p & -Y/p & 0 \\ Y/p & X/p & 0 \\ 0 & 0 & 1 \end{bmatrix} \begin{bmatrix} \sin\gamma \cos\theta \\ \cos\gamma \\ \sin\gamma \sin\theta \end{bmatrix} \tag{4.8}$$

where X/p and Y/p are substituted for $\cos\psi$ and $\sin\psi$, respectively, with $p = \sqrt{X^2 + Y^2}$

IMU Configuration

The IMU configuration yields the thrust acceleration estimate as $T_m = T^* + \varepsilon_m(t)$. The function $\varepsilon_m(t)$ is made up of the deviation of the thrust acceleration from the nominal and the IMU errors. It arises basically from two sources, accelerometer error, ε_a, and platform misaglinment, δ.

Accelerometer errors can include scale factor errors, anisoelastic effects, aging effects, null uncertainties, etc. Platform misalignment can result from initial misaglinment and gyro drift caused by acceleration and vibration-sensitive drifts (mass unbalance, anisoelastic effects, etc.). The data, which is available, regarding the performance characteristics of very low-threshold accelerometers is inadequate for determining a complete statistical description of their behavior. In the past, it has been common practice to express accelerometer errors in the form

$$\varepsilon_a = k_o + k_1 a + k_2 a^2 + \text{H.O.T.} \tag{4.9}$$

where a is the input acceleration. The coefficient, k_o, represents the null errors. The term, $k_1 a$, arises from the linear scale factor and mass unbalances. The term, $k_2 a^2$, is due primarily to anisoelastic effects. In high thrust applications the linear and quadratic terms can be expected to have significant contributions to accelerometer errors; however, for low-thrust applications these effects can reasonably be ignored because of the very low acceleration values encountered (31). The remaining null errors (sensitivity and null uncertainty) are caused by such things as mechanical friction and electrical dead zones, and are assumed here to be a major accelerometer error source. Initial constant biases are assumed zero, and in the study null errors are assumed as random accelerometer outputs characterized as $N(0,\sigma_{ax}^2)$.

An additional accelerometer error source to be considered is the effect of aging. During the mission, it is suggested that possible temperature changes or vibration effects may cause changes in accelerometer characteristics producing output errors which may become significant over long periods of time. Such effects are assumed to be bounded; the net result can

be considered as a slowly changing null error. In this study, it appears reasonable to assume this aging effect to be of the form $k_3(1 - e^{-\xi t})$. Thus, the total accelerometer error sources are simulated as

$$\varepsilon_a = k_o + k_3(1 - e^{-\xi t}) \tag{4.10}$$

where t is the accumulated mission time and ξ is a constant chosen such that 95% of the aging effect has occurred during the first one-third of the mission ($\xi = .07132$ days^{-1}). k_o is a random null error with $E[k_o] = 0$, $E[k_o^2] = \sigma_{ax}^2$.

In general, gyros suffer the same maladies as accelerometers, and their error compensation is similar (i.e., errors are proportional to acceleration and acceleration squared). Of course, a particularly significant error source is gyro drift. However, as mentioned previously the use of a star tracker to provide continuous realignment information effectively eliminates gyro drift as an error source, replacing it with errors in the star tracker. Star tracker errors and, hence, realignment errors modeled as white noise (except in one case where the effects of cumulative drift are shown). The platform misaglinment angles, δ, are then characterized as $N(0,\sigma_{pl}^2)$.

Since the misalignment angles are presumed to be very small, the transformation relating the misaligned axes and aligned axes may be approximated as:

$$\begin{bmatrix} \cos\delta_2 \cos\delta_3 & \cos\delta_2 \sin\delta_3 & \sin\delta_2 \\ (\sin\delta_1 \sin\delta_2 \cos\delta_3 - \cos\delta_1 \sin\delta_3) & (\cos\delta_1 \cos\delta_3 + \sin\delta_1 \sin\delta_2 \sin\delta_3) & \sin\delta_1 \cos\delta_2 \\ (\sin\delta_1 \sin\delta_3 + \cos\delta_1 \sin\delta_2 \cos\delta_3) & (\cos\delta_1 \sin\delta_2 \sin\delta_3 - \sin\delta_1 \cos\delta_3) & \cos\delta_1 \cos\delta_2 \end{bmatrix} \tag{4.11}$$

$$\approx \begin{bmatrix} 1 & \delta_3 & -\delta_2 \\ -\delta_3 & 1 & \delta_1 \\ \delta_2 & -\delta_1 & 1 \end{bmatrix} \triangleq L$$

Thus, the acceleration output from the IMU may be written as

$$T_m = L(T + \varepsilon_a) \tag{4.12}$$

Defining $T' \triangleq T + \varepsilon_a$, it is also possible to write

$$T_m = T' + \begin{bmatrix} 0 & -T'_Z & T'_Y \\ T'_Z & 0 & -T'_X \\ -T'_Y & T'_X & 0 \end{bmatrix} \begin{bmatrix} \delta_1 \\ \delta_2 \\ \delta_3 \end{bmatrix} = T' + T' \times \delta = T' + \varepsilon_g \tag{4.13}$$

treating δ as a pseudo-vector. For the purposes of the simulation δ is generated in the following manner. In the majority of the cases investigated the components of δ are generated by randomly sampling an appropriate normal distribution. In one case where gyro drift is considered, the magnitude of δ, $|\delta|$, is generated as a constant drift rate times the mission time. Letting r_n represent a random sample from a standardized uniform distribution, the direction cosines, c_n, of δ are given by

$$c_n = \begin{bmatrix} c_1 \\ c_2 \\ c_3 \end{bmatrix} = \begin{bmatrix} .707\ r_1 \\ .707\ r_2 \\ \sqrt{1 - c_1^2 - c_2^2} \end{bmatrix} \tag{4.14}$$

Thus, in this case,

$$\delta = |\delta| c_n + u_\delta \tag{4.15}$$

where u_δ is the random sampling from the appropriate normal distribution.

In summary, the IMU errors are

$$\begin{aligned} \varepsilon_a &= k_o + k_3(1 - e^{-\xi t}) \\ \varepsilon_g &= (T + \varepsilon_a) \times \delta \end{aligned} \tag{4.16}$$

and

$$T_m = T + \varepsilon_a + \varepsilon_g \tag{4.17}$$

Estimation of Unmodeled Acceleration Errors

As described previously, three models for estimating the unmodeled acceleration effects are examined in the study. These are each developed below.

Model 1. - The unknown acceleration error components are modeled by an exponentially correlated process, i.e., a first-order Gauss-Markov process, in a heliocentric reference system. The differential equations are then

$$\begin{aligned} \dot{r} &= v \\ \dot{v} &= -\frac{\mu}{r^3} r + T^* + \varepsilon \quad ; \\ \dot{\varepsilon} &= -B\varepsilon + u_\varepsilon \quad , \quad \dot{\beta} = 0 \end{aligned} \tag{4.18}$$

where

$$\varepsilon = \begin{bmatrix} \varepsilon_1 \\ \varepsilon_2 \\ \varepsilon_3 \end{bmatrix} \quad , \quad \beta = \begin{bmatrix} \beta_1 & 0 & 0 \\ 0 & \beta_2 & 0 \\ 0 & 0 & \beta_3 \end{bmatrix} \quad ; \tag{4.19}$$

The random component u_ε is assumed to have the statistics

$$\begin{aligned} E[u_\varepsilon] &= 0 \\ E[u_\varepsilon u_\varepsilon^T] &= q_\varepsilon \end{aligned} \tag{4.20}$$

where q_ε is assumed to be diagonal. The state vector which is estimated is defined then as

$$X^T = [r^T \vdots v^T \vdots \varepsilon^T \vdots \beta^T] \quad .$$

Model 2. - The unknown control components are modeled by exponentially correlated random process, where the acceleration components are expressed in a vehicle fixed reference system. The thrust acceleration magnitude is assumed to be exponentially autocorrelated with the angles γ and θ modeled as white noise. They are estimated in a vehicle or local reference. The corresponding acceleration equation is

$$\begin{aligned} \dot{v} &= -\frac{\mu}{r^3} r + R \begin{bmatrix} (a_0 + \varepsilon_1) & \sin(\varepsilon_2) & \cos(\varepsilon_3) \\ (a_0 + \varepsilon_1) & \cos(\varepsilon_2) & \\ (a_0 + \varepsilon_1) & \sin(\varepsilon_2) & \sin(\varepsilon_3) \end{bmatrix} \quad , \quad \dot{r} = v \\ \dot{\varepsilon} &= -B\varepsilon + u_\varepsilon \quad , \quad \dot{\beta} = 0 \end{aligned} \tag{4.21}$$

where $B = \begin{bmatrix} \beta_1 & 0 & 0 \\ 0 & \beta_2 & 0 \\ 0 & 0 & \beta_3 \end{bmatrix}$

$$E[u_\varepsilon] = 0 \quad , \quad E[u_\varepsilon u_\varepsilon^T] = q_\varepsilon \tag{4.22}$$

The 3×3 matrix q_ε is assumed diagonal. The augmented state vector which is estimated is $X^T = [r^T \vdots v^T \vdots \varepsilon^T \vdots \beta^T]$.

Model 3. - The unknown control components are modeled by a second-order Gauss-Markov process referenced to the vehicle fixed reference frame. The thrust acceleration magnitude is assumed to be represented by a second-order Gauss-Markov process with the angles γ and θ modeled as white noise. They are estimated in a vehicle centered reference frame. The corresponding acceleration equation is

$$\begin{aligned}
\dot{r} &= v \\
\dot{v} &= -\frac{\mu}{r^3} r + R \begin{bmatrix} (a_0 + \varepsilon_1) & \sin(\varepsilon_2) & \cos(\varepsilon_3) \\ (a_0 + \varepsilon_1) & \cos(\varepsilon_2) & \\ (a_0 + \varepsilon_1) & \sin(\varepsilon_2) & \sin(\varepsilon_3) \end{bmatrix} \\
\dot{\varepsilon} &= \eta \\
\dot{\eta} &= -B\varepsilon + u_\eta \quad , \quad \dot{\beta} = 0
\end{aligned} \tag{4.23}$$

where $B = \begin{bmatrix} \beta_1 & 0 & 0 \\ 0 & 0 & 0 \\ 0 & 0 & 0 \end{bmatrix}$

$$E[u_\eta] = 0 \quad , \quad E[u_\eta u_\eta^T] = q_\eta \tag{4.24}$$

The 3×3 matrix q_η is assumed to be diagonal. The augmented state vector which is estimated is $X^T = [r^T \vdots v^T \vdots \varepsilon^T \vdots \eta^T \vdots \beta_1^T]$.

The models discussed in the previous section were programmed for numerical solution on the CDC 6400-6600 digital computer at The University of Texas at Austin. The data obtained during the study is described in the following section.

V. NUMERICAL SIMULATIONS AND DATA PRESENTATION

The general characteristics of the nominal Eros mission are summarized in Table 1. Except as otherwise noted, these characteristics are common to all simulation runs.

Certain abbreviations are used to indicate the observation types employed and are defined according to the following legend:

RR - Radar range rate	Sn-Pl - Sun-planet angle
St-Pl - Star-planet angle	Sn-St - Sun-star angle

Table 2 summarizes the models for estimating the unknown accelerations and defines the 1σ and $\frac{1}{3}\sigma$ error values used in the thrust acceleration error simulations.

Figure 2 shows the projection of the trajectory path into the ecliptic with various time points indicated along the path.

Standard Orbit Determination

Table 3 summarizes the performance characteristics of the trajectory estimation process for the nominal Eros mission for three cases. For the first two cases, no model errors are considered in the estimation process; however, (a) 1σ and (b) $\frac{1}{3}\sigma$ acceleration error values are simulated. In the third case (c), thrust acceleration uncertainties are considered in the estimation process as additive white noise with zero mean and covariance matrix q. The values of the components of the state noise covariance matrix used in the third case are indicated below the table.

In each case the terminal position and velocity components are indicated, along with the terminal position and velocity norms and RSS

uncertainties. Figures 3a.1 through 3c.3 show the error behavior of the position, velocity, and acceleration components in the heliocentric frame. As would be expected, divergence of the estimation process occurs after a short time for the first two cases. In the third case, inclusion of the effects of the model uncertainty statistics delays the error divergence, but the estimate of the state is generally unacceptable.

Orbit Determination Using IMU Measurements

Table 4 summarizes the performance characteristics for the state estimation process with both the nominal observation types and with IMU measurements. Except as noted in the last case, nominal platform alignment was simulated continuously with alignment errors represented as zero mean, uncorrelated random misalignment angles with 1σ values as indicated. Accelerometer error simulation values are given corresponding to the simulation model defined previously. In all cases the aging constant is $\xi = .071327$. The accelerometer error values for each case correspond, respectively, to the following percentages of the nominal thrust acceleration thrust:

a) $k_3 = 13.33\%$, $\sigma_{ax} = 1.33\%$

b) $k_3 = 10\%$, $\sigma_{ax} = 1.0\%$

c) $k_3 = 6.67\%$, $\sigma_{ax} = .67\%$

d) $k_3 = 3.33\%$, $\sigma_{ax} = .33\%$

The integration step for all IMU simulation runs is 6.9444×10^{-2} days, or 100 minutes, and the terminal time is 152.0129 days .

Figures 4a.1 - 4d.3 show the position and velocity component error history for approximately 24 days (Case c also has plots for 152 days). For Case e), constant platform drift, the error history is shown for 84.821 days.

No attempt is made to estimate model uncertainties in the IMU runs; hence, $q(t) = 0$. It is anticipated that the accuracy in the estimate of the state using the IMU data could be improved by compensating for state noise by adding Q-matrix compensation as in Eq. (3.13) or by estimating the error in the accelerometer output using the dynamic model compensation technique described in Section II.

Orbit Determination Estimating Unmodeled Acceleration Characteristics

Data for Models 1 and 2 are presented in Tables 5 and 6, respectively, with simulation data for Model 3 given in Tables 7 and 8. The apriori state error covariances for the model parameters, and the appropriate submatrix components of the state noise covariance matrices are given beneath each table.

The two model 1 cases in Table 5 represent simulations for two seperate values of the diagonal state noise covariance matrix, q , and corresponding position, velocity and acceleration error histories for 24 days are given in Figures 5a.1 - 5b.3 (heliocentric reference). As is apparent from these data, the use of Model 1 yields unsatisfactory performance of the estimation algorithm; some aspects of this performance will be discussed later.

Table 6 presents the data for three runs using Model 2 to structure the unmodeled accelerations. The results obtained here by estimating the control parameters are encouraging. Figures 6a.1 - 6c.3 give the error histories for the position, velocity and acceleration components. The position and velocity errors are referenced to the heliocentric frame; however, the acceleration error history is referenced to the local or vehicle frame.

Extensive data associated with Model 3 simulations are presented in Tables 7 and 8. In Table 7 the effects of decreasing values of the purely

random components in the control parameters are indicated with generally better state estimates occurring for smaller values of these components. Figures 7a.1 - 7c.3 provide the corresponding error histories for position, velocity (heliocentric frame), and acceleration (local frame).

Table 8 shows the effects of using different observation types as well as varying the data sampling interval. The last two cases, h) and i), show the performance of the estimation algorithm when the assumed components of the state noise covariance matrix, q , are perturbed by a decrease and increase, respectively, of 1%. As is apparent, the algorithm is extremely sensitive to the choice of q . Figures 8a.1 - 8i.3 correspond to the Table 8 data and provide the error histories. As before, position and velocity are in the heliocentric reference; acceleration, in the local reference.

VI. DATA ANALYSIS AND COMPARISON

In examining the results presented in the previous section one of the most striking aspects of the mission simulation data is the extent to which thrust acceleration errors affect the position and velocity estimates. From the Table 3 data for the 1σ acceleration errors, the position error estimate has diverged to over 10,000 km within the first twenty days of the observations. See for example, Figure 3a.1. Even for the $\frac{1}{3}\sigma$ acceleration errors the estimates diverge rapidly. For the third case in Table 3, Case 3c*, the use of the state noise covariance matrix to provide a lower bound on the value of the state error covariance matrix improves the error histories by at least an order of magnitude or more. However, for practical purposes the navigation performance indicated by the data is unacceptable. Based on the results shown in Table 4 and Figures 4, the IMU simulations do not appear to yield good estimates until misalignment errors and accelerometer errors are down to the values indicated by Case 4c ($\sigma_{pl} = .01°$, $k_3 = 1.965E-5$, $\sigma_{ax} = 1.965E-6$). Even then, the Z-components of error are significantly large compared with the other two components. This is a characteristic common not only to all the IMU simulation runs, but the majority of the other simulations as well. The reason for this behavior is not apparent. One aspect of this characteristic is that the randomness of the thrust direction will apparently play a large part in the navigation error. It is noted in Case 7c (purely deterministic thrust acceleration error simulation) that the terminal Z-component of the error is not only reasonable, it is minimal. Thus, the Earth-Sun-vehicle dynamical configuration

*In the sequel, simulation runs will generally be identified by their table number and the letter identifying them within the table.

and observation types are not believed to be solely responsible. It should be pointed out, however, that for vehicle motion confined to the X-Y plane, it can be shown that poor information is available from radar range-rate measurements. In the nominal mission simulation there is very little motion in the Z-direction; hence, from the range-rate measurements one would expect little information concerning the Z-components. That the large Z-component errors are most pronounced for the inertial measurements tends to imply more strongly that the behavior is due to the randomness of the thrust acceleration error. This problem is not considered further; however, it is apparent that a careful investigation of this characteristic is needed.

Several conclusions are immediately apparent from the IMU simulation data. Quite obviously, the more accurate the IMU equipment, the better the navigation will be. In addition, the use of a stellar monitoring device to maintain platform alignment appears to be indispensable in configuring an inertial measuring system for long duration, low-thrust missions.

Cases 5a and 5b reflect attempts to compensate for thrusting errors by structuring the error components as exponentially correlated in the heliocentric frame. The data indicates these attempts met with little success. In fact, Case 3c (employing a state noise covariance matrix only) yields better navigation accuracies. Consideration of this fact must be made in light of the dynamics of the system. Recall that initially the simulation begins with the vehicle located on the heliocentric X-axis, the nominal thrust acceleration being directed in the positive Y-direction. The simulation is such that in this configuration the acceleration error has both a time correlated and a purely random component in the Y-direction; in the X-direction the error component is purely random (see Figure 9).

Consider the parameters for the thrust acceleration error simulation.

Since γ is simulated as a normally distributed random variable and θ is a uniformly distributed random variable, the errors for the heliocentric X- and Z-components are nearly purely random. On the other hand, the initial values of the Y-component of the error has both a time correlated component and a purely random component. As the mission progresses, the natures of the X- and Y-components at a later time are beginning to reverse; the X-error is picking up a time correlated component simultaneous with the loss of the time-correlated Y-component. The parameters associated with the differential equations representing the acceleration errors are constants. Hence, no allowance is made for the non-stationary properties of this formulation and, as might be expected, the approach does not yield good results. As a consequence of these considerations, the reasonable alternative of directly modeling the behavior of the control parameters was selected (Model 2).

The data for the Model 2 simulations show a significant increase in navigation accuracies. For the first 24 days the performance is quite good for the 1σ cases. Thereafter, the estimates degrade in accuracy, and at about 85 days a very large deviation in the position estimate occurs. The estimate of the velocity remains generally quite good throughout the simulation run (Case 6a). For the $\frac{1}{3}\sigma$ acceleration errors (Case 6c), the same general behavior occurs, even to the extent that the terminal errors are within an order of magnitude of one another. It would seem reasonable to expect that a $\frac{2}{3}$ reduction in the random errors would result in at least some improvement in the navigation error history. One candidate for the source of the trouble is the state noise covariance matrix employed for case 6c. The values used were found simply by taking $\frac{1}{9}$ of those used in Case 6a (except for σ_θ which remains the same). However, partial data obtained by employing the arbitrary values of

$q_{11} = 4.876E - 22\ (m/s^3)^2$, $q_{22} = .1334E - 5\ (rad/s)^2$,

$q_{33} = 3.3\ (rad/s)^2$, $q_{ij} = 0$, $i \neq j$

yield the error components and norms (at 152 days) given below.

	X	Y	Z	Norm
Position (km)	-2.926×10^3	-1.118×10^3	3.641×10^3	4.818×10^3
Velocity (m/s)	-.1189	-.2675	-9.870	.3089

These values are a significant improvement over Case 6c and the immediate implication is that the performance of the estimation algorithm is fairly sensitive to the selection of the state noise covariance matrix. This aspect of the estimation process is examined further in conjunction with the Model 3 simulations.

In going to the Model 3 structure for the unmodeled accelerations, it was expected that a very significant improvement in the navigation accuracies could be obtained. The results were somewhat less than spectacular, at least for the same 1σ error values. The X- and Z-terminal error components were reduced by a factor of 2, while the Y-component of the terminal error was reduced by an order of magnitude. The velocity error history exhibited basically the same characteristics as for the Model 2 structure. Although the terminal velocity errors actually increased for Model 3, the norm of these values was still slightly less than the maximum velocity error norm for case 6a.

The data for Case 7b ($\frac{1}{3}\sigma$ error values) shows an expected improvement in navigation accuracy. To carry through the implication that the smaller the random errors, the better the estimation accuracy, Case 7c (deterministic error only) was run and the data indicated considerable improvement in the navigation performance. Similar attempts utilizing the Model 2

structure produced the expected large errors in the state estimate (i.e., the mean position error norm was several Earth radii) which resulted in divergence of the estimate at approximately 70 days. These simulations reinforce the conclusion that better structuring of the model will provide more accurate state estimates. There is, however, a rather subtle distinction to be pointed out in this statement. The term "correct mathematical structuring" refers to the form or type of the functions used to represent the unmodeled effects, not the values of the parameters associated with a particular function. If the structure is well-defined, the corresponding parameters may be accurately estimated. As detailed modeling is replaced by the assumption of purely random behavior (no structure in the functional sense) the state estimates become less accurate and a stable estimation procedure is harder to maintain.

Closely associated with this aspect of the estimation problem is the choice of the state noise covariance matrix value. This sets a lower bound on the state error covariance matrix, which in turn controls the asymptotic values of the gain matrix, K, and, hence, the state estimate. An indication of the sensitivity of the estimation procedure to the values of the q-matrix was pointed out in conjunction with the Model 2 runs. An even more dramatic sensitivity to the state noise covariance matrix is shown by Cases 8h and 8i in which the q-matrix is decreased and increased, respectively, by 1% of the nominal q-matrix value. The data given in Table 8 is somewhat misleading in this respect. It indicates a significant reduction in the terminal error conditions for Case 8h. However, examination of Figures 8h.1 and 8h.5 show that maximum values of the position and velocity error norms occur at approximately 80 days, and these are an order of magnitude greater than those where the nominal value of q is used. In case 8i

a slight improvement in the overall velocity error norm is indicated, but the terminal position error norm (which is also the maximum in this case) is greater by a factor slightly greater than 3. These results should not be interpreted to imply that the nominal value of q used in the simulation is the optimum value. It was the one, selected from a large number of values, which yielded good overall performance.

As a result of the indicated sensitivity of the estimation procedure to the values adopted for the q-matrix, it is felt that further investigations should employ some adaptive scheme for estimating the proper state noise covariance matrix. Some preliminary investigations of the feasibility of such an approach have been made, and at least one scheme due to Jazwinski (4) appears promising.

It is interesting to examine the estimates of the acceleration error frequency. As mentioned above, accurate structuring allows reasonably accurate estimates of the associated parameters in the model; as more randomness is introduced such estimation becomes difficult. These conjectures are sustained by examining the history of the frequency estimates. Figure 10 shows the actual frequency error history for Cases 7a through 7c. The period of the thrust acceleration magnitude variation is .1 days, or a frequency of $.2\pi$ radians/day. As expected, the accuracy of the frequency estimate improves when the magnitude of the purely random noise is decreased. Thus, since the time correlated components of the thrust acceleration error has its structure characterized by the frequency, the accuracy of the unmodeled acceleration estimate is also dependent upon the extent to which purely random noise is included (see also Figures 7c).

The effects of different observation types and varying sampling

and integration intervals are pointed out by Cases 8a through 8g. Cases 8a through 8c show the combined effects of a more rapid sampling interval plus the effect of more accurately simulating the random acceleration errors. As indicated previously (Section IV) the simulation is constructed such that random fluctuations in the acceleration vector are constant over the integration interval; the smaller the interval, the more nearly are white noise effects simulated.

These results tend to indicate that an increased sampling rate generally increases the overall accuracy of the estimate. (Too small an interval, however, results in a rapid decrease of the state error covariance matrix, corresponding ill conditioning of the observation deviation covariance and subsequent numerical problems).

In all cases where the observation interval was varied, the observation covariance was correspondingly scaled inversely proportional to the interval. Cases 8b and 8c employed the same total number of range-rate observations, with 8c showing a marked improvement over 8b. All three Cases (8a through 8c) reflect divergence in the estimate with the Z-position error components showing a generally linear divergence. This tends to support the earlier statement that little information about the Z-components is derived from the range-rate measurements for vehicle motion restricted to being near the X-Y plane.

On the other hand, the on-board angles in general might be expected to yield more information depending, of course, upon the direction of the navigation star(s) employed. Recall that the on-board angle used for the majority of cases was the star-planet angle, with Earth as the selected planet. The star was selected near the X-Y plane so that generally more information would be available for the X-Y components than if the star direction

had a large Z-component.

Note that somewhat better performance was obtained for the star-planet angle measurements than for range-rate measurements for the same observation schedule, 100-minute intervals (Cases 8a and 8d).

Case 8e provides comparison of the star-planet and sun-star angles. The results of Case 8d (star-planet angle) indicate better performance. An explanation of this is that Earth is closer to the vehicle, hence, the corresponding star-planet angle is more sensitive to position errors.

Cases 8f and 8g combine the range-rate and star-planet angle measurements for two different schedules. These results again tend to indicate that a more rapid sampling increases the accuracy. However, it is cautioned that these results are for short time periods and as shown by Figures 8g the estimate errors are growing slightly.

VII. CONCLUSIONS AND RECOMMENDATIONS

Based on the data presented in the previous sections, the following conclusions can be made regarding the navigation procedures for the low-thrust space vehicles. Some of the conclusions are regarded as preliminary since in several areas additional numerical studies are required to complete the investigation. In particular, it is anticipated that further study of the utilization of the Inertial Measuring Units is warranted. The general conclusions are as follows:

1. The estimate of the state obtained with the standard and Q-matrix-compensated sequential estimation algorithms will diverge due to the errors in the thrust program. The divergence occurs within a few days (less than 20) for the standard sequential estimation algorithm.

2. The IMU techniques for compensating for the unmodeled accelerations by measuring the acceleration directly leads to unacceptable navigation accuracies unless precise gyro-platform alignment (within .01°) and very low noise-to-signal ratios (< .07) in the accelerometers are maintained.

3. The results obtained in the simulation indicate that the Dynamic Model Compensation (DMC) algorithm will yield a significant improvement over the navigation accuracies obtained with the Standard- and Q-matrix Compensated Sequential Estimation algorithms. In addition, the DMC algorithm will yield better navigation accuracies than the IMU-Standard Orbit Determination algorithm except for extremely precise IMU measurements, i.e., gyro-platform alignment < .01° and accelerometer signal-to-noise ratio > .07.

4. In addition to yielding a more accurate estimate of the state, the Dynamic Model Compensation algorithm will produce an accurate estimate

of the bias and long period components of the unmodeled accelerations. The long-period components are those with periods considerably greater than the observation interval. The short-period (on the order of the observation interval) and purely random components are averaged out by the DMC algorithm.

5. The accuracy of the estimate with the DMC algorithm is quite sensitive to the observation interval and to the accuracy of the observations. For best results for the low-thrust Eros missions simulated in this study, range-rate data points should be processed at intervals $\leq$ 10 minutes. The higher observation rates per given time interval will lead to a more accurate estimate.

6. The navigation accuracy obtained with the Dynamic Model Compensation algorithms is quite sensitive to the value of the variance in the random noise in the approximating equation. As a consequence, further study of means of estimating this parameter is warranted.

7. For the DMC algorithm, the state error covariance matrix represents a conservative bound on the estimation error. However, the state error covariance matrix does not bound the state error for the standard or for the majority of the IMU compensated results.

8. Detailed and flexible structuring of the approximation for the unmodeled accelerations is necessary for accurate navigation. In general, the assumption of a purely random noise should be avoided in favor of approximations that are combinations of purely random and auto-correlated functions of time. In this study, both first-order and second-order Gauss-Markov processes were used to approximate the unmodeled acceleration. The second-order process leads to a more accurate navigation procedure.

9. The first-order Gauss-Markov process does not represent periodic phenomena very well; however, the second order process (i.e., a damped

harmonic oscillator forced by zero-mean random noise) can be used to represent both decaying and periodic phenomena.

In view of the conclusions presented in the previous paragraphs, the following recommendations for further study are made:

1. Based on the sensitivity of the estimation algorithm to the value assigned to the state noise covariance matrix, it is recommended that DMC algorithm be modified to allow estimation of the value of the covariance matrix during the estimation process. By this procedure, a completely adaptive estimation algorithm for compensating for the unmodeled acceleration can be developed.

2. Based on the less than satisfactory performance of the IMU-Standard Orbit Determination algorithm, it is recommended that a study be made to determine the effectiveness of the DMC algorithm in compensating for the noise introduced in the IMU acceleration measurements due to gyro and accelerometer error.

3. It is recommended that an estimation procedure be evaluated in which the IMU measurements are treated as observations rather than as a direct input to the state equations. Since with the DMC algorithms, the unmodeled accelerations are treated as additional state variables, the accelerometer output will be related directly to the state. As a consequence, the estimation process should be improved by this data. It should be noted that, since the accelerometer output will be a continuous signal, a continuous observation algorithm rather than the discrete-observation algorithm used in this investigation will be required to process the observation.

REFERENCES

1. Jordan, J. F., G. A. Madrid and G. E. Pease, "The Effects of Major Error Sources in Planetary Spacecraft Navigation Accuracies", Journal of Spacecraft and Rockets, Vol. 9, No. 3, March, 1972, pp. 196-204.

2. Rourke, K. H. and J. F. Jordan, "Guidance and Navigation for Solar Electric Interplanetary Missions", Journal of Spacecraft and Rockets, Vol. 8, No. 9, September, 1971, pp. 920-926.

3. Kalman, R. E. and R. S. Bucy, "New Results in Linear Filtering and Prediction Theory", Trans. ASME, Journal of Basic Engineering, Series D, Vol. 82, March, 1960, pp. 35-45.

4. Jazwinski, A. H., Stochastic Processes and Filtering Theory, Academic Press, New York, New York, 1969, pp. 276-277.

5. Squires, R. K., et al, "Response of Orbit Determination Systems to Model Errors", C-643-69-503, Goddard Space Flight Center, Greenbelt, Maryland, 1969.

6. Gapcynski, J. P., W. T. Blackshear and H. R. Campton, "The Lunar Gravitational Field as Determined from the Tracking Data of the Lunar Orbiter Series of Spacecraft", AAS/AIAA Astrodynamics Specialist Conference, AAS Paper No. 68-132, Jackson, Wyoming, September, 1968.

7. Hamer, H. A. and K. G. Johnson, "Effect of Gravitational-Model Selection on the Accuracy of Lunar Orbit Determination from Short Data Arcs", NASA TN D-5105, Langley Research Center, March, 1969.

8. Anderle, R. J., P. A. Malyevac and H. L. Green, Jr., "Effect of Neglected Gravity Coefficients on Computed Satellite Orbits and Geodetic Parameters", AIAA/AGU Symposium on Astrodynamics and Related Planetary Sciences, Washington, D. C., April 21-25, 1969.

9. Schlee, F. H., C. J. Standish and N. F. Toda, "Divergence in the Kalman Filter", AIAA Journal, Vol. 5, No. 6, June, 1967, pp. 1114-1120.

10. Schmidt, S. F., "Computational Techniques in Kalman Filtering", Theory and Applications of Kalman Filtering, NATO AGARDograph 139, Ed. by C. T. Leondes, February, 1970, Chapter 3.

11. Sorenson, H. W., "Kalman Filtering Techniques", Advances in Control Systems, Vol. 3, Ed. by C. T. Leondes, 1966, pp. 219-292.

12. Potter, J. E. and J. C. Decker, "The Minimal Bound on the Estimation Error Covariance Matrix in the Presence of Correlated Driving Noise", SIAM Journal of Control, Vol. 8, pp. 513-526, November, 1970.

13. Miller, R. S., "Asymptotic Behavior of the Kalman Filter with Exponential Aging", AIAA Journal, Vol. 9, March, 1971, pp. 537-539.

14. Wishner, R. P., R. E. Larson and M. Athans, "Status of Radar Tracking Algorithms", Proceedings of the Symposium on Nonlinear Estimation Theory and Its Applications, IEEE No. 70C66-AC, San Diego, California, September, 1970, pp. 32-54.

15. Friedland, B., "Treatment of Bias in Recursive Filtering", IEEE Transactions on Automatic Control, Vol. AC-14, No. 4, August, 1960, pp. 359-367.

16. Russell, R. K. and D. W. Curkendall, "On Modeling Continuous Accelerations as Piecewise Constant Functions", JPL Technical Report 32-1526, Vol. VIII, pp. 45-52.

17. Carpenter, G. C. and E. T. Pitkin, "Orbit Determination for a Thrusted Space Vehicle", Vol. 8, No. 12, December, 1970, pp. 2265-2270.

18. Potter, J. E. and W. E. Van der Velde, "Optimum Mixing in Gyroscope and Star Tracker Data", MIT Experimental Astronomy Lab. Report RE-26, February, 1967.

19. Erzberger, H., "Application of Kalman Filtering to Error Correction of Inertial Navigators", NASA TND-3874, Ames Research Center, February, 1967.

20. Fitzgerald, R. J., "Filtering Horizon-Sensor Measurements for Orbital Navigation", Proceedings of the AIAA/JACC Guidance and Control Conference, Seattle, Washington, August, 1966, pp. 500-509.

21. Mehra, R. K., "Application of Statistical Smoothing Techniques", Harvard University, Technical Report No. 560, April, 1968.

22. Rauch, H. E., "Optimum Estimation of Satellite Trajectories Including Random Fluctuations in Drag", AIAA Journal, Vol. 3, No. 4, April, 1965, pp. 717-722.

23. Lear, W. M., "Mathematical Model for Estimation of Powered (and Free Flight) Trajectories in the Earth-Moon Gravity Field", Program Technical Report Task MSC/TRW A-48, TRW Systems, February, 1966.

24. Duxbury, T. C. and H. Ohtakay, "In-Flight Calibration of a Navigation Instrument", AIAA Guidance, Control and Flight Mechanics Conference, AIAA Paper No. 70-1023, August, 1970.

25. Jordan, J. F., "Optimal Stochastic Control Theory Applied to Interplanetary Guidance", EMRL Technical Report No. 1004, The University of Texas at Austin, August, 1966.

26. Esposito, P. B., et al, "Classical Least Squares and Sequential Estimation Techniques as Applied to the Analysis of the Mariner

27. Bryson, A. E. and L. J. Henrikson, "Estimation Using Sampled-Data Containing Sequentially Correlated Noise", Harvard University, Technical Report No. 533, June, 1967.

28. Ingram, D. S., "Orbit Determination in the Presence of Unmodeled Accelerations", Applied Mechanics Research Laboratory, Report No. AMRL-1022, The University of Texas at Austin, January, 1971. (Also, Ph.D. Dissertation).

29. Ingram, D. S. and B. D. Tapley, "Lunar Orbit Determination in the Presence of Unmodeled Accelerations", AAS/AIAA Astrodynamics Specialist Conference 1971, AAS Paper No. 71-37, August, 1971.

30. Tapley, B. D. and D. S. Ingram, "Orbit Determination in the Presence of Unmodeled Accelerations", Proceedings of the Second Symposium on Nonlinear Estimation Theory, San Diego, California, September, 1971.

31. Friedlander, A. L., "Analysis of an Optimal Celestial-Inertial Navigation Concept for Low-Thrust Interplanetary Vehicles", IIT Report No. E-6037, August, 1965.

32. Friedlander, A. L., "Solar Electric Propulsion - A Survey of Technology Status and Mission Applications", ITT Research Institute, March, 1970.

33. Pitman, G. R. (ed.), Inertial Guidance, John Wiley and Sons, Inc., New York, New York, 1962.

Initial Conditions		Initial Condition Uncertainties (1σ)
X	.150523632E9 km	6378.12 km
Y	0.	6378.12 km
Z	-6378.12 km	6378.12 km
$\dot{X}$	0.	73.82083 m/sec
$\dot{Y}$	31,742.95833 m/sec	73.82083 m/sec
$\dot{Z}$	73.82083 m/sec	73.82083 m/sec

Nominal Thrust Acceleration (Vehicle Reference)		Nominal Observations		
		Type	Sample Interval	Variance
$\ddot{x}_t$	0	Range-rate (RR)	100 min	1 mm/sec @ 1 min
$\ddot{y}_t$	3.0 E - 4 m/sec^2	star planet	100 min	10 arc sec @ 100 min
$\ddot{z}_t$	0	angle (St-Pl)		

Navigation Star Direction Cosines (X,Y,Z)	.553846	.738426	.384615

Table 1. Nominal Trajectory Characteristics

Models	Thrust Acceleration Simulation Errors	
1. Exponentially autocorrelated acceleration errors estimated in heliocentric frame	1σ	δa_o = 6% a_o = .18E-4 m/sec^2 σ_a = 1% a_o = 3.E-6 m/sec^2 σ_γ = .01745 rad σ_θ = 1.8166 rad Period = .1 days
2. Exponentially autocorrelated control parameter errors; acceleration errors referenced to vehicle frame. 3. Sinusoidally autocorrelated control parameter errors; acceleration errors referenced to vehicle frame	$\frac{1}{3}\sigma$	δa_o = 6% a_o = .18E-4 m/sec^2 σ_a = .33% a_o = .99E-6 m/sec^2 σ_γ = .006 rad. σ_θ = 1.8166 rad. Period = .1 days

Table 2. Models Used in Simulation

Model	Acceleration Simulation Errors	Time/ integration step (days)	Observations	*Terminal Errors*					
				Position Components (X,Y,Z;km)	Position Norm (km)	Position RSS (km)	Velocity Components ($\dot{X},\dot{Y},\dot{Z}$;m/s)	Velocity Norm (m/s)	Velocity RSS (m/s)
a) No compensation	1σ	152.08/ 6.944E-2	RR, St-Pl	-4.191E5 -1.687E5 -3.614E6	3.642E6	1.469	13.74 -63.42 51.54	86.87	6.000E-5
b) No compensation	$\frac{1}{3}\sigma$	152.08/ 6.944E-2	RR, St-Pl	5.456E3 4.817E3 4.807E4	4.807E4	1.862	.6083 1.213 -18.79	18.84	9.500E-5
c) Uncorrelated state noise	1σ	152.08/ 6.944E-2	RR, St-Pl	1.204E4 -3.952E2 -1.871E4	2.225E4	1.467E4	-.1292 1.014 -.5809	1.176	.1539

For Case c): $q_{11} = q_{22} = 3.067E-11\ (m/sec^2)^2$; $q_{33} = 2.183E-12\ (m/sec^2)^2$; $q_{ij} = 0$, $i \neq j$

Table 3. Terminal Navigation Error With Standard Estimation Methods

IMU error sim: misalign/ accelerometer	Acceleration Simulation Errors	Time/ integration step (days)	Observations	Terminal Errors					
				Position Components (X,Y,Z;km)	Position Norm (km)	Position RSS (km)	Velocity Components ($\dot{X},\dot{Y},\dot{Z}$;m/s)	Velocity Norm (m/s)	Velocity RSS (m/s)
a) σ_{pl} = 1°/ k_3 = 4.101E-5 (m/s^2) σ_{ax} = 4.101E-6 (m/s^2)	1σ	152.0/ 6.944E-2	RR, St-Pl	-2.568E4 -2.411E4 -1.048E6	1.049E6	1.336	-6.745 -5.643 67.28	67.85	1.000E-4
b) σ_{pl} = .1°/ k_3 = 2.990E-5 σ_{ax} = 2.990E-6	1σ	152.0/ 6.944E-2	RR, St-Pl	-6.304E2 -3.776E2 1.352E5	1.352E5	1.596	-.6748 -.2471 8.089	8.120	2.415E-4
c) σ_{pl} = .01°/ k_3 = 1.965E-5 σ_{ax} = 1.965E-6	1σ	152.0/ 6.944E-2	RR, St-Pl	-5.174 -5.981 -1.505E4	1.505E4	1.894	-6.617E-2 -1.894E-2 .6731	.6766	2.929E-4
d) σ_{pl} = .001° k_3 = 1.025E-5 σ_{ax} = 1.025E-6	1σ	152.0/ 6.944E-2	RR, St-Pl	1.073 .2118 -1.530E3	1.530E3	1.908	-6.372E-3 -1.843E-3 6.655E-2	6.688E-2	2.937E-4
e) No platform realignment; constant drift of .001°/hr random misalignment σ_{pl} = .001° ; k_3 = 1.025E-5 σ_{ax} = 1.025E-6	1σ	152.0/ 6.944E-2	RR, St-Pl	-2.940E5 -2.583E4 -1.819E6	1.819E6	.7830	8.170 -41.37 1.024E2	1.107E2	2.088E-4

Table 4. Terminal Navigation Errors Using IMU Measurements

Model	Acceleration Simulation Errors	Time/ Integration step (days)	Observations	Terminal Errors					
				Position Components (X,Y,Z;km)	Position Norm (km)	Position RSS (km)	Velocity Components ($\dot{X},\dot{Y},\dot{Z}$;m/s)	Velocity Norm (m/s)	Velocity RSS (m/s)
a) 1	1σ	25./ 6.944E-2	RR, St-P1	-5.317E4 1.048E4 5.486E4	7.712E4	1.762E3	-47.96 6.138 58.31	75.75	1.979
b) 1	1σ	25./ 6.944E-2	RR, St-P1	-5.907E4 -6.092E3 5.632E4	8.185E4	8.219E2	-29.95 1.934 42.80	52.27	1.166

a) $q_{11} = q_{22} = q_{33} = 4.178E-21\ (m/sec^3)^2$, $q_{11} = 0$, $i \neq j$

b) $q_{11} = q_{22} = 1.198E-21\ (m/sec^3)^2$, $q_{33} = 4.178E-21\ (m/sec^3)^2$, $q_{ij} = 0$, $i \neq j$

Table 5. Terminal Navigation Errors Using Heliocentric First-Order Acceleration Error Approximation

Model	Acceleration Simulation Errors	Time/ integration step (days)	Observations	Position Components (X,Y,Z;km)	Position Norm (km)	Position RSS (km)	Velocity Components ($\dot{X},\dot{Y},\dot{Z}$;m/s)	Velocity Norm (m/s)	Velocity RSS (m/s)
a) 2	1σ	152.0/ 6.944E-2	RR, St-P1	-1.075E4 -1.231E3 1.662E4	1.983E4	2.208E3	.8573 -.8574 .3560	1.264	.4974
b) 2	1σ	25.0/ 6.944E-2	RR, St-P1	6.156E2 -1.390E3 -9.827E2	1.810E3	5.904E2	.7812 -7.733E-2 -1.131	1.377	.4061
c) 2	$\frac{1}{3}\sigma$	152.0/ 6.944E-2	RR, St-P1	-1.051E4 -2.754E3 1.637E4	1.965E4	1.554E3	-1.907 -1.067 .4717	2.236	.4018

a),b) q_{11} = 1.198E - 21 $(m/s^3)^2$, q_{22} = .324E - 3 $(rad/s)^2$, q_{33} = 3.3 $(rad/s)^2$, q_{ij} = 0 , i ≠ j

c) q_{11} = 1.331E - 22 $(m/s^3)^2$, q_{22} = .36E - 4 $(rad/s)^2$, q_{33} = 3.3 $(rad/s)^2$, q_{ij} = 0 , i ≠ j

Model 2 apriori covariances:

σ_ε^2 = 6.570E - 10 $(m/s^2)^2$ σ_γ^2 = .4E - 3 rad^2 σ_θ^2 = 3.5 rad^2 $\sigma_{\beta X}^2 = \sigma_{\beta Y}^2 = \sigma_{\beta Z}^2$ = .01 day^{-2}

Table 6. Terminal Navigation Errors Using Vehicle Fixed First-Order Acceleration Error Approximations

Model	Acceleration Simulation Errors	Time/ Integration step (days)	Observations	Terminal Errors: Position Components (X,Y,Z;km)	Position Norm (km)	Position RSS (km)	Velocity Components ($\dot{X},\dot{Y},\dot{Z}$;m/s)	Velocity Norm (m/s)	Velocity RSS (m/s)
a) 3	1σ	152.0/ 6.944E-2	RR, St-Pl	5.125E3 -1.436E2 -7.530E2	9.109E3	2.228E3	3.265 .7109 -3.939	5.165	.4635
b) 3	$\frac{1}{3}\sigma$	152.0/ 6.944E-2	RR, St-Pl	-1.370E3 -76.86 2.509E3	2.859E3	7.341E2	-.4201 -.1462 -.9575	1.056	.1925
c) 3	Deterministic only (no random components)	100.0/ 6.944E-2	RR, St-Pl	13.80 -5.057 3.086	15.01	1.312	-1.193E-4 -2.130E-3 -1.831E-3	2.811E-3	2.403E-4

a) $q_{11} = 1.198E-21\ (m/s^3)^2$, $q_{22} = .324E-3\ (rad/s)^2$, $q_{33} = 3.3\ (rad/s)^2$, $q_{ij} = 0$, $i \neq j$

b) $q_{11} = 1.331E-22\ (m/s^3)^2$, $q_{22} = .36E-4\ (rad/s)^2$, $q_{33} = 3.3\ (rad/s)^2$, $q_{ij} = 0$, $i \neq j$

c) $q_{ij} = 0$, all ij

Model 3 apriori covariances (all cases, except as noted, for Table 8.):

$P^2_\varepsilon = 3.912E-20\ (m/s^3)^2$ $P^2_{\dot\gamma} = P^2_{\dot\theta} = 0$ $P^2_\eta = 8.801E-20\ (m/s^2)^2$ $P^2_\gamma = .4E-3\ rad^2$ (1σ errors)

$P^2_\gamma = .6E-4\ rad^2$ ($\frac{1}{3}\sigma$ errors) $P^2_\theta = 3.5\ rad^2$ $P^2_\beta = .4\ (rad/day)^2$

Table 7. Effects of Magnitude of the Random Acceleration Components

Model	Acceleration Simulation Errors	Time/ Integration step (days)	Observations	Terminal Errors					
				Position Components (X,Y,Z;km)	Position Norm (km)	Position RSS (km)	Velocity Components ($\dot{X},\dot{Y},\dot{Z}$;m/s)	Velocity Norm (m/s)	Velocity RSS (m/s)
a) 3	1σ	25.0/ 6.944E-2	RR only @ 100 min intervals	-2.495E4 6.816E2 2.866E4	3.800E4	4.107E3	-7.857 -.4775 17.31	19.02	2.056
b) 3	1σ	25.0/ 6.944E-3	RR only @ 10 min intervals	-8.365E3 1.561E3 -1.254E4	1.515E4	1.060E3	-3.875 .4271 -6.007	7.161	.5110
c) 3	1σ	2.5/ 6.944E-4	RR only @ 1 min intervals	-3.7027E2 2.769E2 -1.086E3	1.161E3	1.026E3	-.5683 -5.076E-2 -6.027	6.054	1.272
d) 3	1σ	25.0/ 6.944E-2	St-Pl only @ 100 min intervals	-2.444E3 1.270E4 5.918E3	1.422E4	3.026E4	-9.120 7.314 11.57	16.45	14.96
e) 3	1σ	25.0/ 6.944E-2	Sn-St only @ 100 min intervals	4.359E5 9.281E5 -7.028E5	1.2431E6	1.8462E5	1.210E3 4.012E2 6.459E2	1.429E3	1.146E2
f) 3	1σ	1.540/ 6.944E-4	RR @ 1 min, St-Pl @ 10 min intervals	-5.417E2 -2.504E2 1.333E2	6.114E2	4.886E2	.2938 -.3696 -1.800	1.861	.8500
g) 3	1σ	7.700/ 6.944E-3	RR and St-Pl @ 10 min intervals	1.643E2 6.358E2 33.28	6.575E2	43.98	-1.352 .7285 .4159	1.591	5.262E-2
h) 3; U decreased 1%	1σ	152.0/ 6.944E-2	RR, St-Pl	58.66 -8.281E2 1.119E3	1.393E3	2.501E3	3.542 .2852 -.8616	3.657	.6852
i) 3; U increased 1%	1σ	152.0/ 6.944E-2	RR, St-Pl	1.573E4 1.524E3 -2.371E4	2.849E4	2.162E3	2.294 1.537 -1.281	3.044	.4612

Table 8. Effects of Observation Types and Observation Schedules

Table 8. (Continued) Effects of Observation Types and Observation Schedules

a) - g) $q_{11} = 1.198E - 21\ (m/s^3)^2$, $q_{22} = .324E - 3\ (rad/s)^2$,

$q_{33} = 3.30\ (rad/s)^2$, $q_{ij} = 0$, $i \neq j$

i) $q = 1.200E - 21\ (m/s^3)^2$, $q_{22} = .327E - 3\ (rad/s)^2$,

$q_{33} = 3.33\ (rad/s)^2$, $q_{ij} = 0$, $i \neq j$

h) $q_{11} = 1.186E - 21\ (m/s^3)^2$, $q_{22} = .321E - 3\ (rad/s)^2$,

$q_{33} = 3.27\ (rad/s)^2$, $q_{ij} = 0$, $i \neq j$

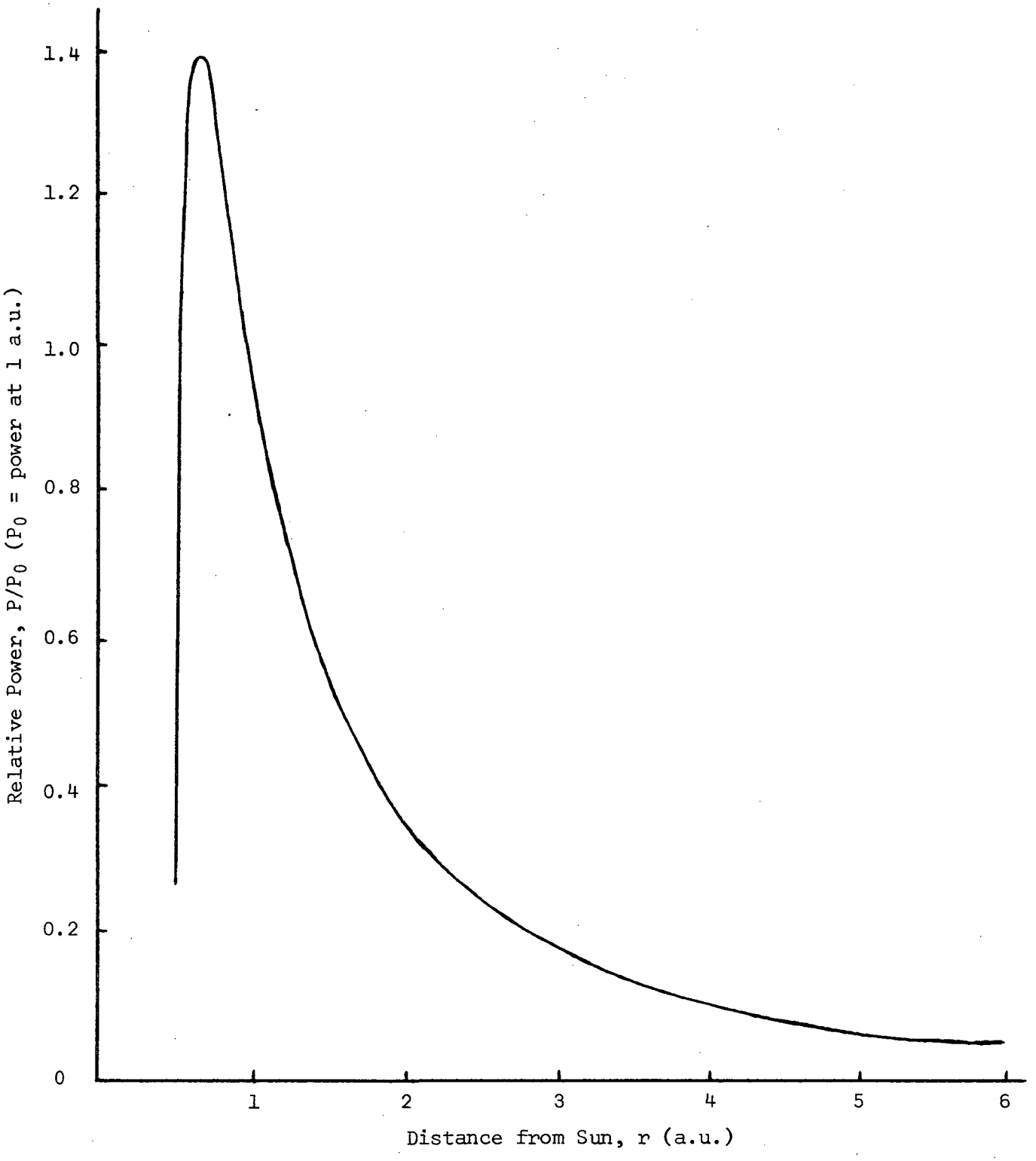

Figure 1a Solar Cell Power Profile

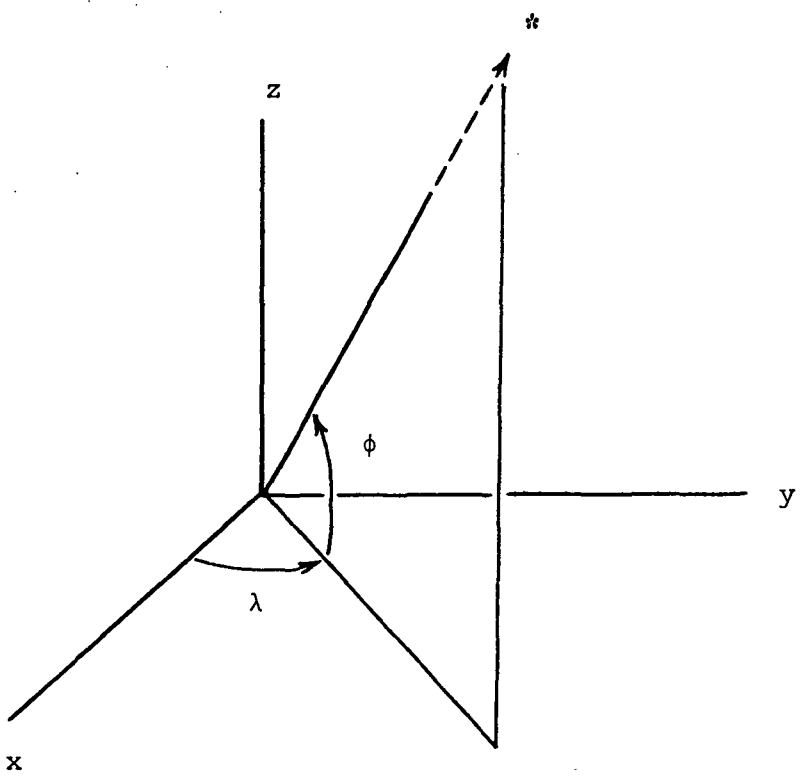

Figure 1b Theodolite Type Measurement

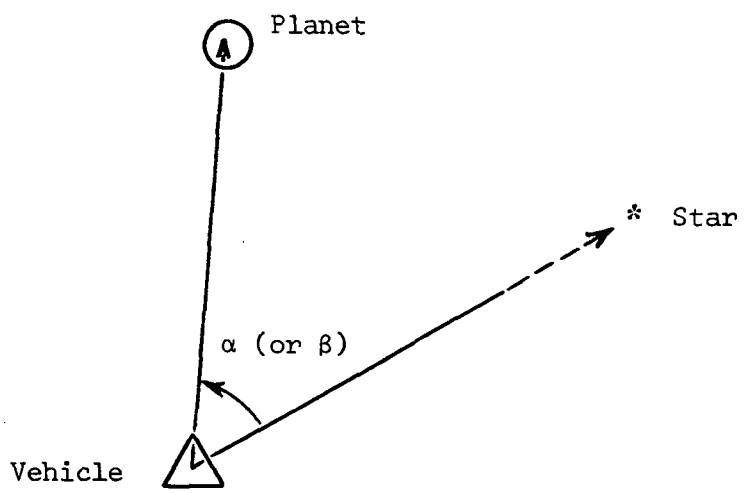

Figure 1c Sextant Type Measurement

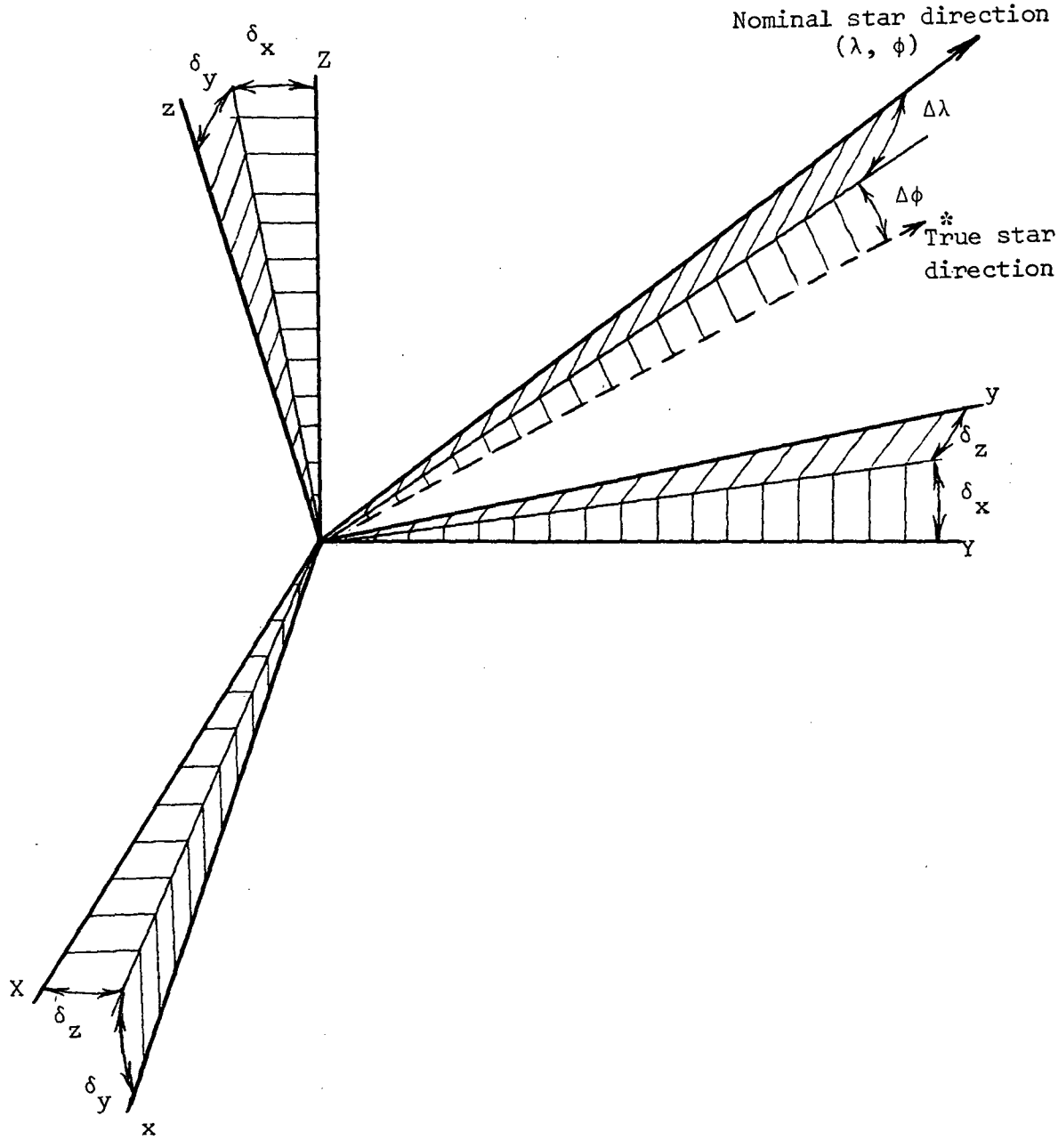

Figure 1d Platform Misalignment and Star Sighting Geometry

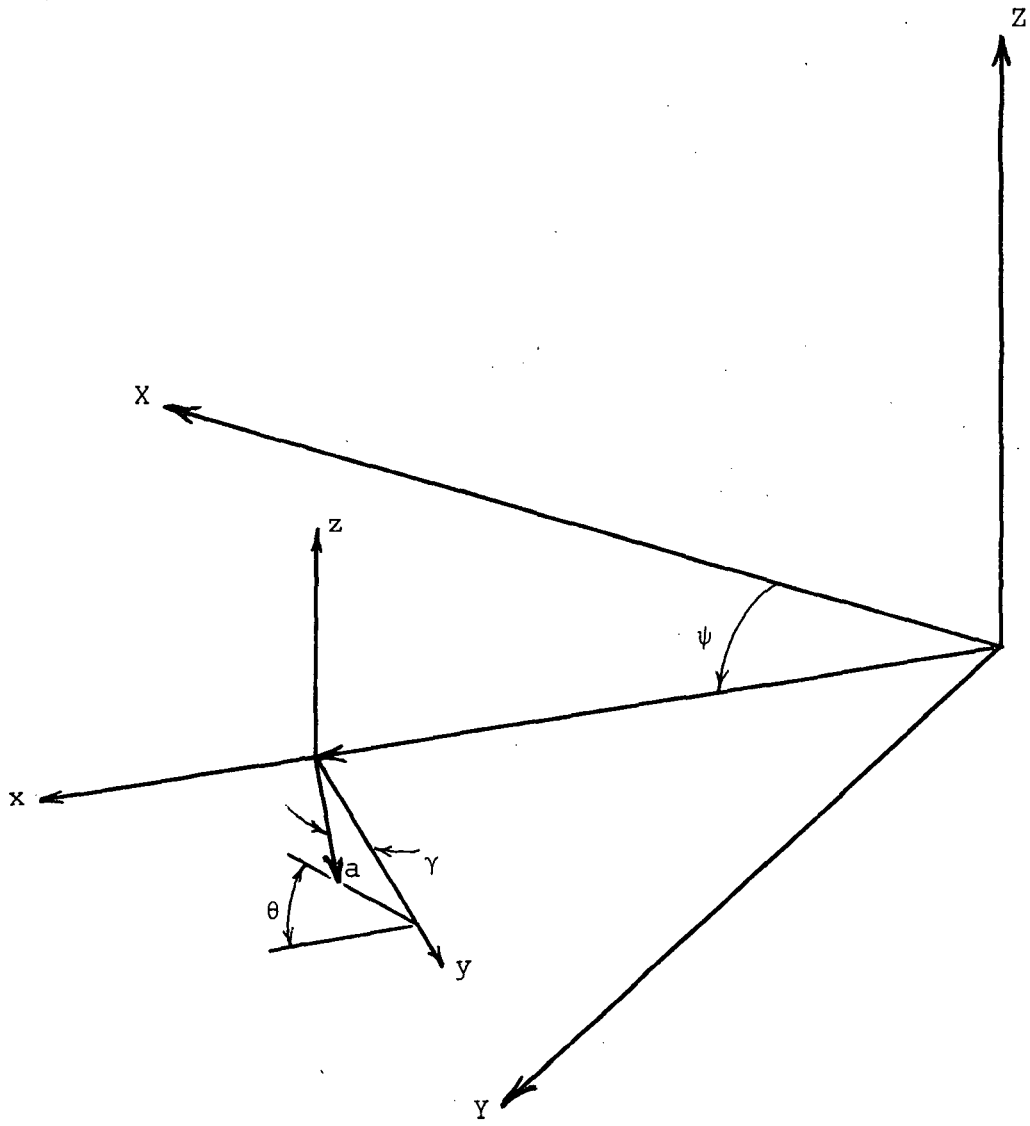

Figure 1e Thrust Acceleration Vector Configuration

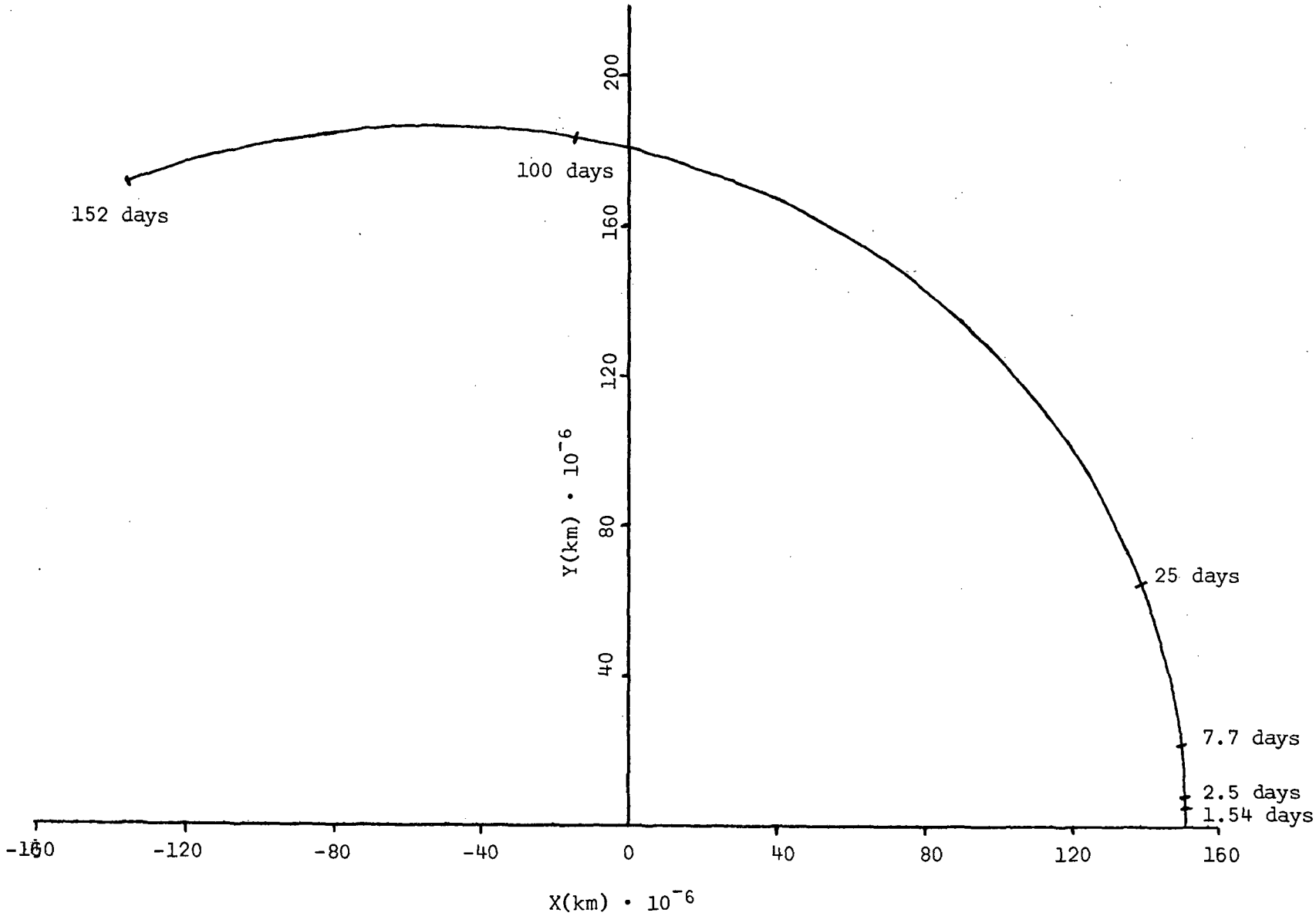

Figure 2 Trajectory Projection in X-Y Plane

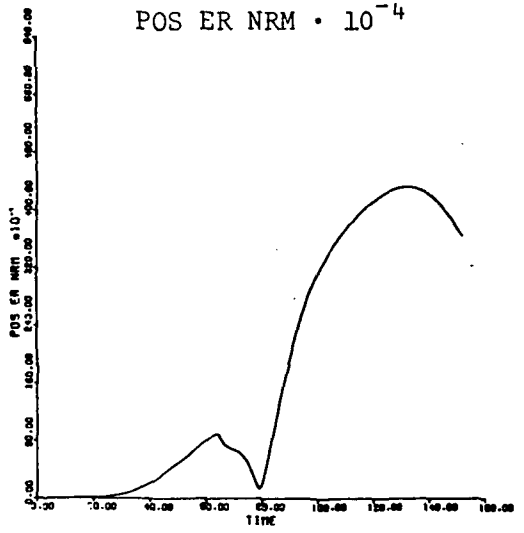

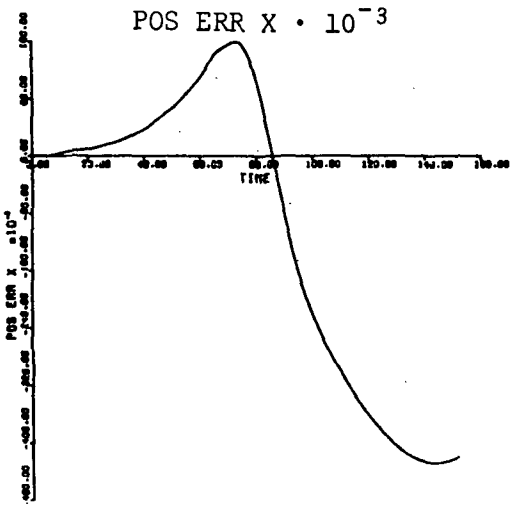

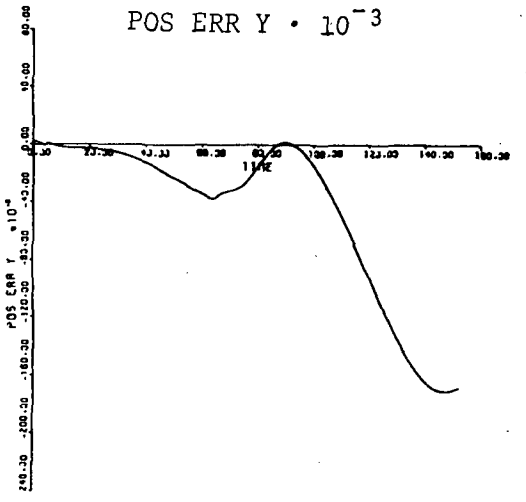

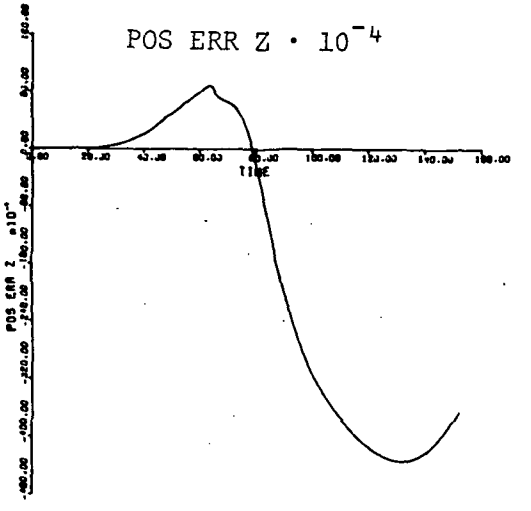

Figure 3a.1 Position Error (km) vs. Time (days) for Standard O. D. (1σ Errors)

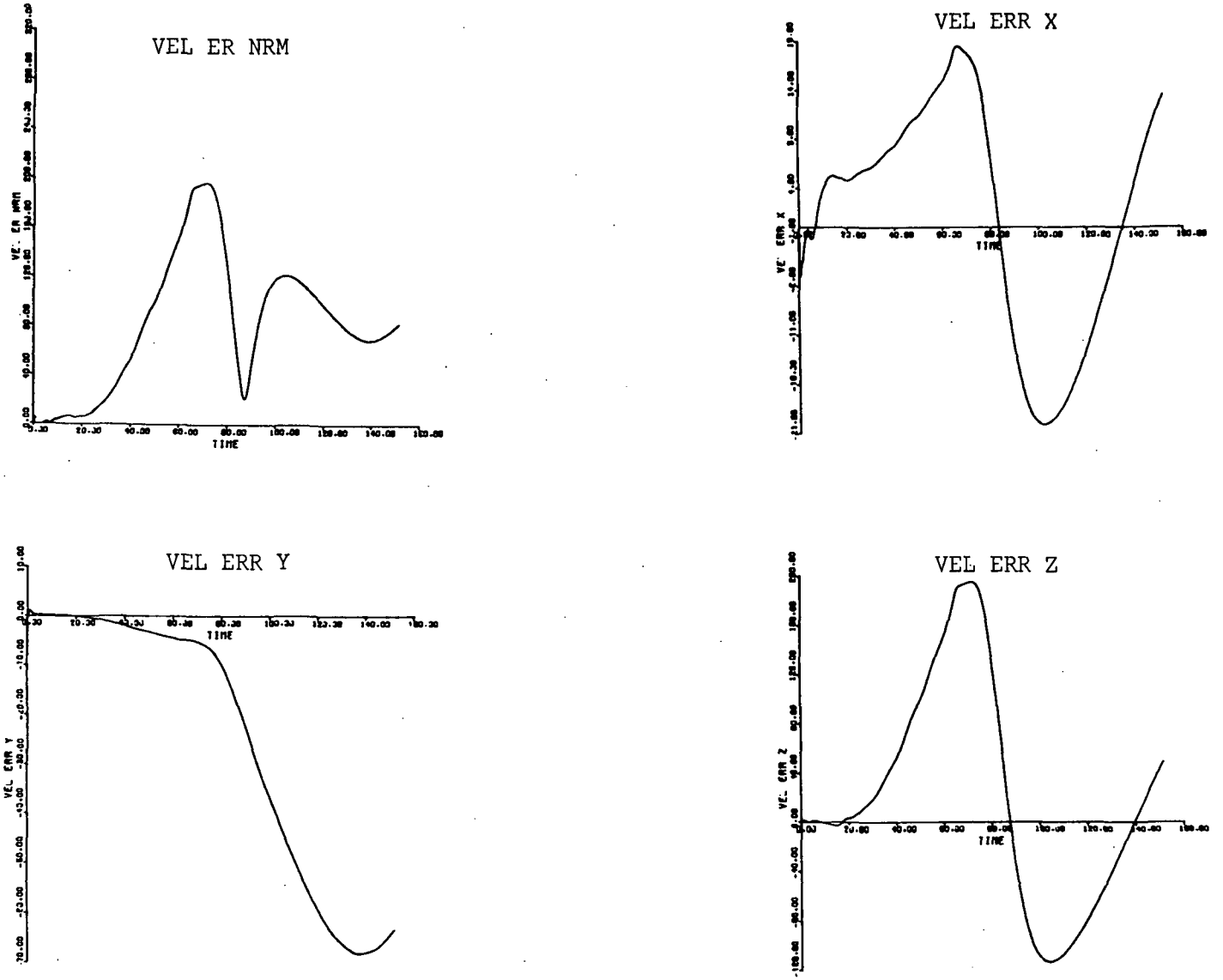

Figure 3a.2 Velocity Error (m/s) vs. Time (days) for Standard O. D. (1σ Errors)

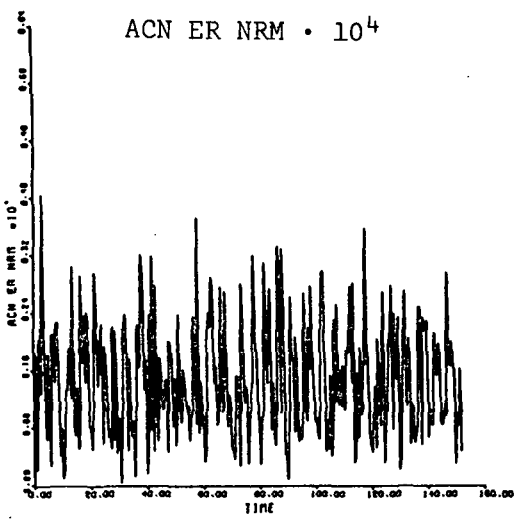

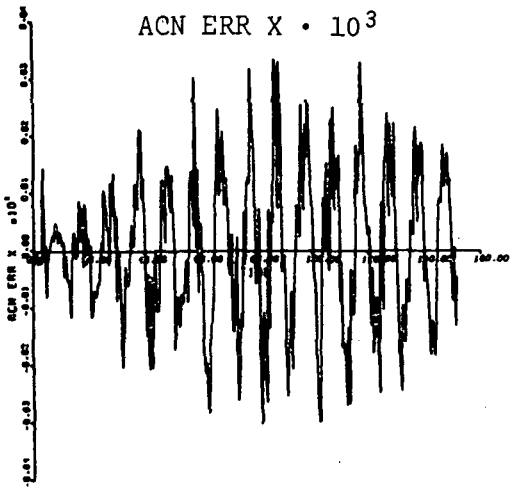

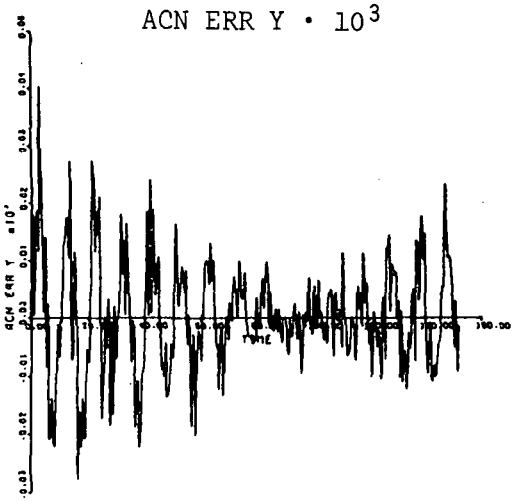

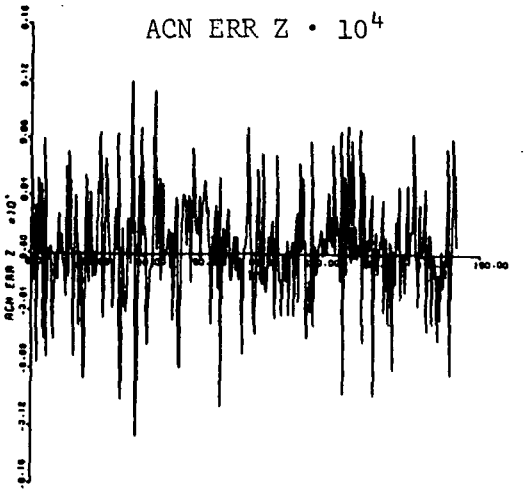

Figure 3a.3 Acceleration Error (m/s^2) vs. Time (days) for Standard O. D. (1σ Errors)

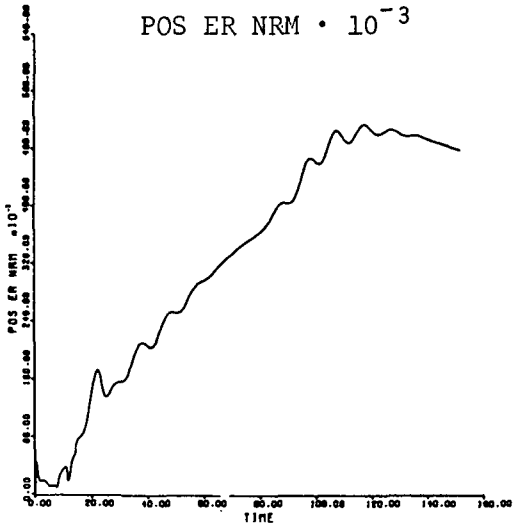

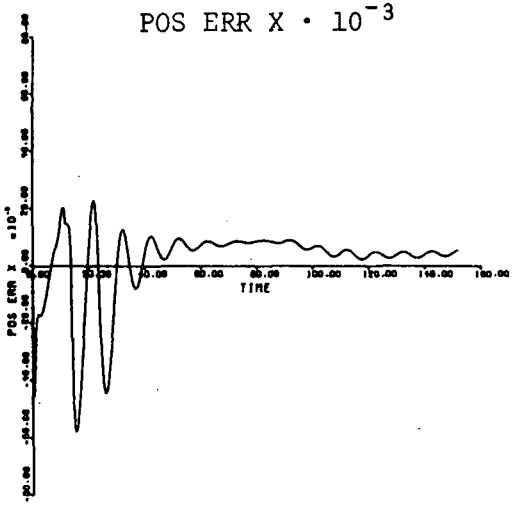

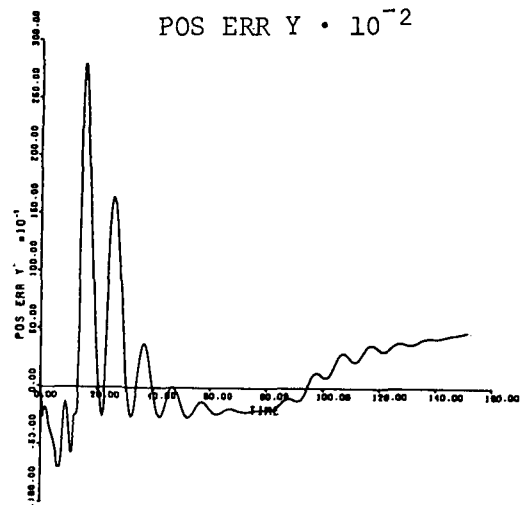

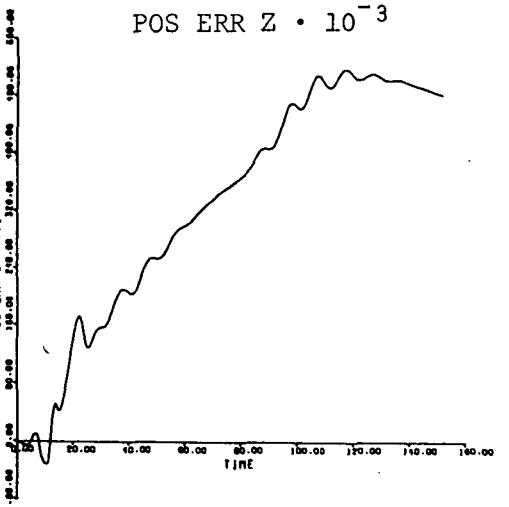

Figure 3b.1 Position Error (km) vs. Time (days) for Standard O. D. (1/3σ Errors)

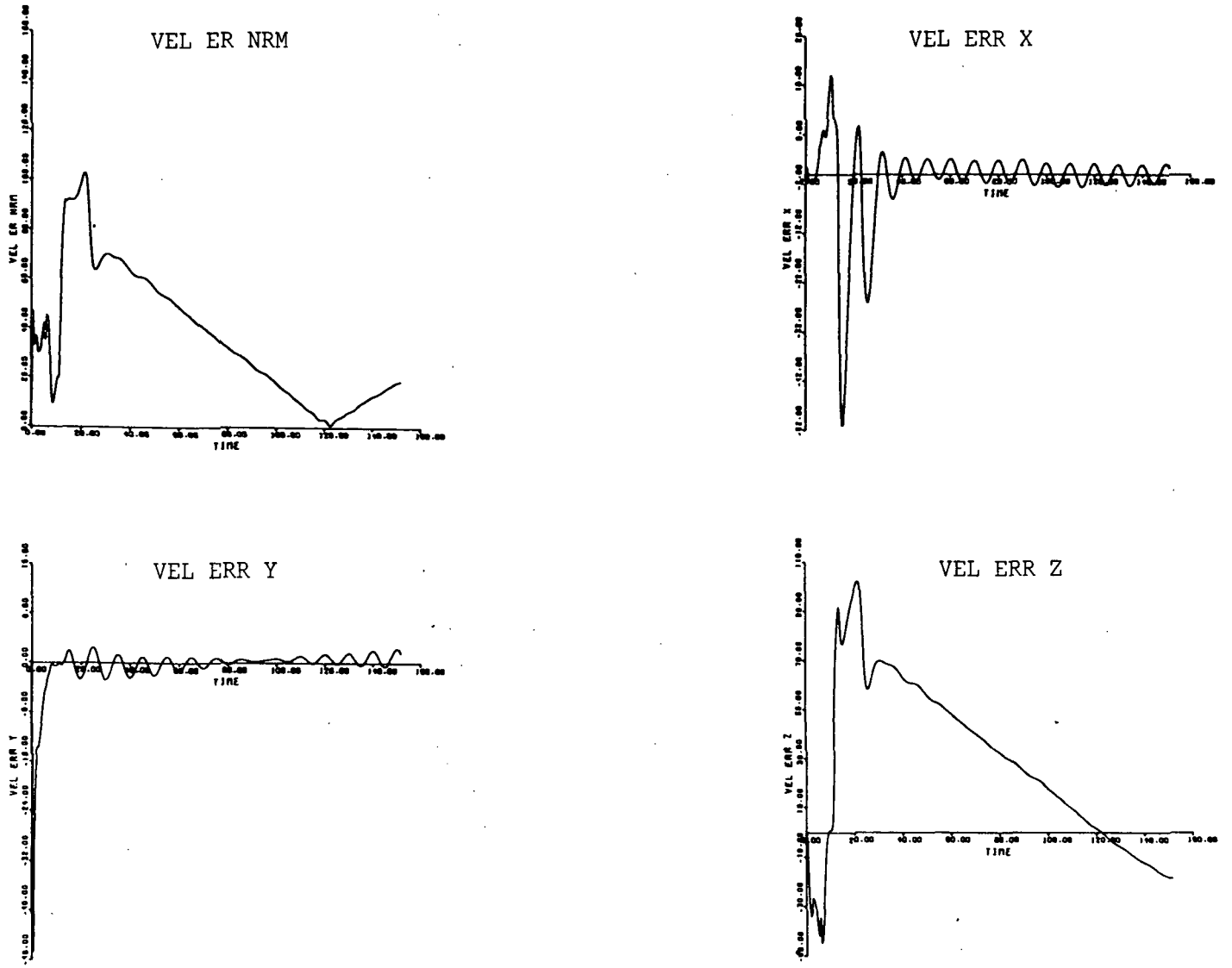

Figure 3b.2 Velocity Error (m/s) vs. Time (days) for Standard O. D. (1/3σ Errors)

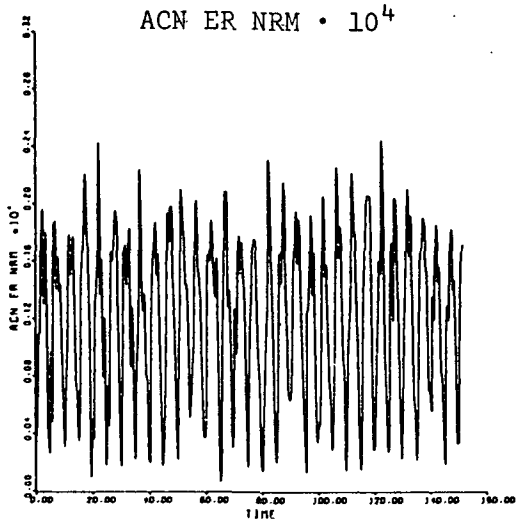

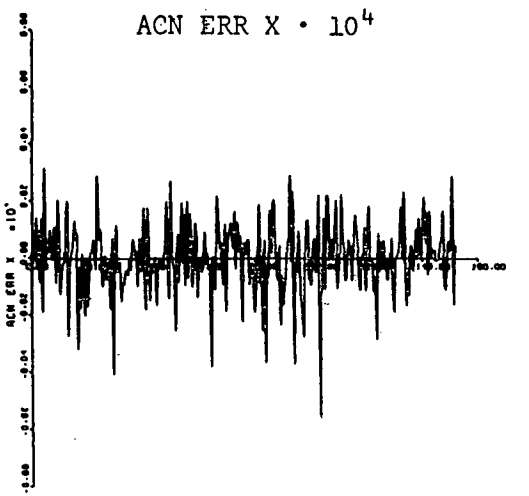

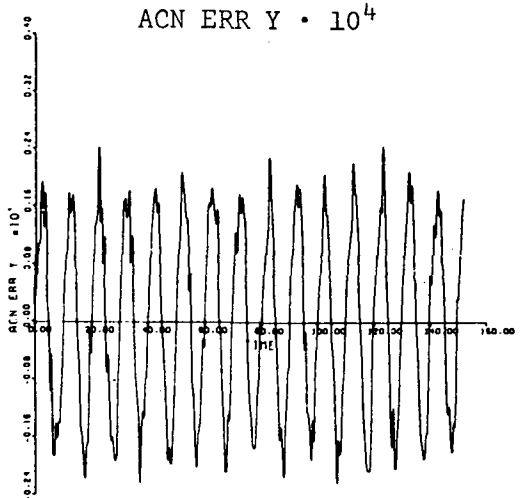

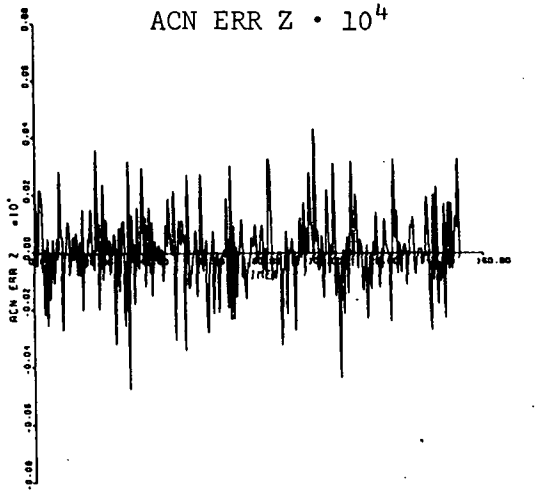

Figure 3b.3 Acceleration Error (m/s^2) vs. Time (days) for Standard O. D. (1/3σ Errors)

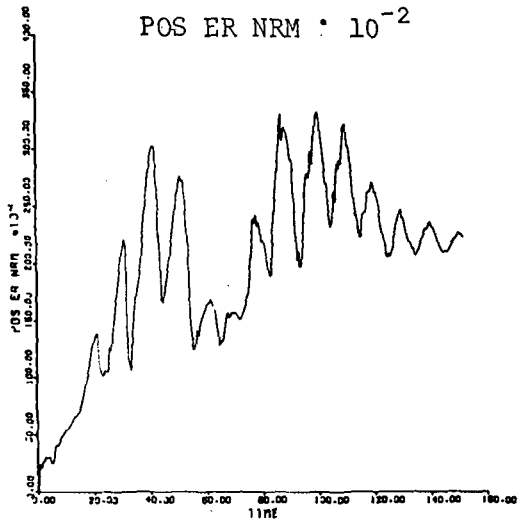

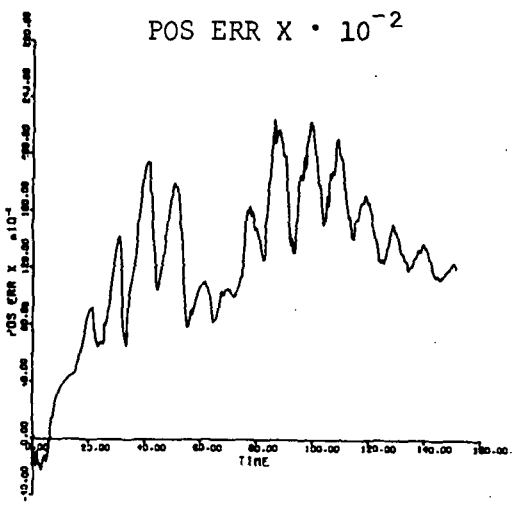

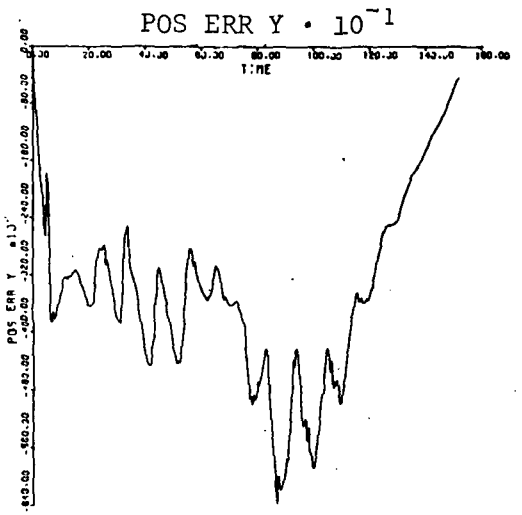

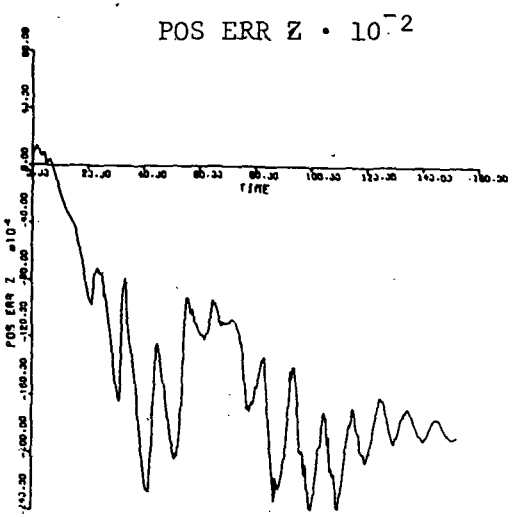

Figure 3c.1 Position Error (km) vs. Time (days) for Standard O. D. with Q-matrix Compensation (1σ Errors)

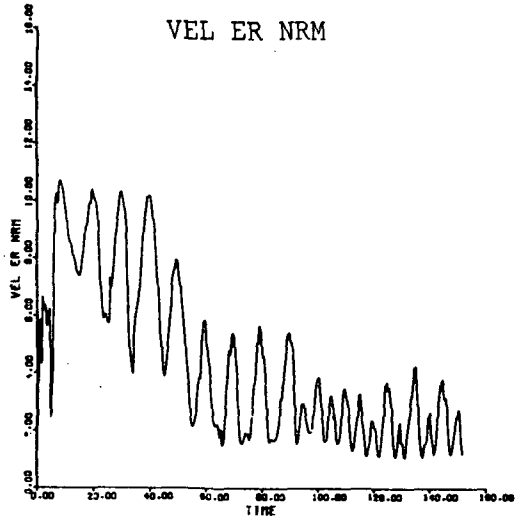

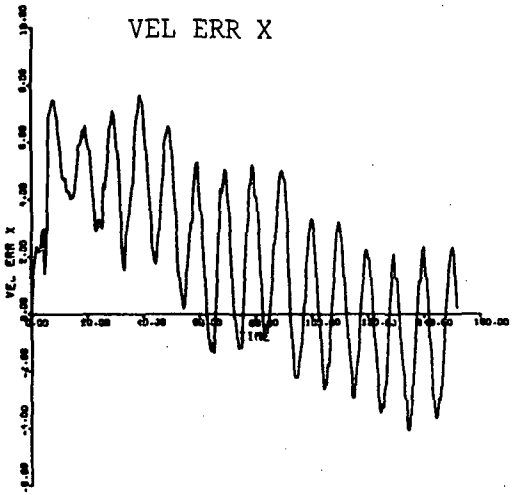

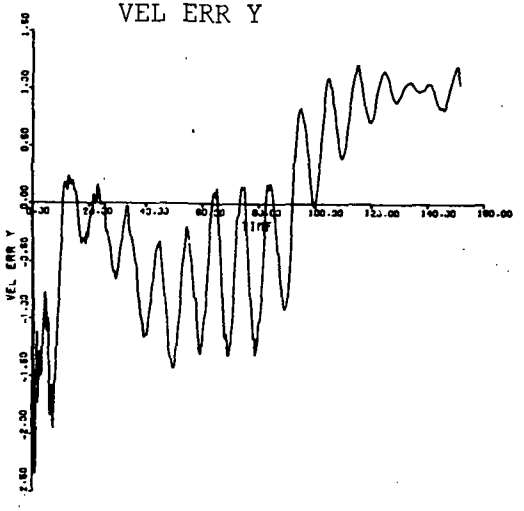

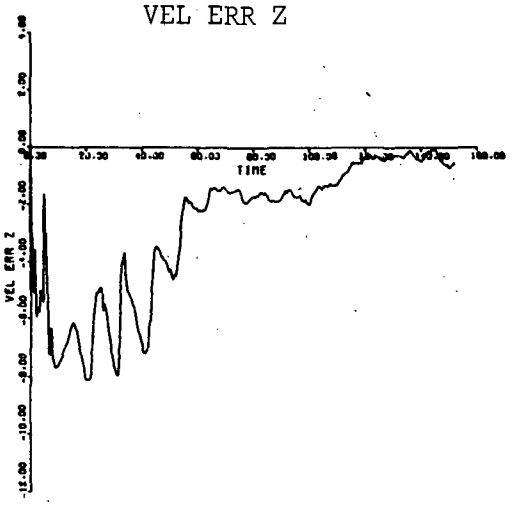

Figure 3c.2 Velocity Error (m/s) vs. Time (days) for Standard O. D. with Q-matrix Compensation (1σ Errors)

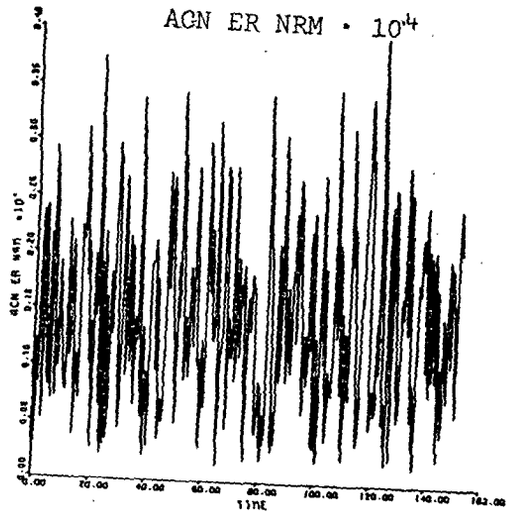

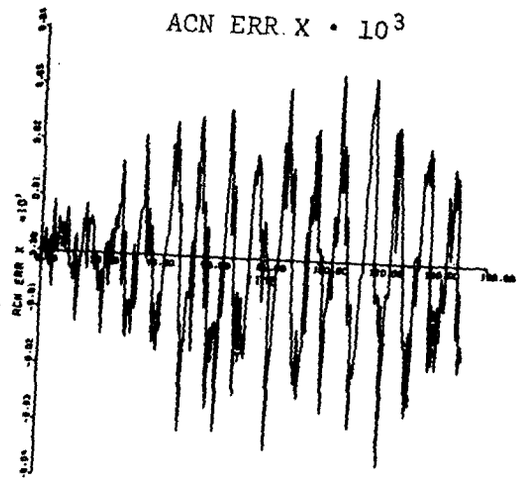

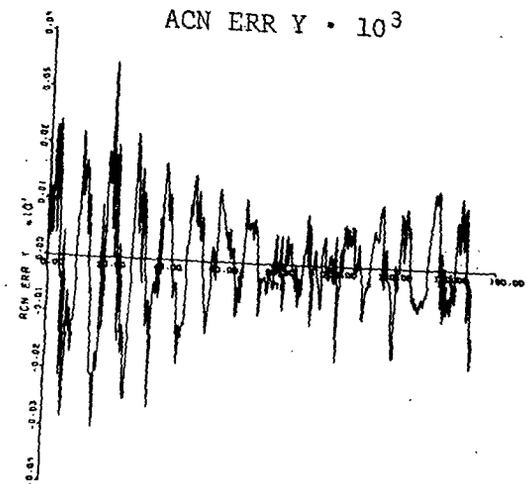

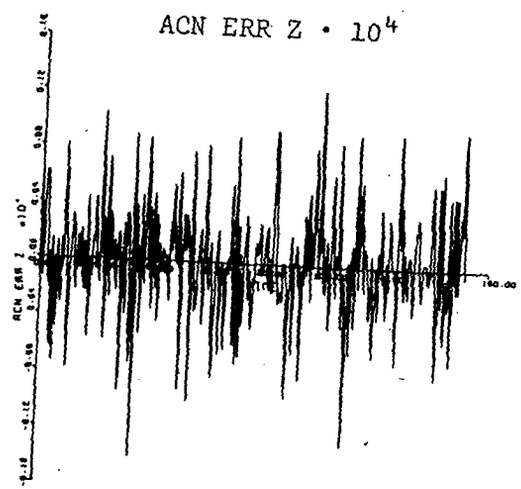

Figure 3c.3 Acceleration Error (m/s^2) vs. Time (days) for Standard O. D. with Q-matrix Compensation (1σ Errors)

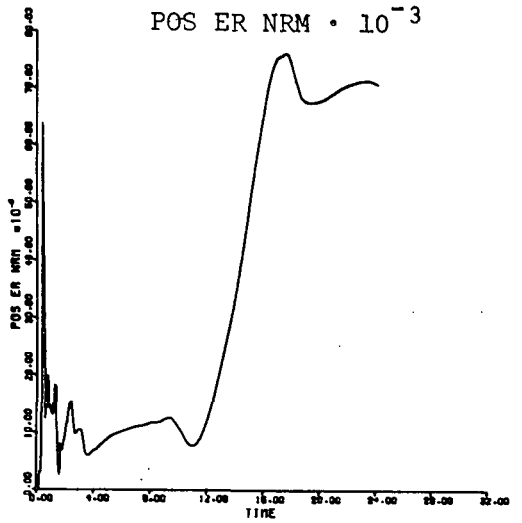

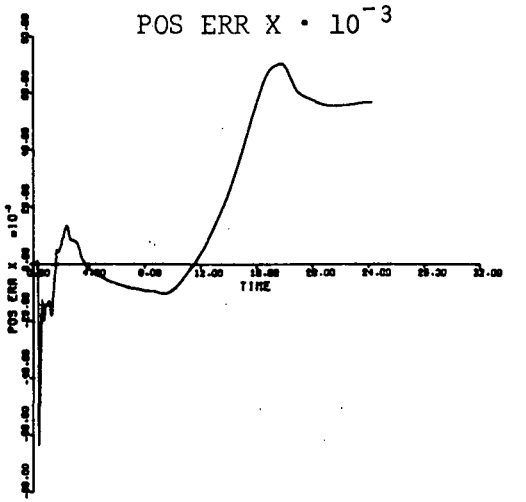

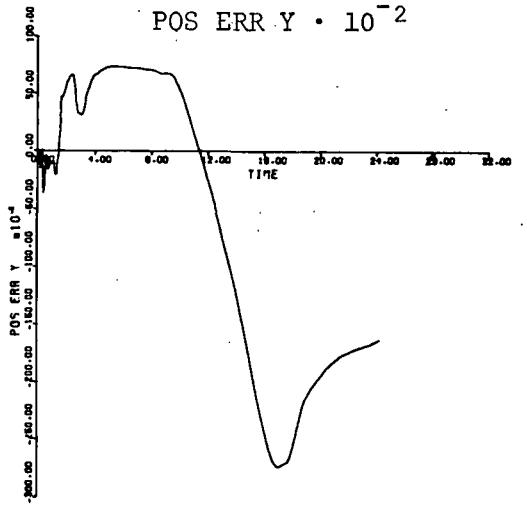

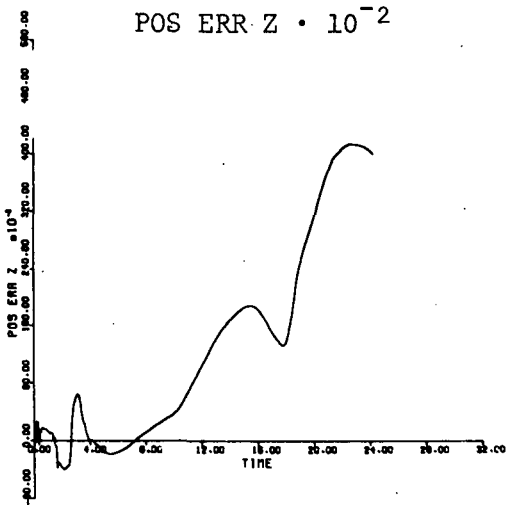

Figure 4a.1 Position Error (km) vs. Time (days) for IMU Errors ($\sigma_{pl} = 1°$, $k_3 = .133a_o$, $\sigma_{ax} = .0133a_o$)

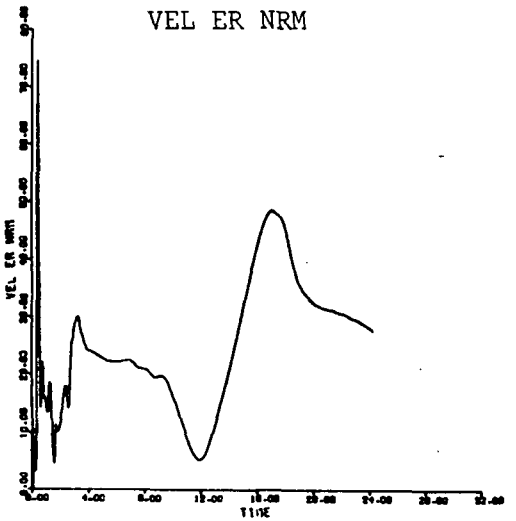

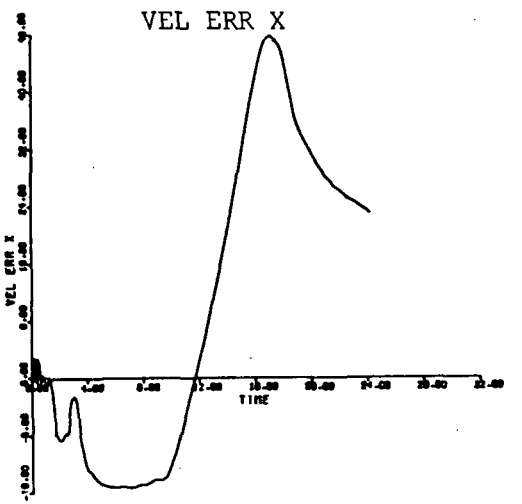

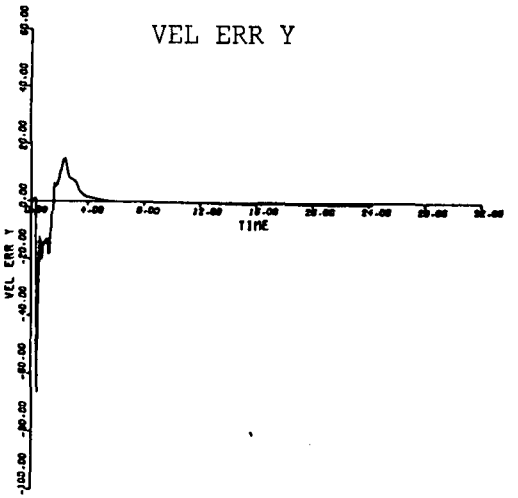

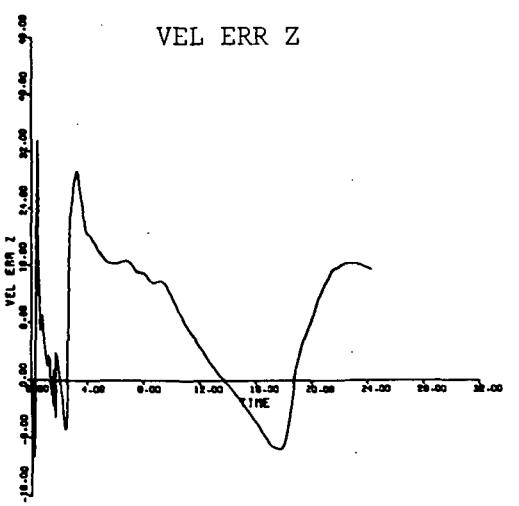

Figure 4a.2 Velocity Error (m/s) vs. Time (days) for IMU Errors ($\sigma_{pl} = 1^{o}$, $k_3 = .133a_o$, $\sigma_{ax} = .0133a_o$)

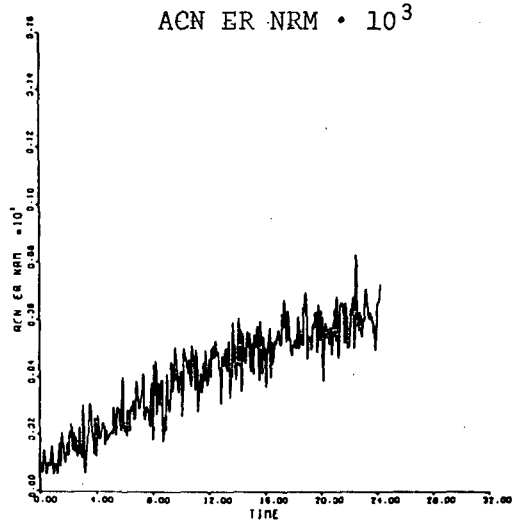

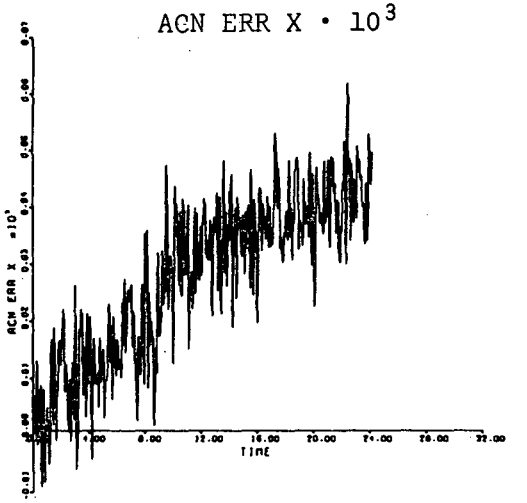

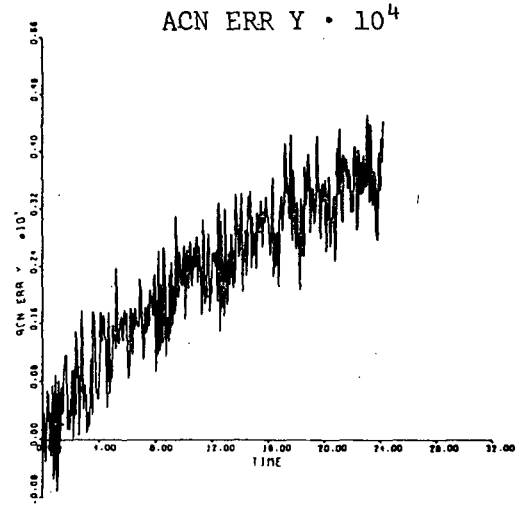

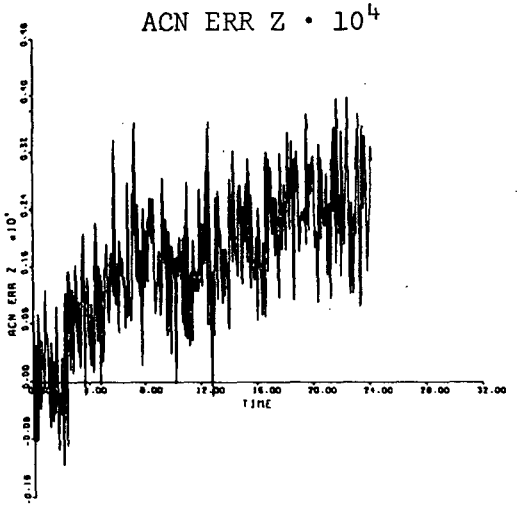

Figure 4a.3 Acceleration Error (m/s^2) vs. Time (days) for IMU Errors ($\sigma_{pl} = 1°$, $k_3 = .133a_o$, $\sigma_{ax} = .0133a_o$)

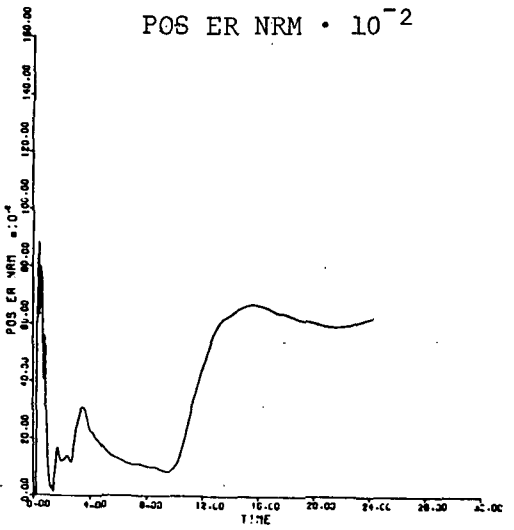

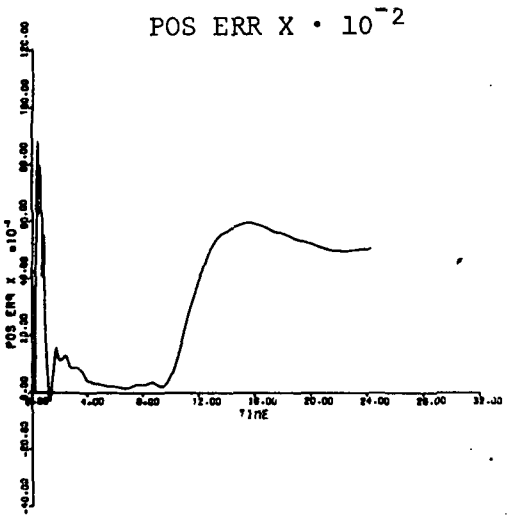

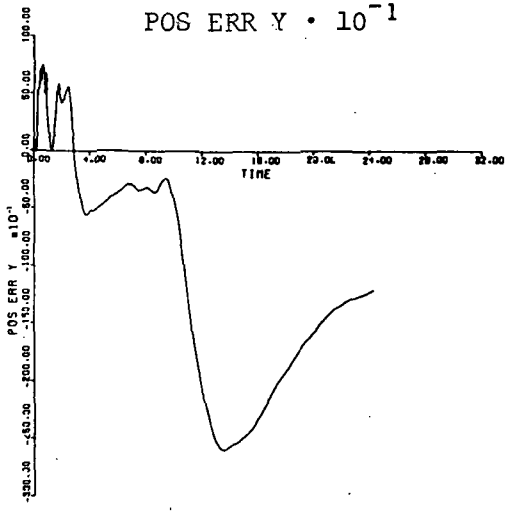

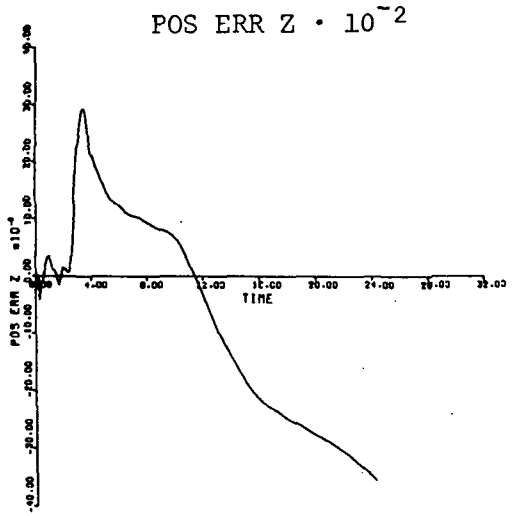

Figure 4b.1 Position Error (km) vs. Time (days) for IMU Errors ($\sigma_{pl} = .1^{o}$, $k_3 = .1a_o$, $\sigma_{ax} = .01a_o$)

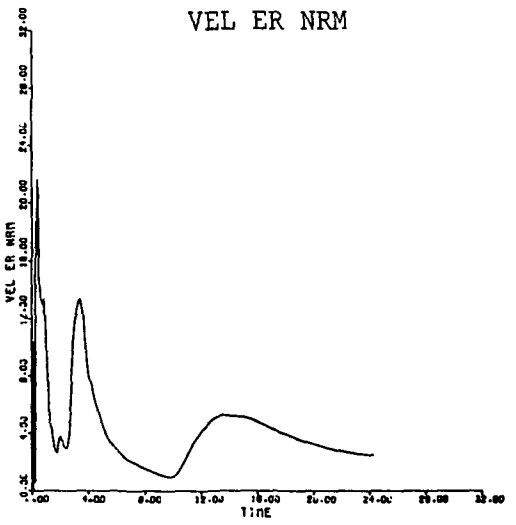

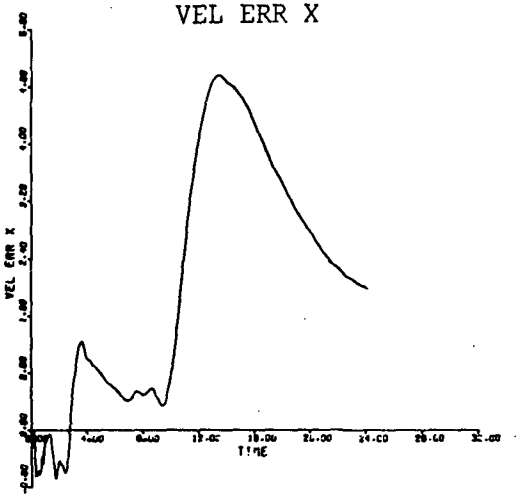

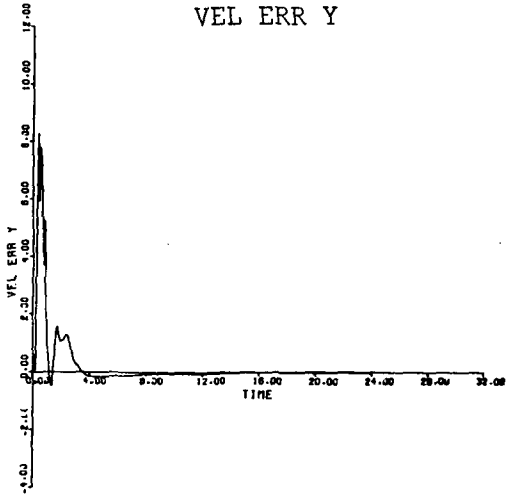

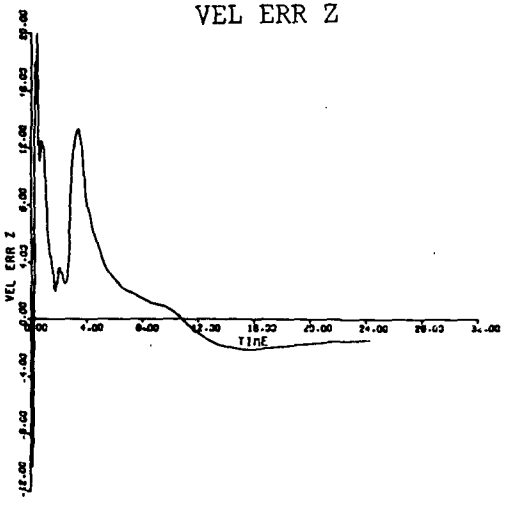

Figure 4b.2 Velocity Error (m/s) vs. Time (days) for IMU Errors ($\sigma_{pl} = .1°$, $k_3 = .1a_o$, $\sigma_{ax} = .01a_o$)

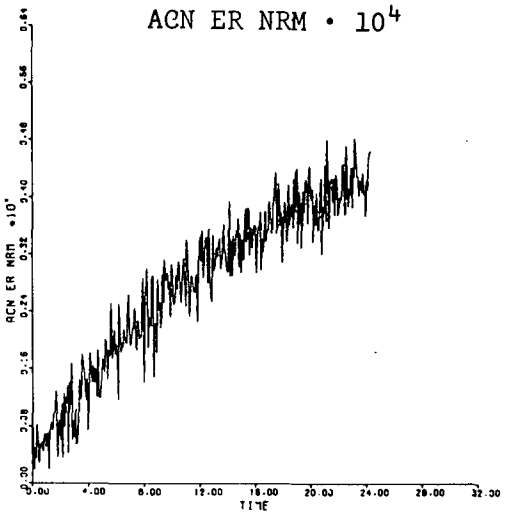

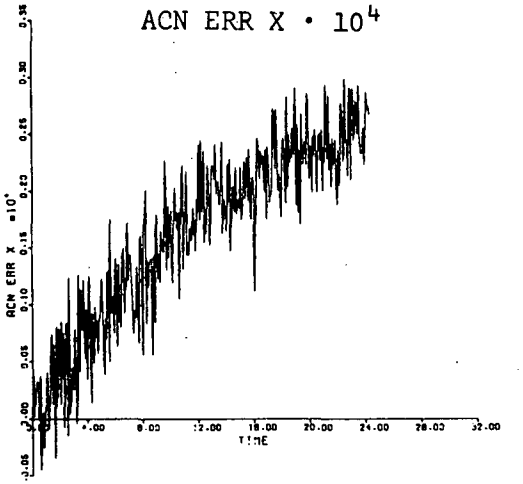

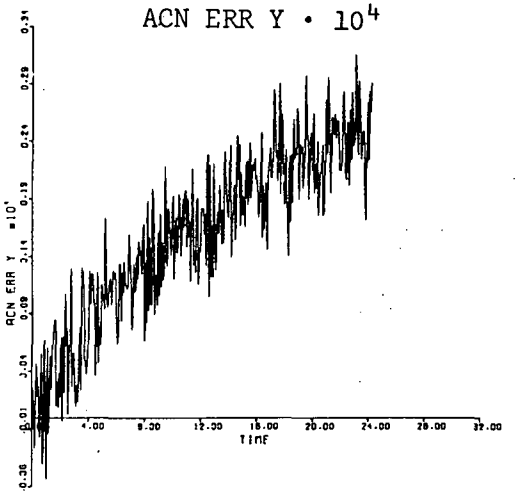

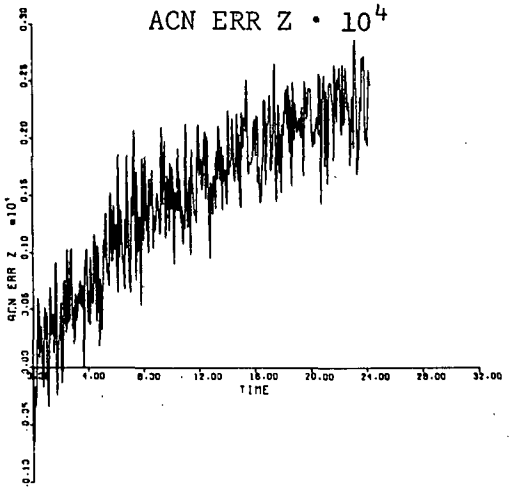

Figure 4b.3 Acceleration Error (m/s^2) vs. Time (days) for IMU Errors ($\sigma_{pl} = .1^o$, $k_3 = .1a_o$, $\sigma_{ax} = .01a_o$)

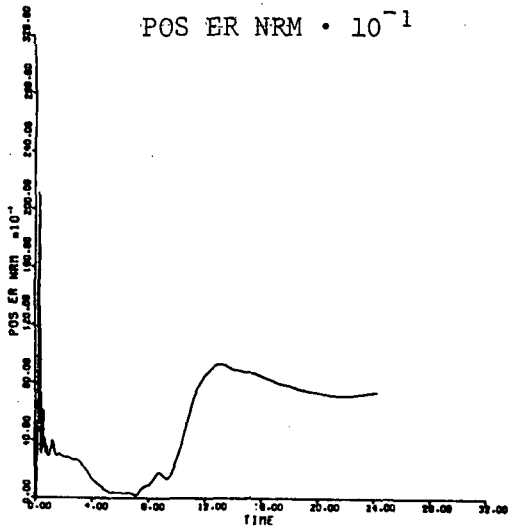

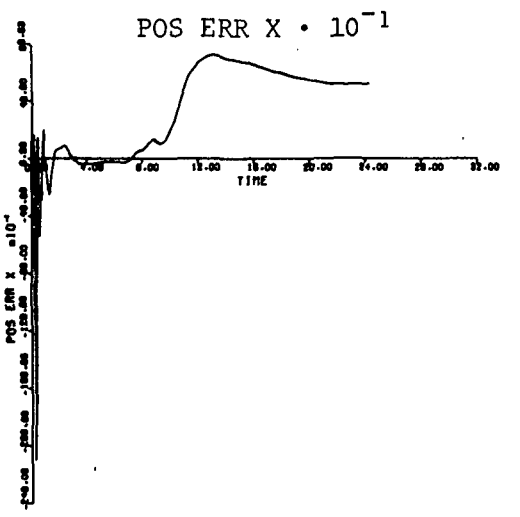

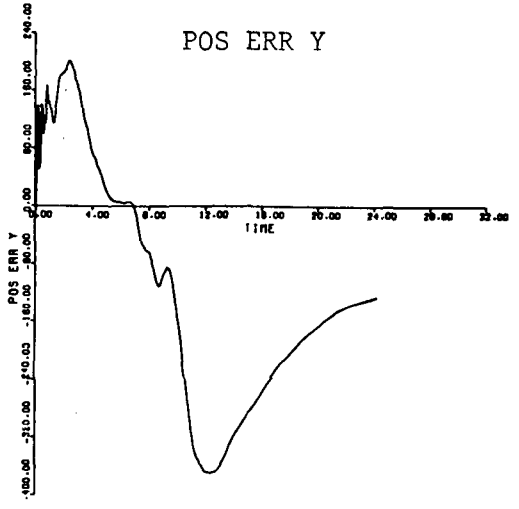

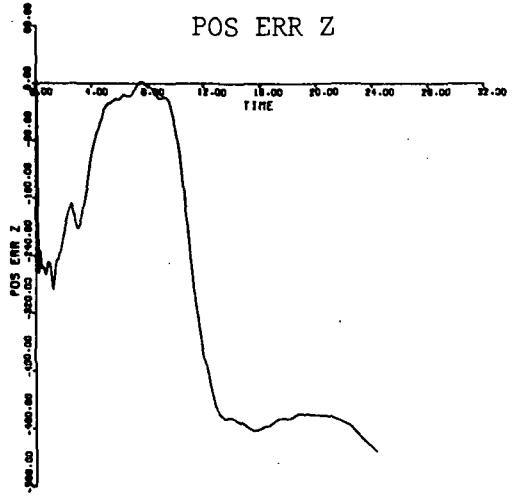

Figure 4c.1 Position Error (km) vs. Time (days) for IMU Errors ($\sigma_{pl} = .01°$, $k_3 = .0667a_o$, $\sigma_{ax} = .00667a_o$)

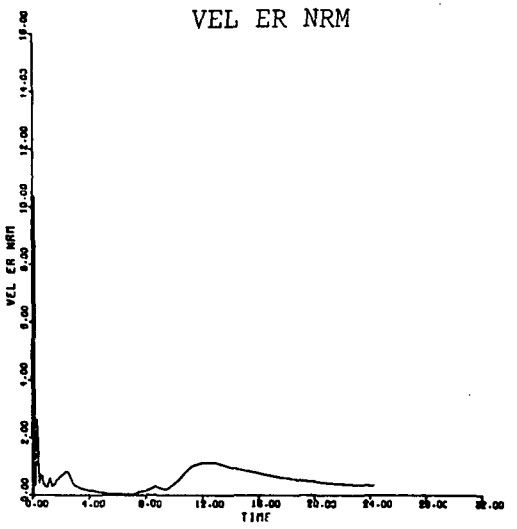

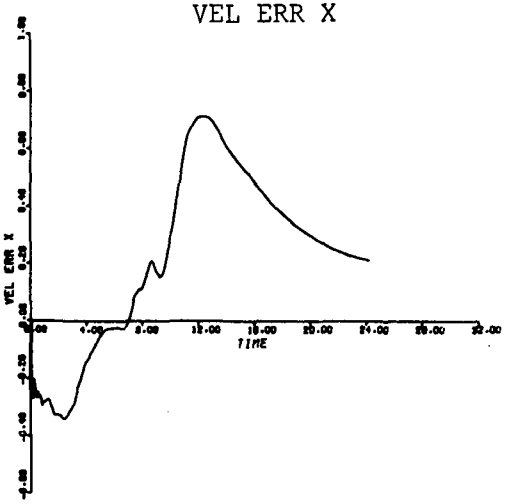

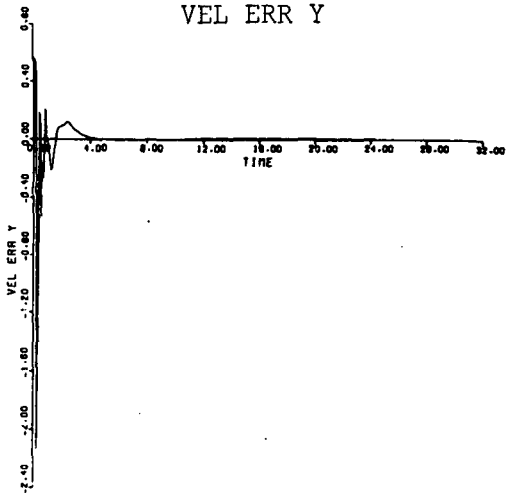

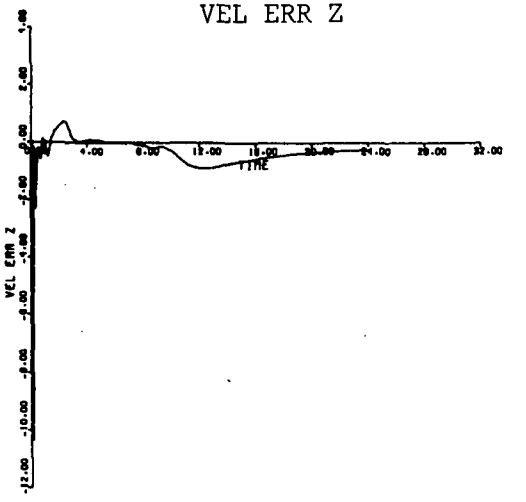

Figure 4c.2 Velocity Error (m/s) vs. Time (days) for IMU Errors ($\sigma_{pl} = .01°$, $k_3 = .0667a_o$, $\sigma_{ax} = .00667a_o$)

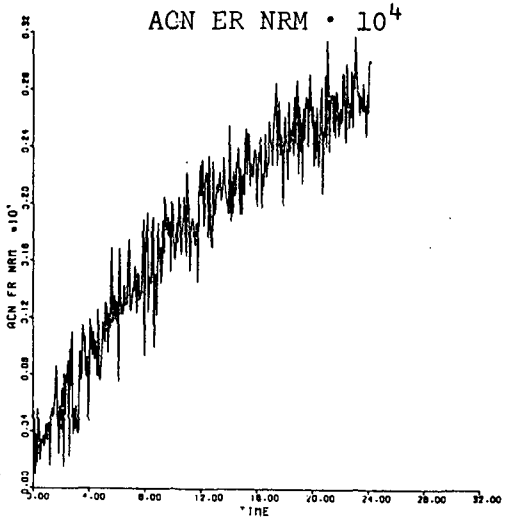

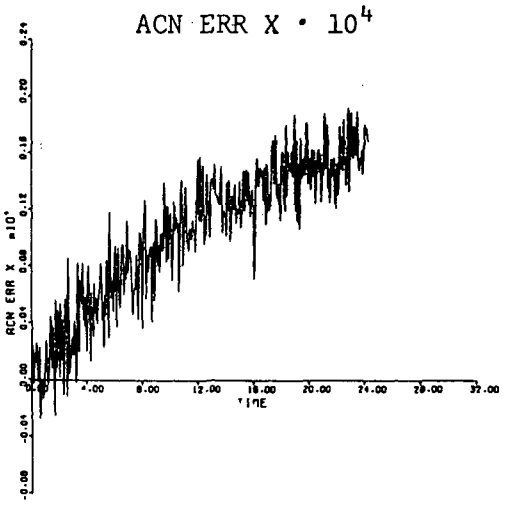

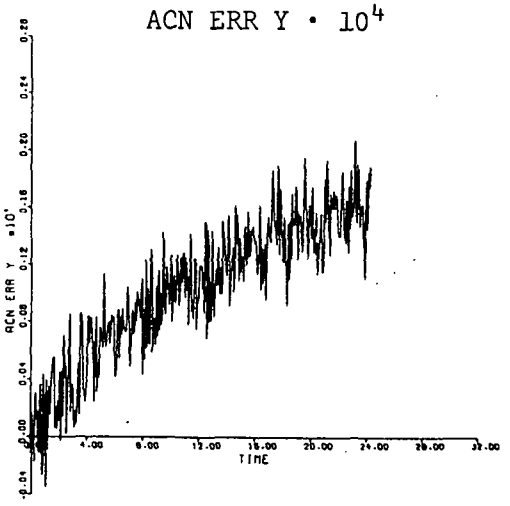

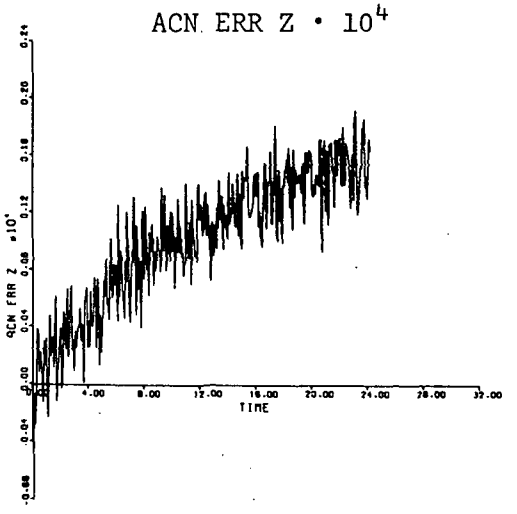

Figure 4c.3 Acceleration Error (m/s^2) vs. Time (days) for IMU Errors ($\sigma_{pl} = .01°$, $k_3 = .0667a_o$, $\sigma_{ax} = .00667a_o$)

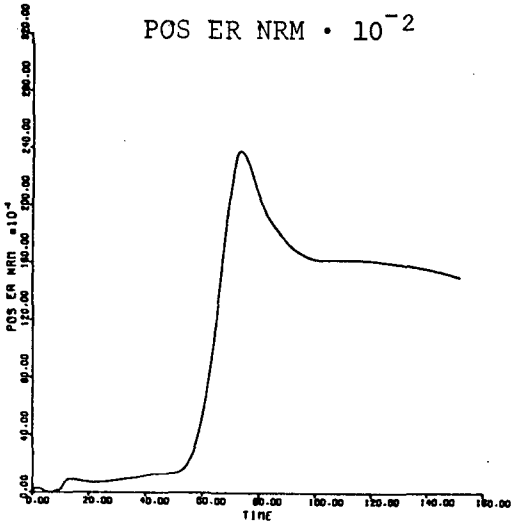

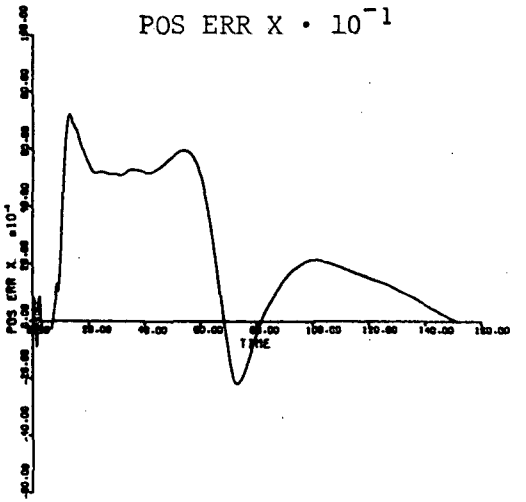

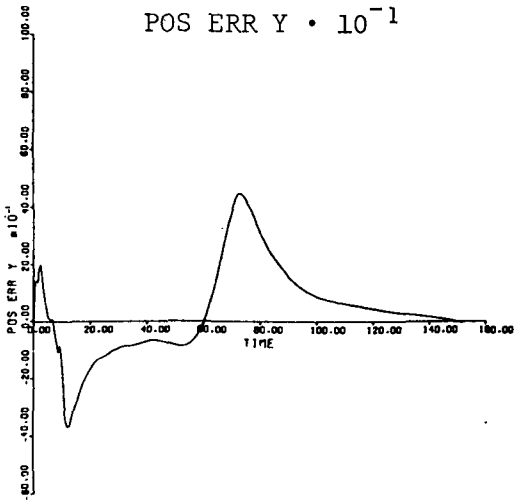

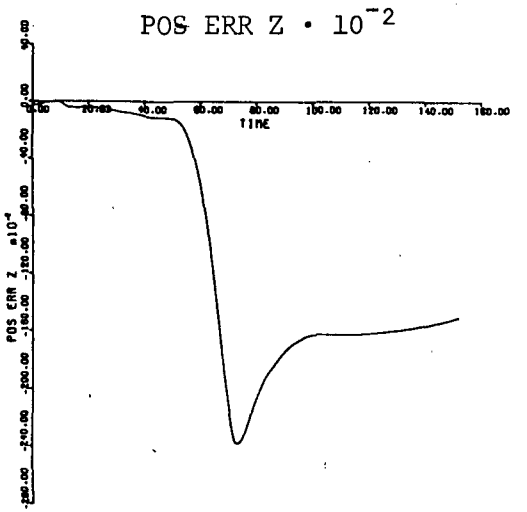

Figure 4c.4 Position Error (km) vs. Time (days) for IMU Errors ($\sigma_{pl} = .01°$, $k_3 = .0667a_o$, $\sigma_{ax} = .00667a_o$)

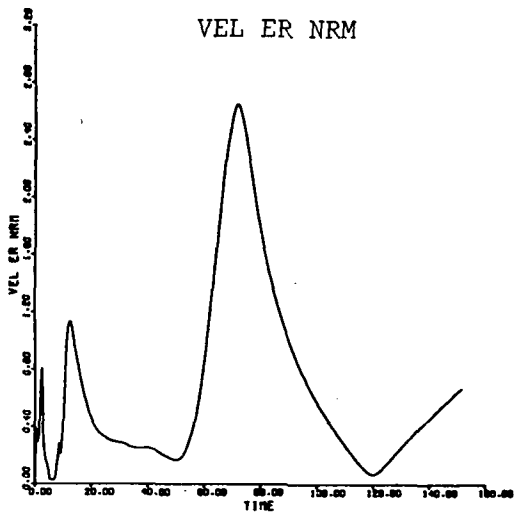

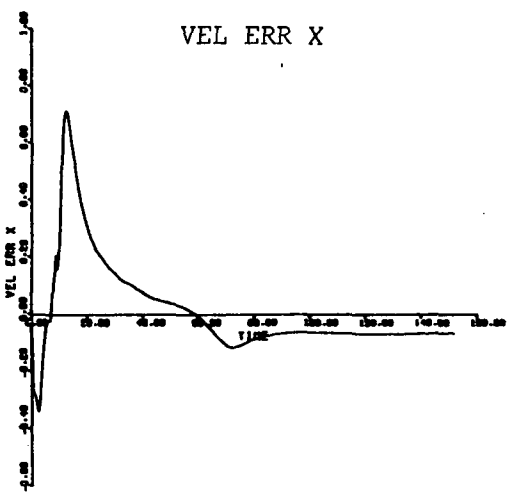

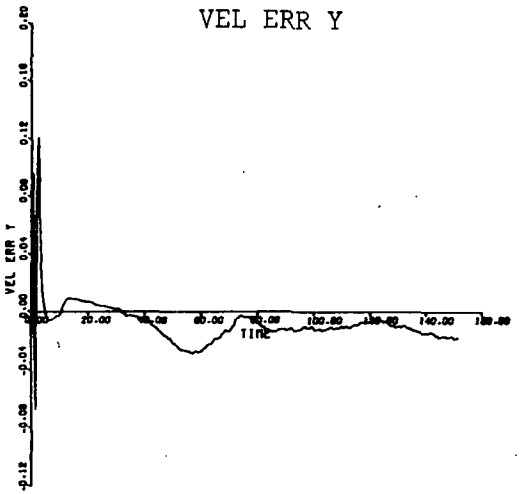

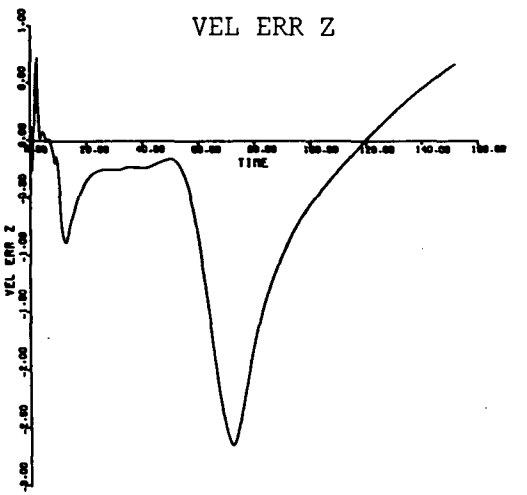

Figure 4c.5 Velocity Error (m/s) vs. Time (days) for IMU Errors ($\sigma_{pl} = .01°$, $k_3 = .0667a_o$, $\sigma_{ax} = .00667a_o$)

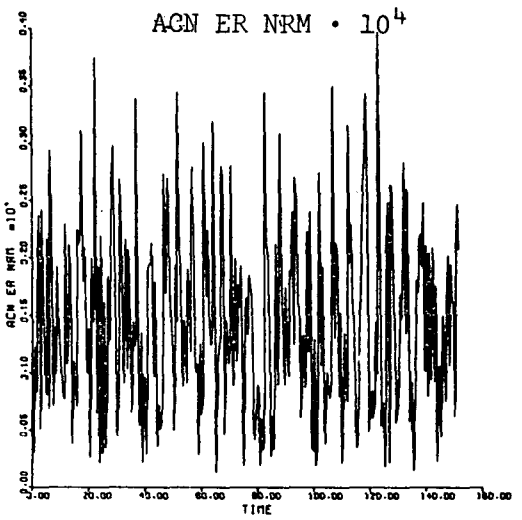

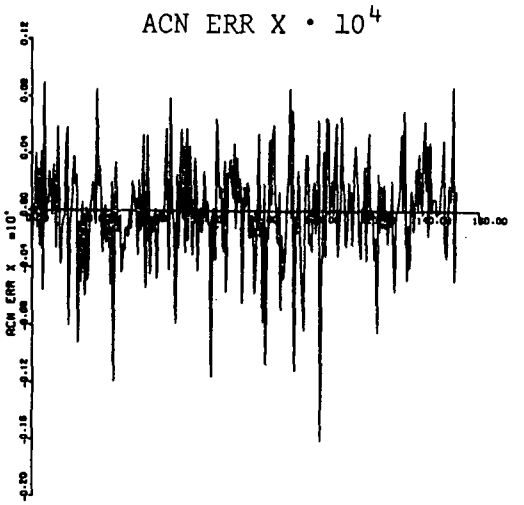

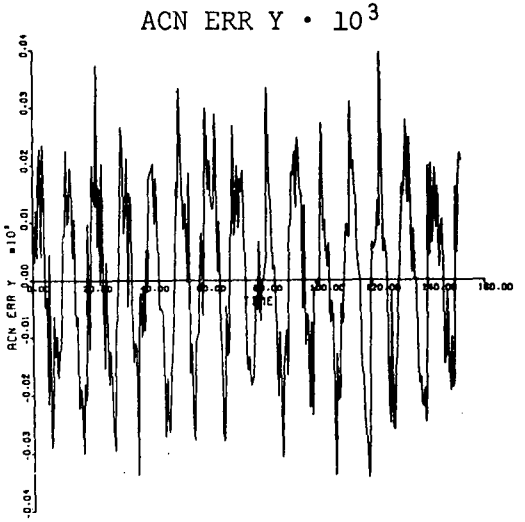

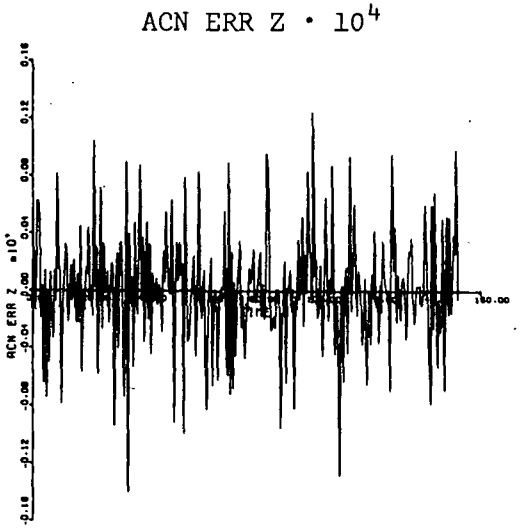

Figure 4c.6 Acceleration Error (m/s^2) vs. Time (days) for IMU Errors ($\sigma_{pl} = .01°$, $k_3 = .0667$, $\sigma_{ax} = .00667a_o$)

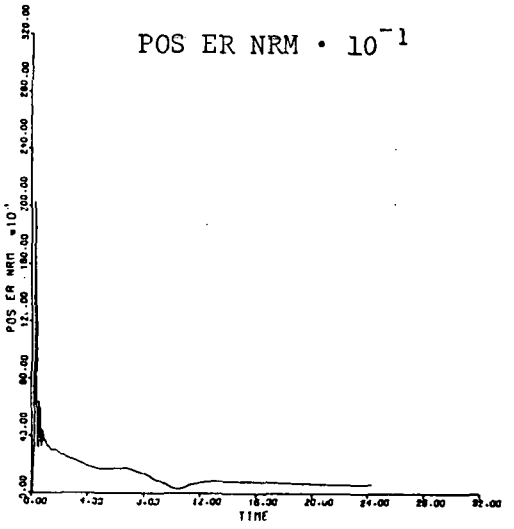

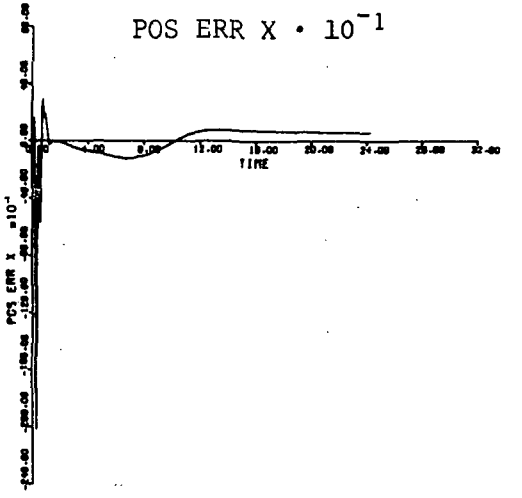

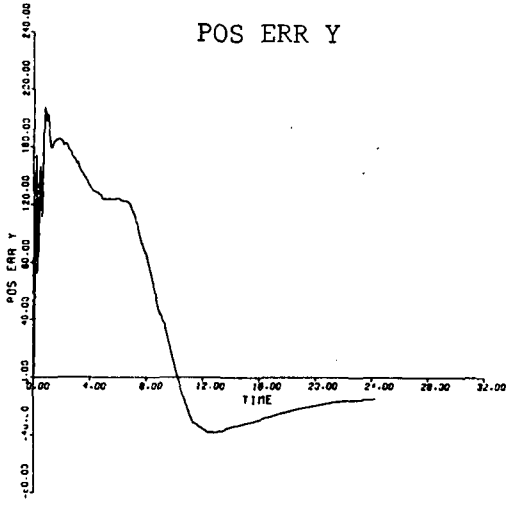

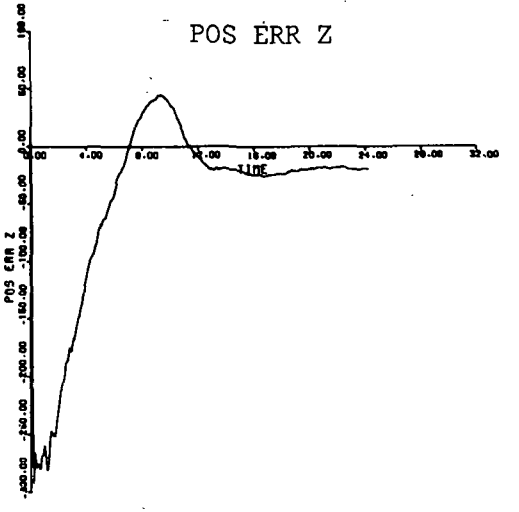

Figure 4d.1 Position Error (km) vs. Time (days) for IMU Errors ($\sigma_{pl} = .001^{o}$, $k_3 = .0333a_o$, $\sigma_{ax} = .00333a_o$)

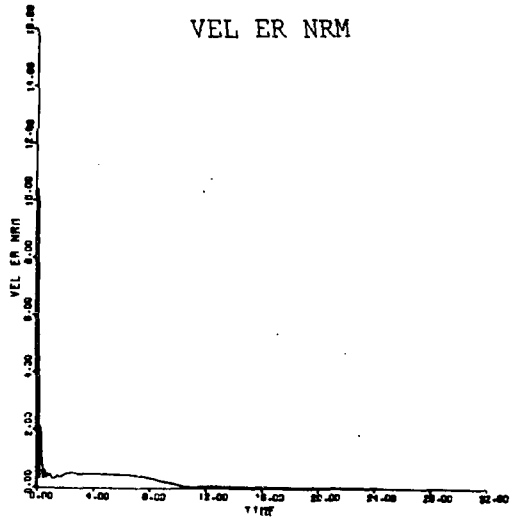

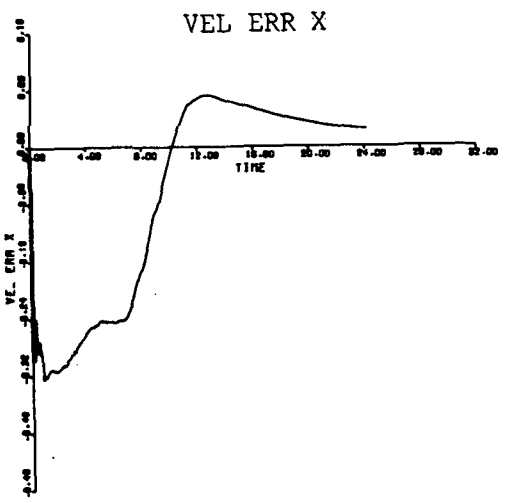

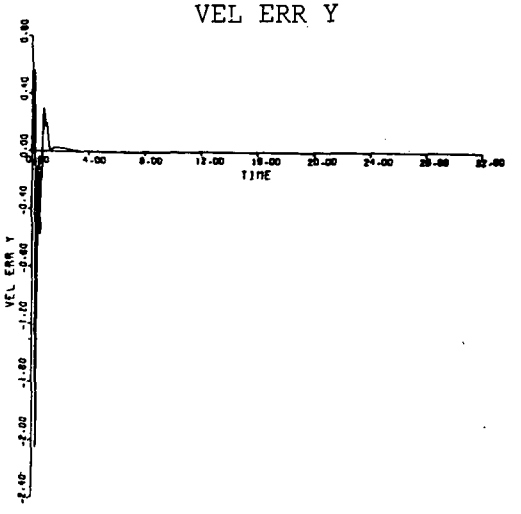

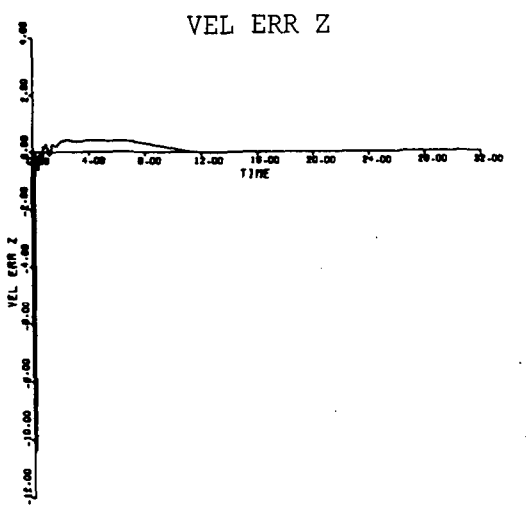

Figure 4d.2 Velocity Error (m/s) vs. Time (days) for IMU Errors ($\sigma_{pl} = .001°$, $k_3 = .0333a_o$, $\sigma_{ax} = .00333a_o$)

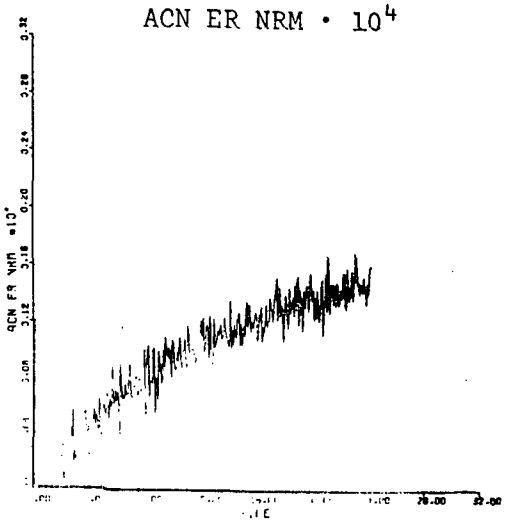

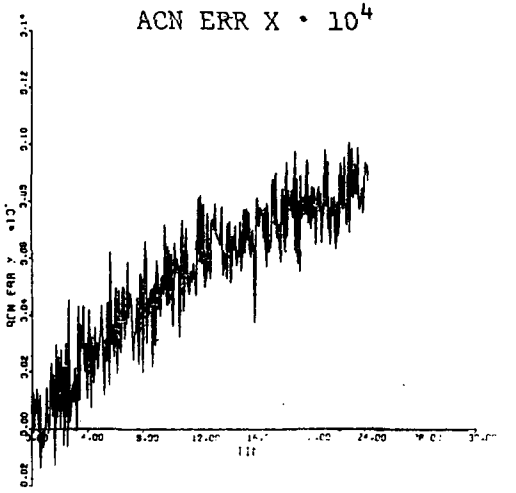

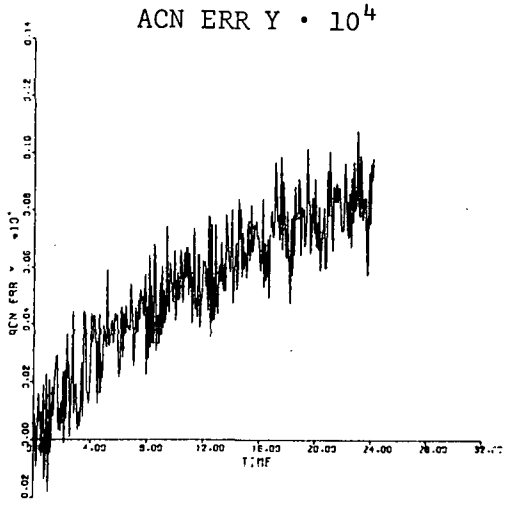

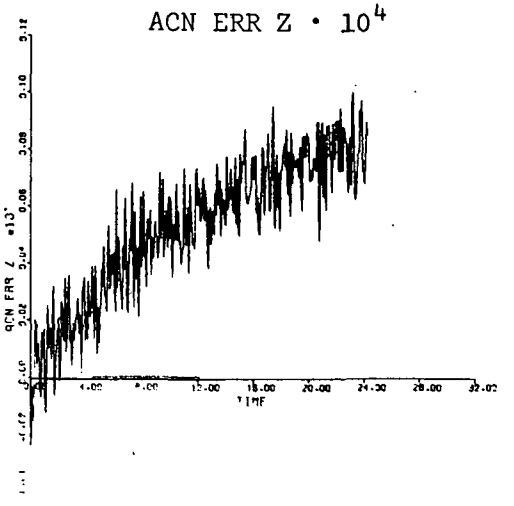

Figure 4d.3 Acceleration Error (m/s^2) vs. Time (days) for IMU Errors ($\sigma_{pl} = .001^o$, $k_3 = .0333a_o$, $\sigma_{ax} = .00333a_o$)

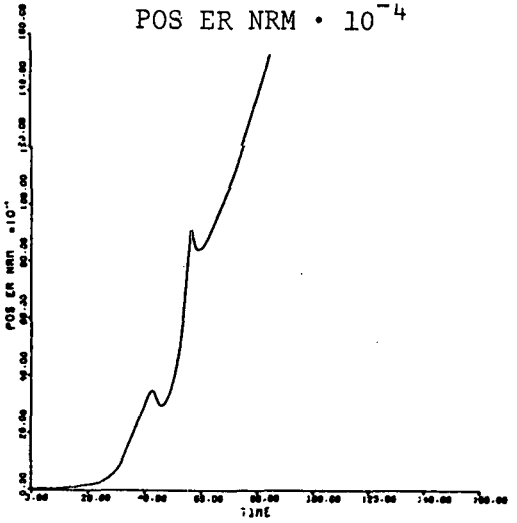

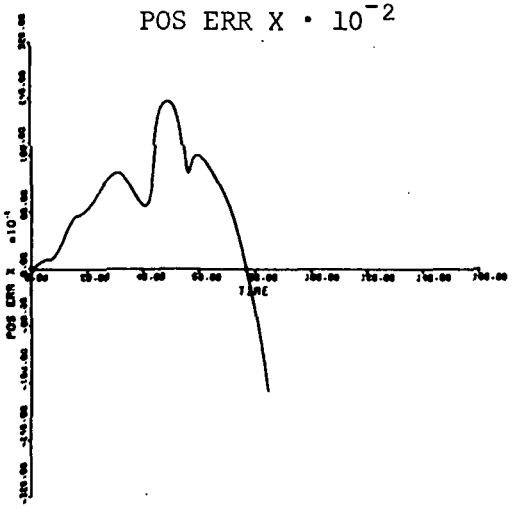

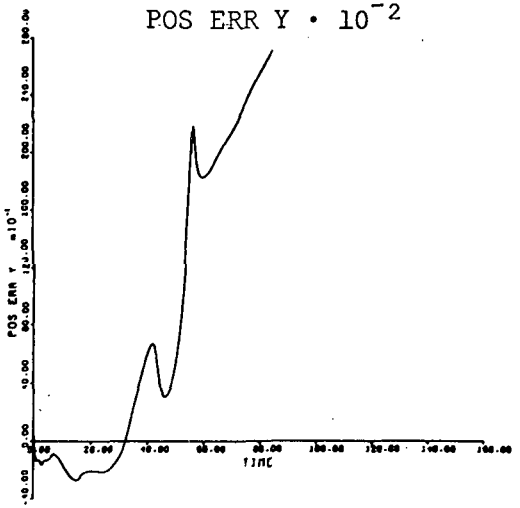

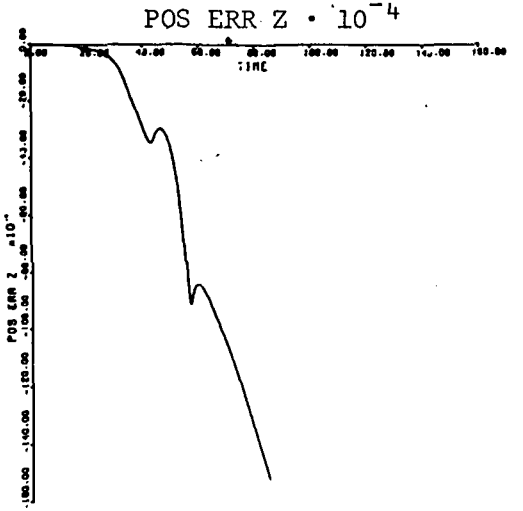

Figure 4e.1 Position Error (km) vs. Time (days) for IMU Errors (σ_{pl} = .001°, $k_3 = .0333a_o$, $\sigma_{ax} = .00333a_o$), No Platform Realignment

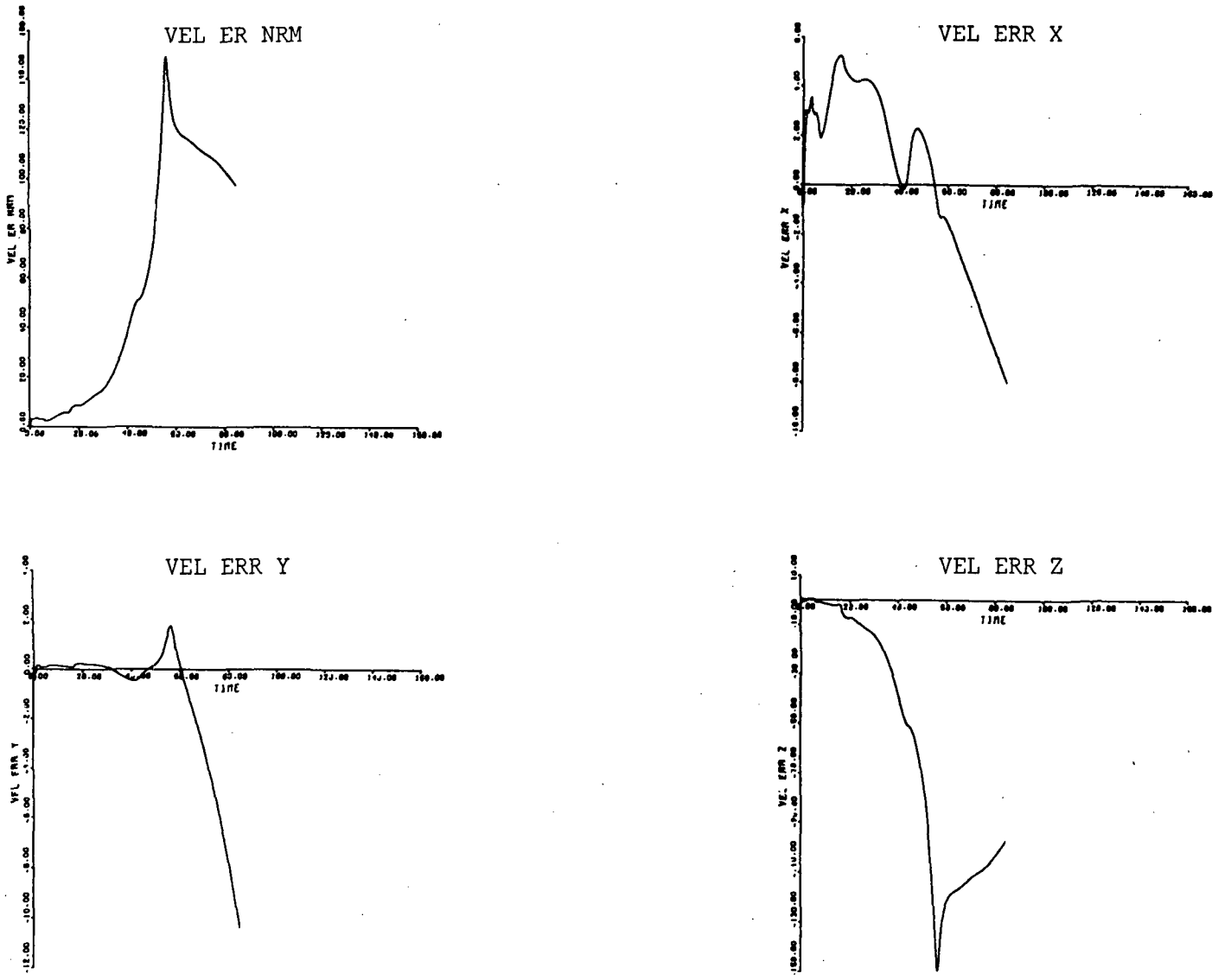

Figure 4e.2 Velocity Error (m/s) vs. Time (days) for IMU Errors ($\sigma_{pl} = .001°$, $k_3 = .0333a_o$, $\sigma_{ax} = .00333a_o$), No Platform Realignment

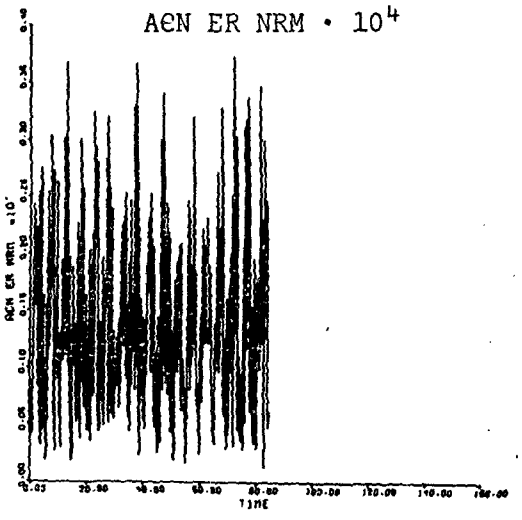

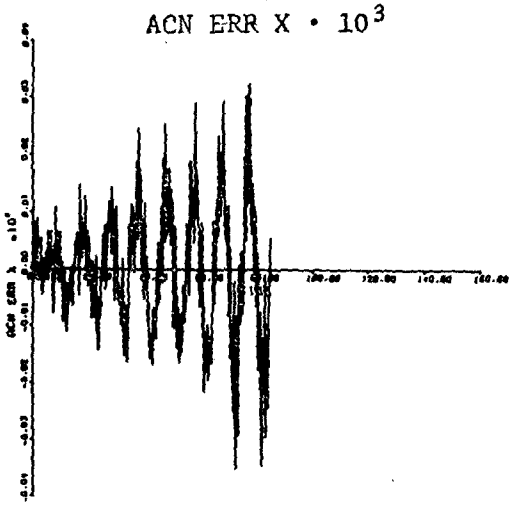

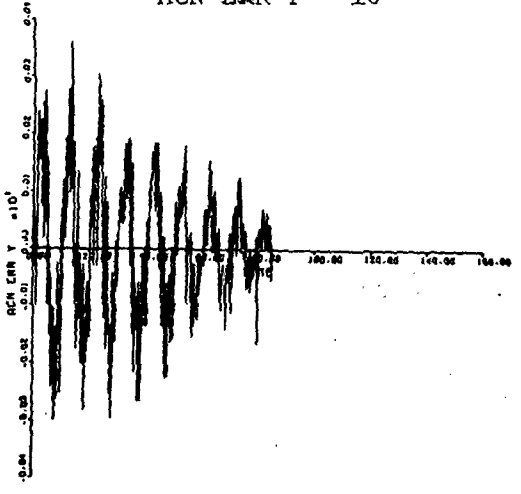

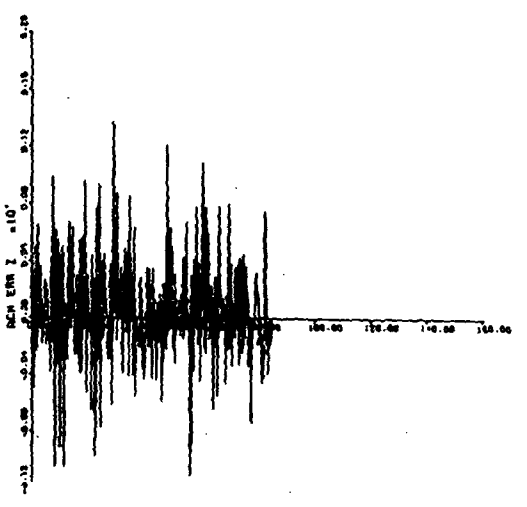

Figure 4e.3 Acceleration Error (m/s^2) vs. Time (days) for IMU Errors ($\sigma_{pl} = .001°$, $k_3 = .0333a_o$, $\sigma_{ax} = .00333a_o$), No Platform Realignment

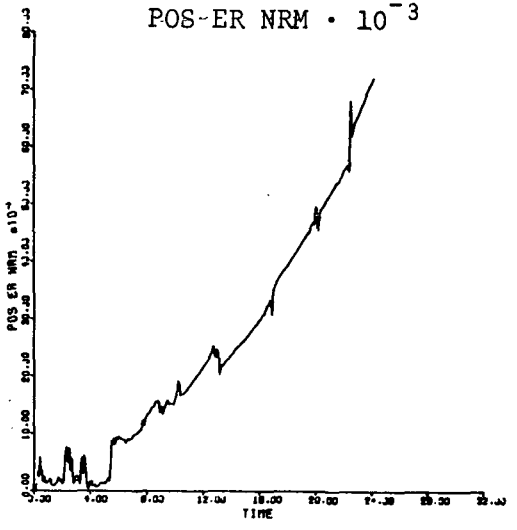

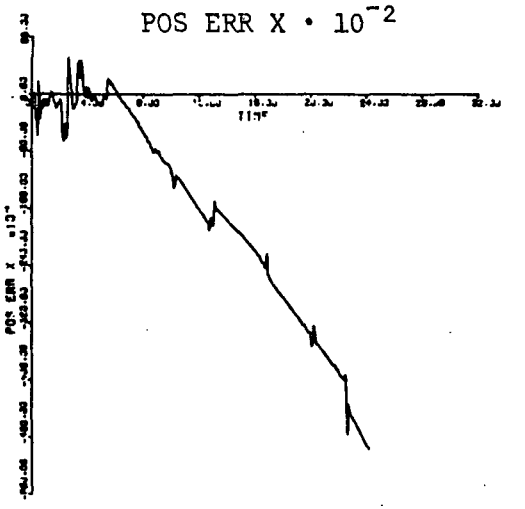

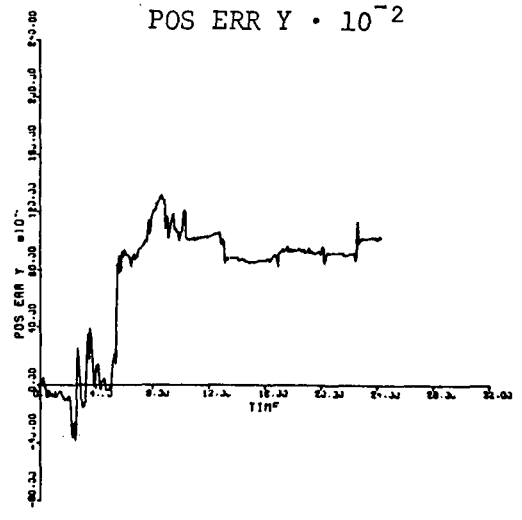

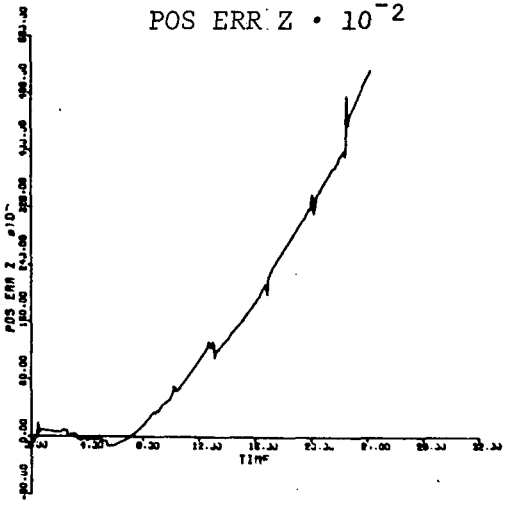

Figure 5a.1 Position Error (km) vs. Time (days) for Model 1 Acceleration Error Compensation

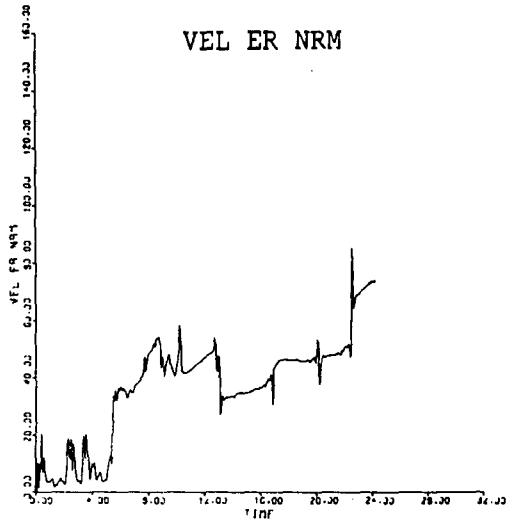

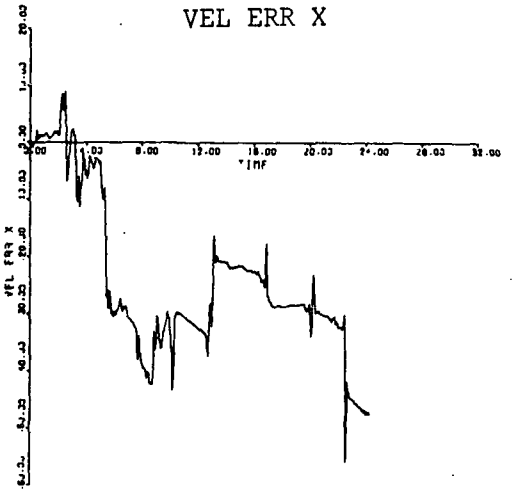

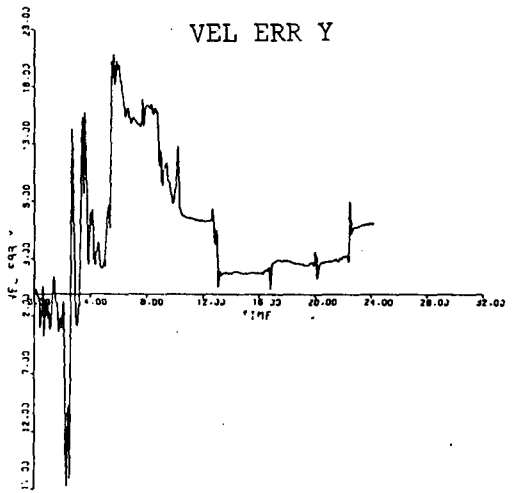

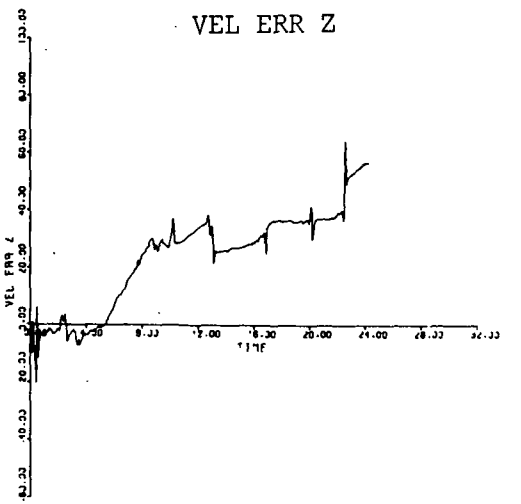

Figure 5a.2 Velocity Error (m/s) vs. Time (days) for Model 1 Acceleration Error Compensation

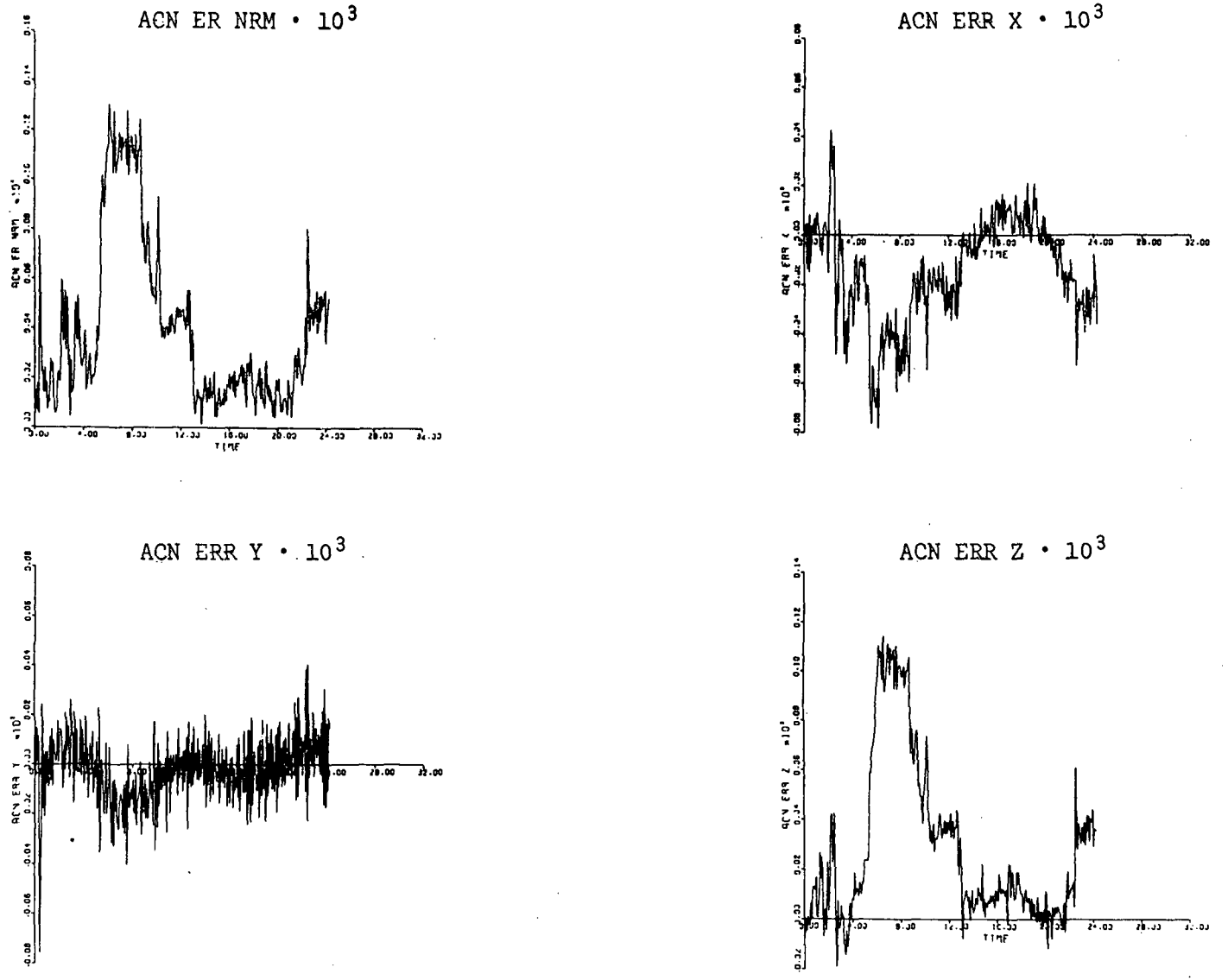

Figure 5a.3 Acceleration Error (m/s^2) vs. Time (days) for Model 1 Acceleration Error Compensation

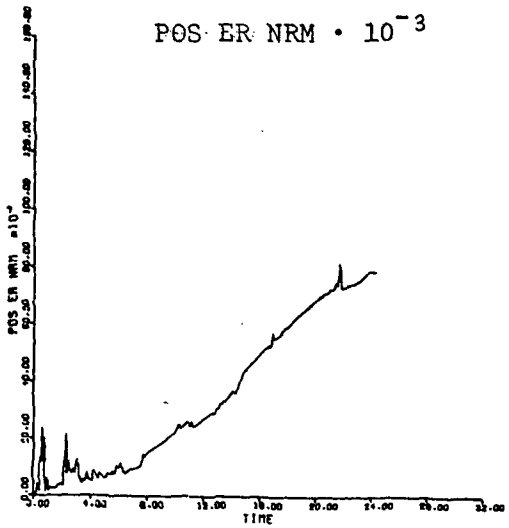

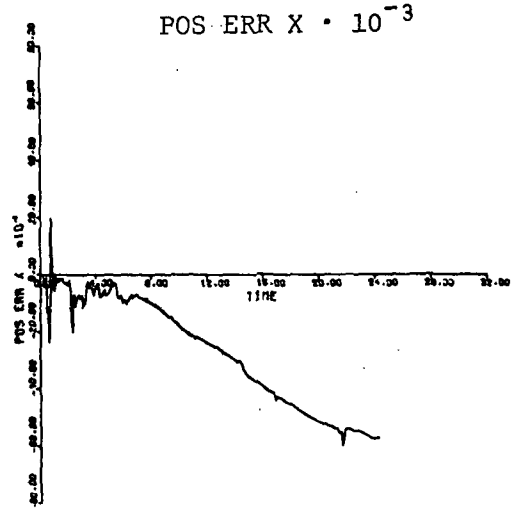

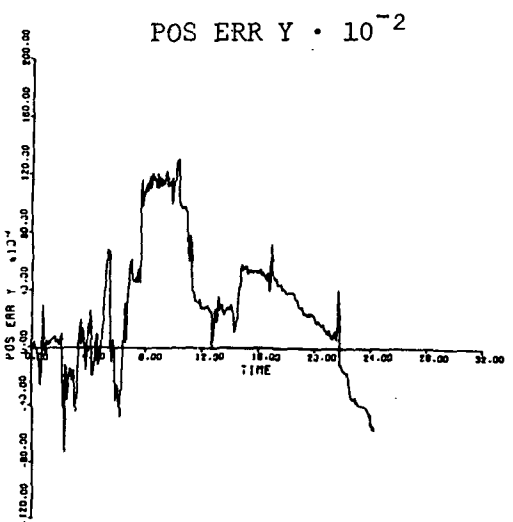

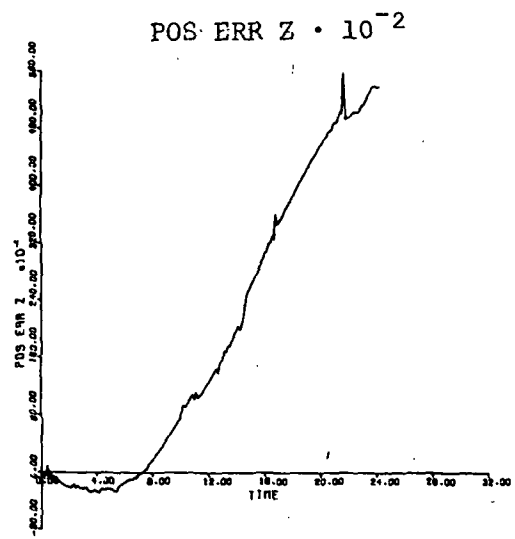

Figure 5b.1 Position Error (km) vs. Time (days) for Model 1 Acceleration Error Compensation (Alternate q-Matrix)

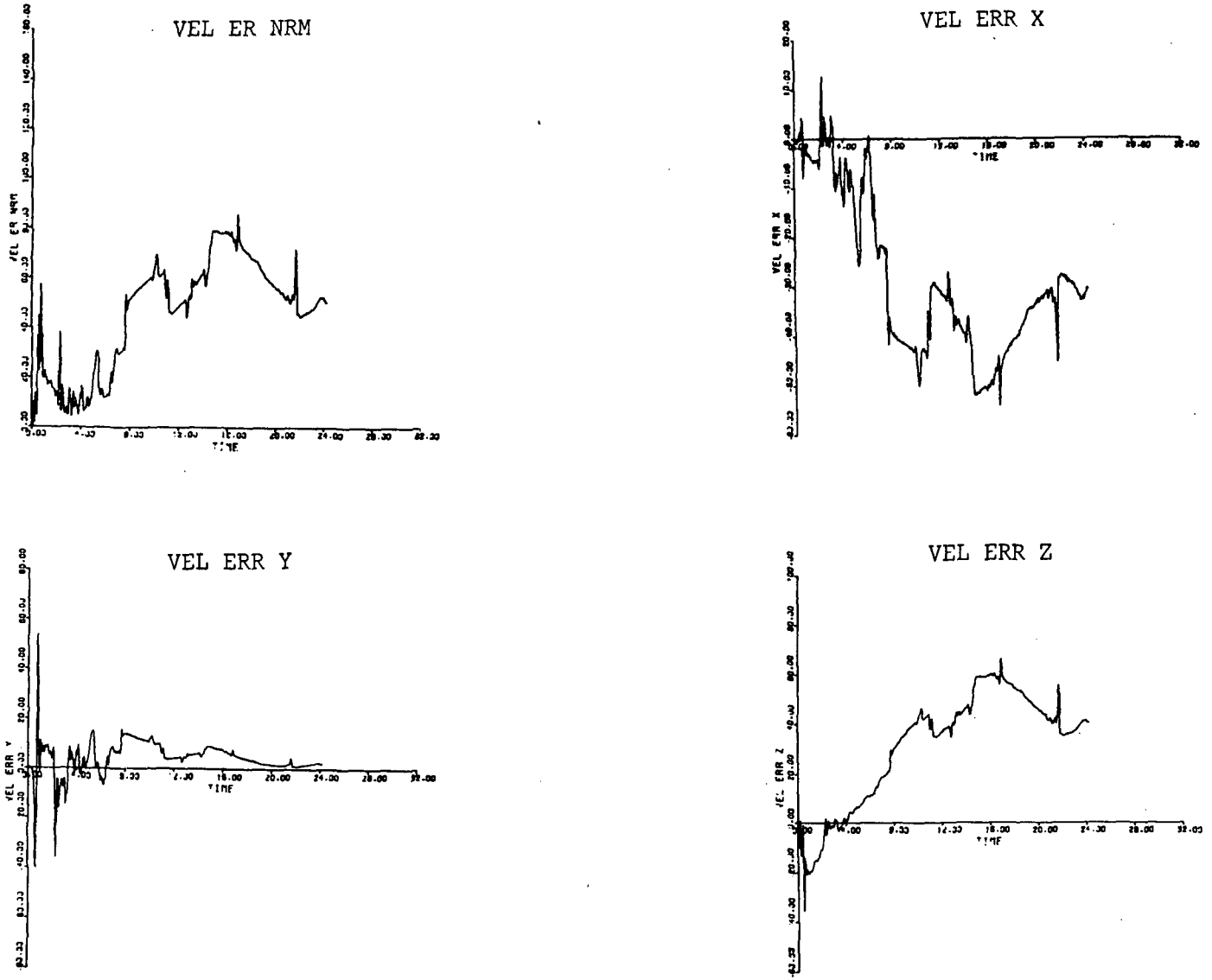

Figure 5b.2 Velocity Error (m/s) vs. Time (days) for Model 1 Acceleration Error Compensation (Alternate q-Matrix)

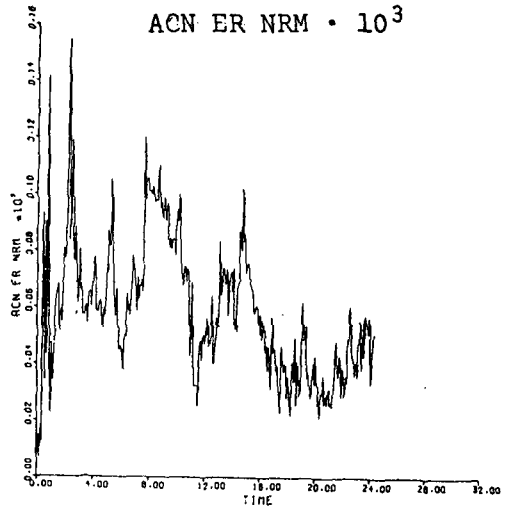

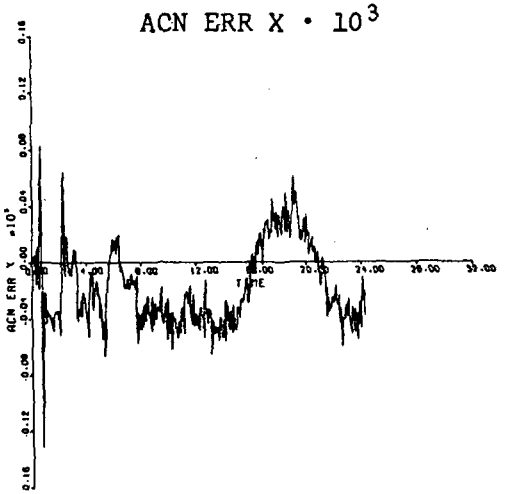

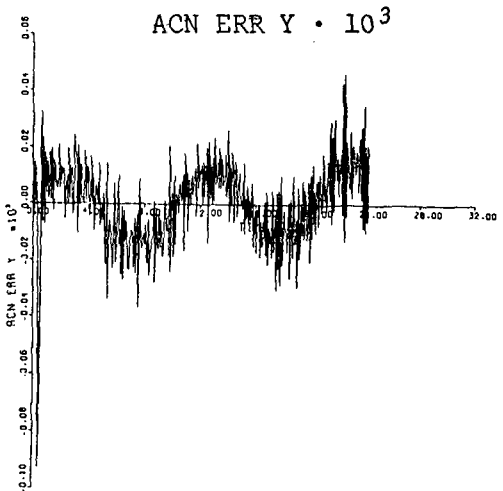

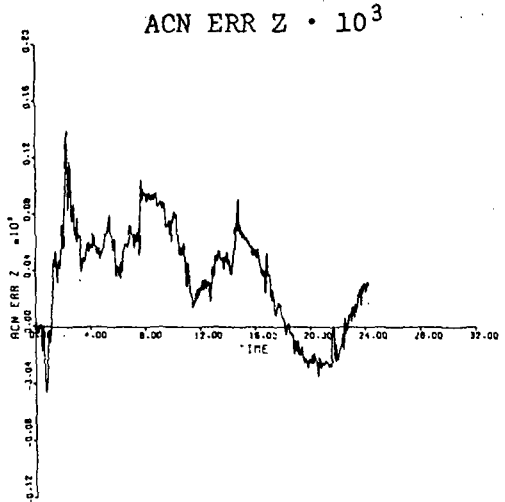

Figure 5b.3 Acceleration Error (m/s^2) vs. Time (days) for Model 1 Acceleration Error Compensation (Alternate q-Matrix)

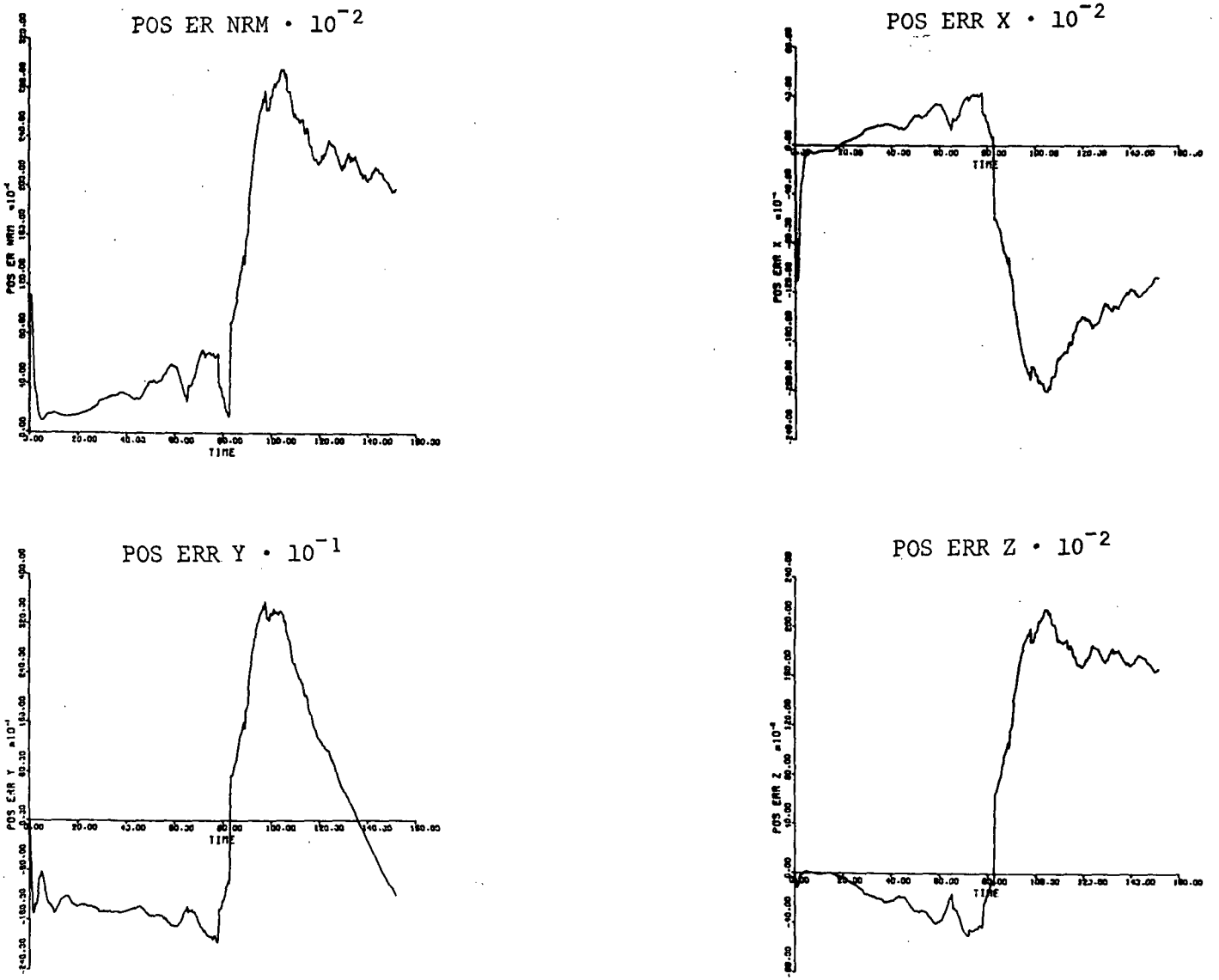

Figure 6a.1 Position Error (km) vs. Time (days) for Model 2 Acceleration Error Compensation (1σ Errors)

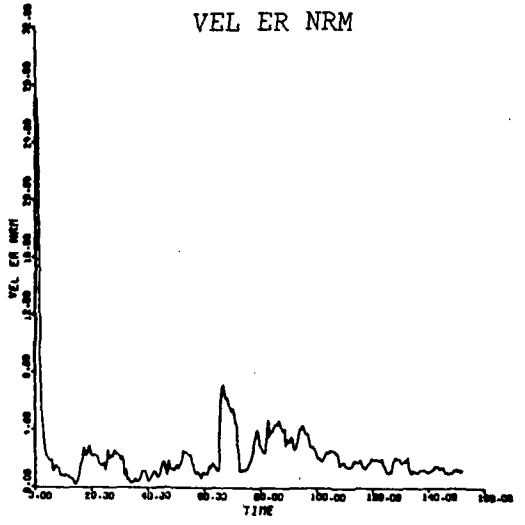

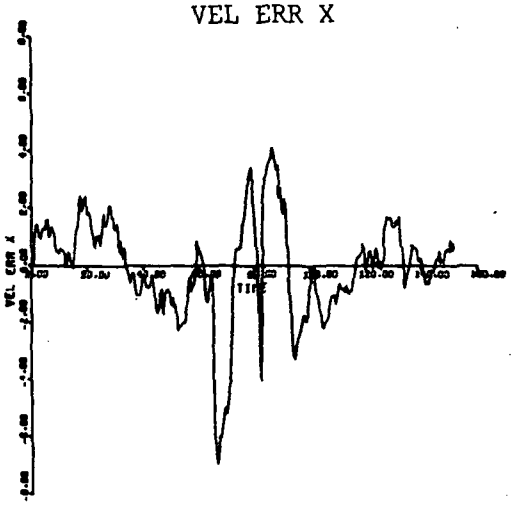

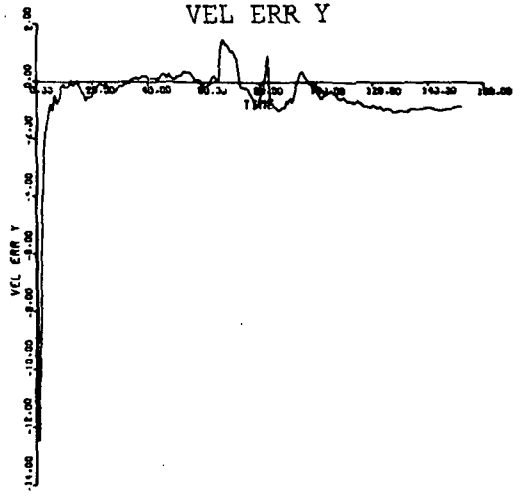

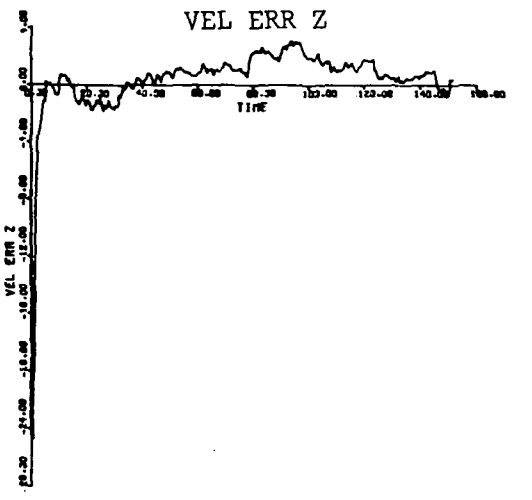

Figure 6a.2 Velocity Error (m/s) vs. Time (days) for Model 2 Acceleration Error Compensation (1σ Errors)

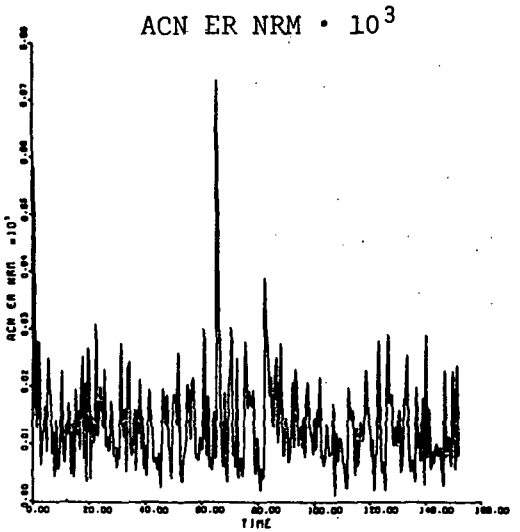

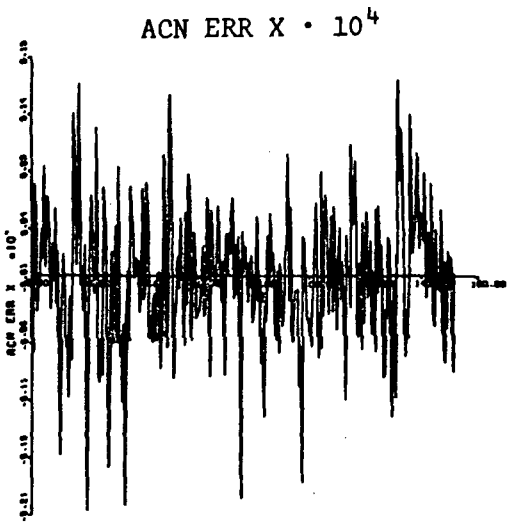

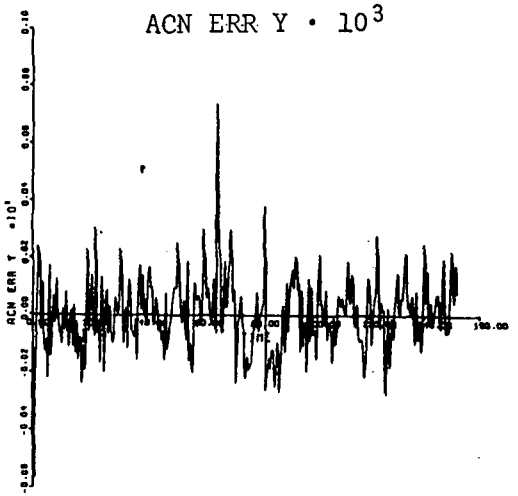

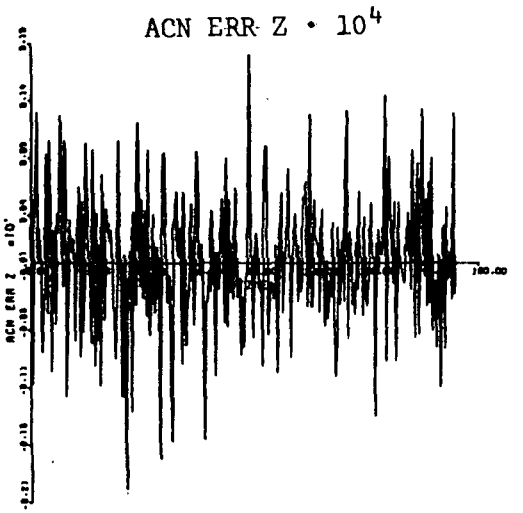

Figure 6a.3 Acceleration Error (m/s^2) vs. Time (days) for Model 2 Acceleration Error Compensation (1σ Errors)

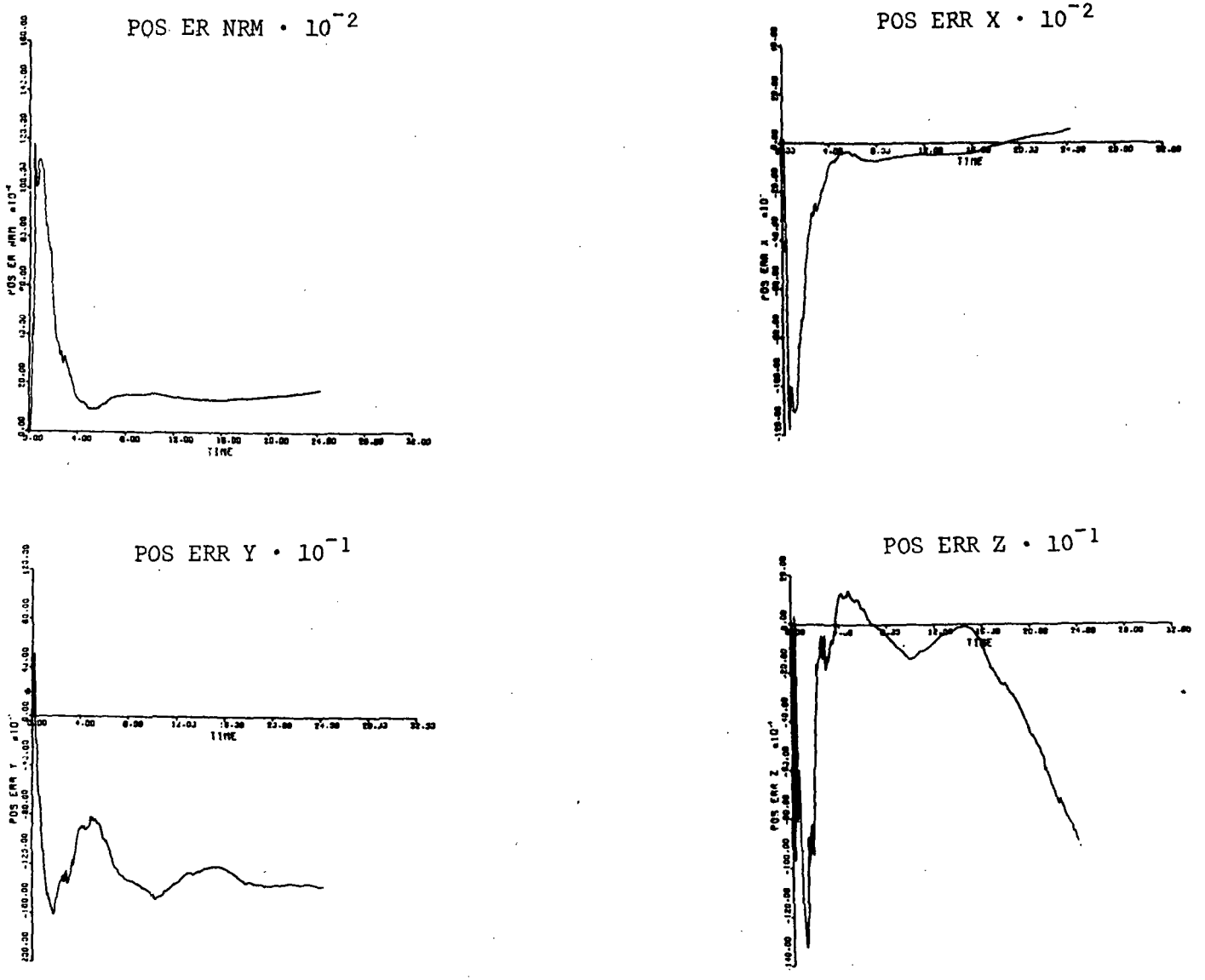

Figure 6b.1 Position Error (km) vs. Time (days) for Model 2 Acceleration Error Compensation (1σ Errors)

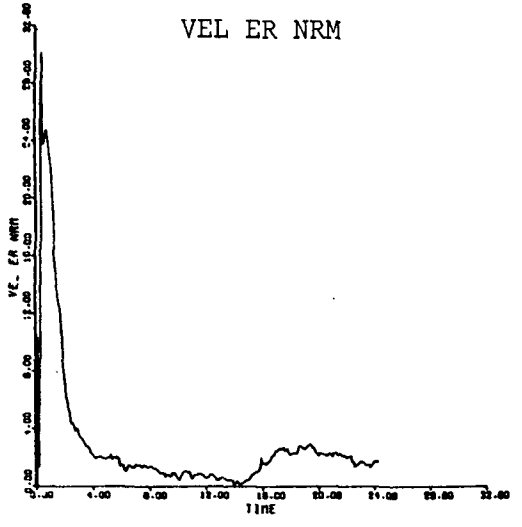

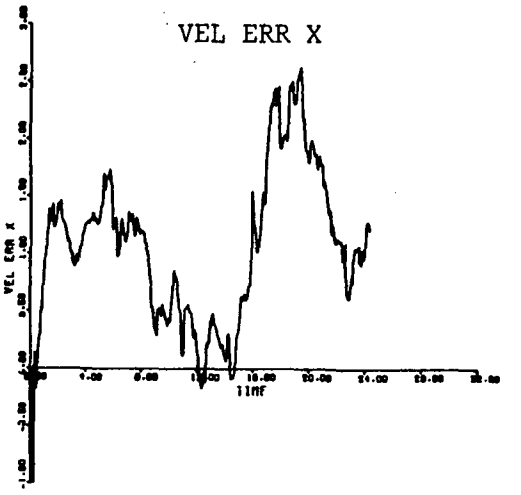

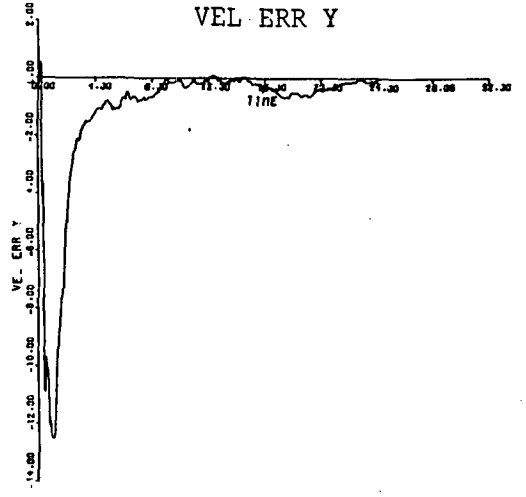

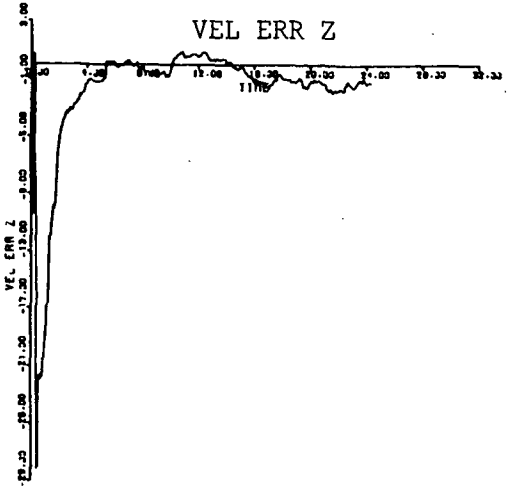

Figure 6b.2 Velocity Error (m/s) vs. Time (days) for Model 2 Acceleration Error Compensation (1σ Errors)

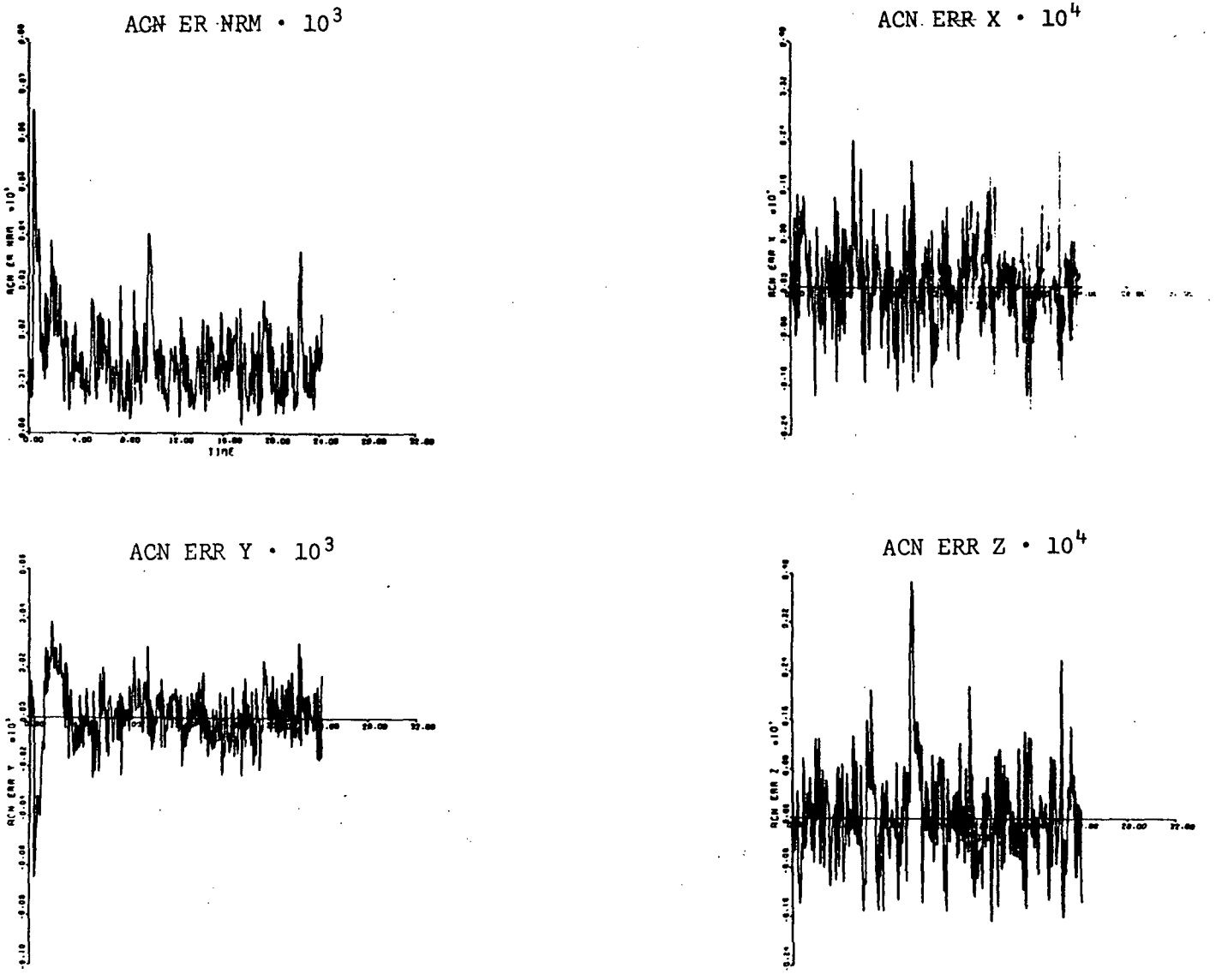

Figure 6b.3 Acceleration Error (m/s^2) vs. Time (days) for Model 2 Acceleration Error Compensation (1σ Errors)

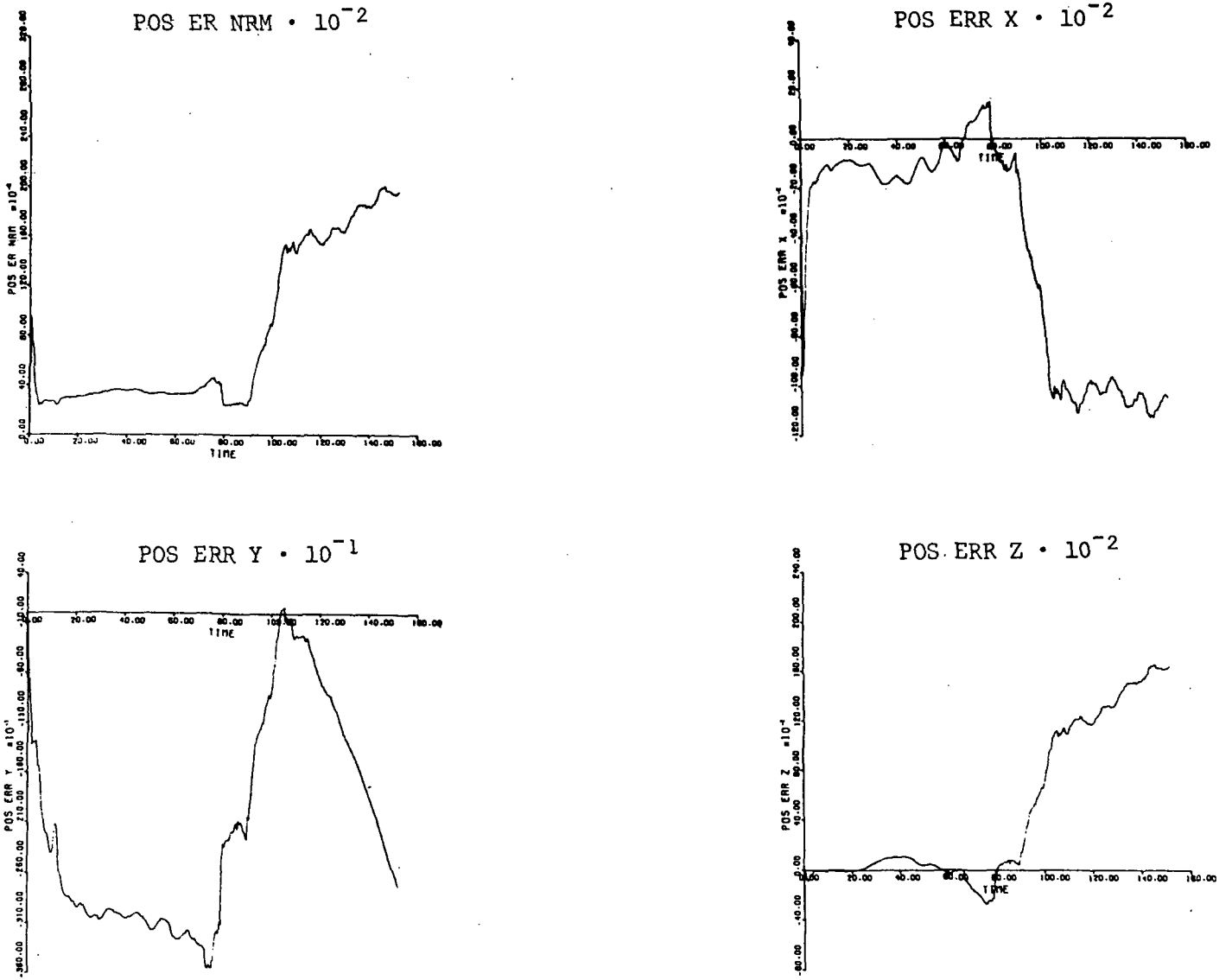

Figure 6c.1 Position Error (km) vs. Time (days) for Model 2 Acceleration Error Compensation (1/3σ Errors)

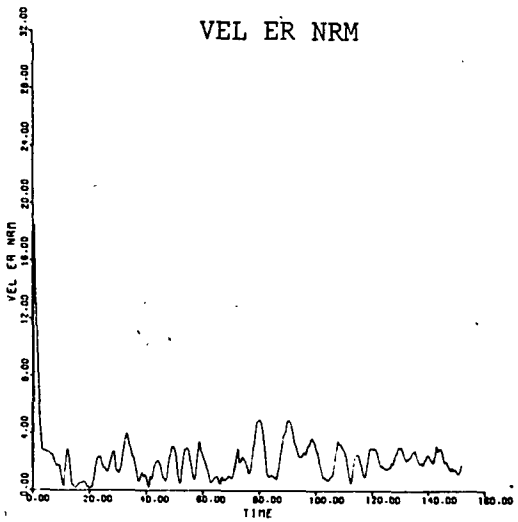

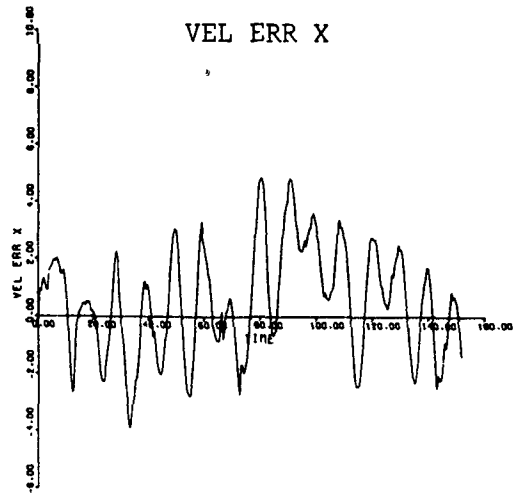

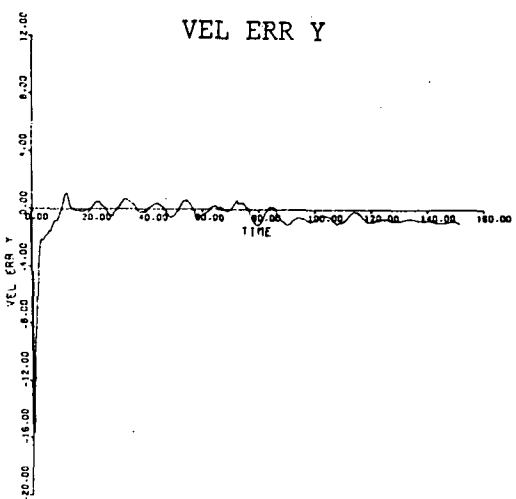

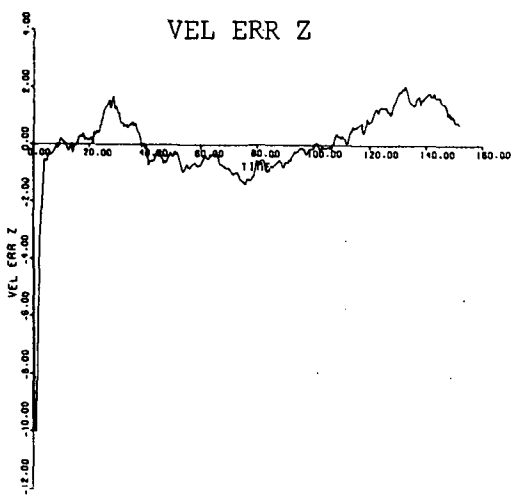

Figure 6c.2 Velocity Error (m/s) vs. Time (days) for Model 2 Acceleration Error Compensation (1/3σ Errors)

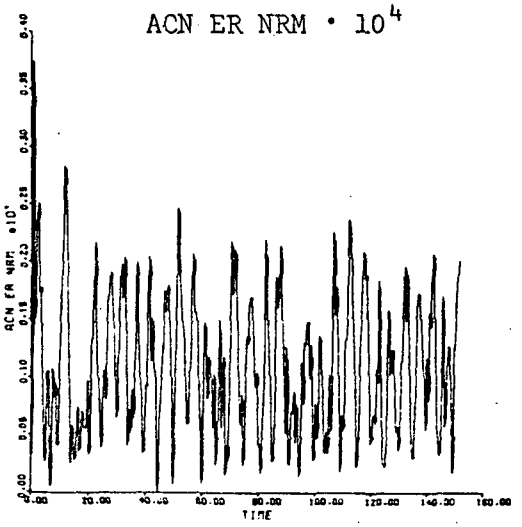

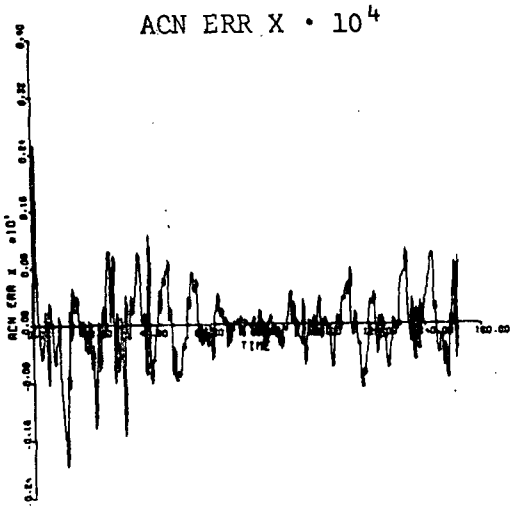

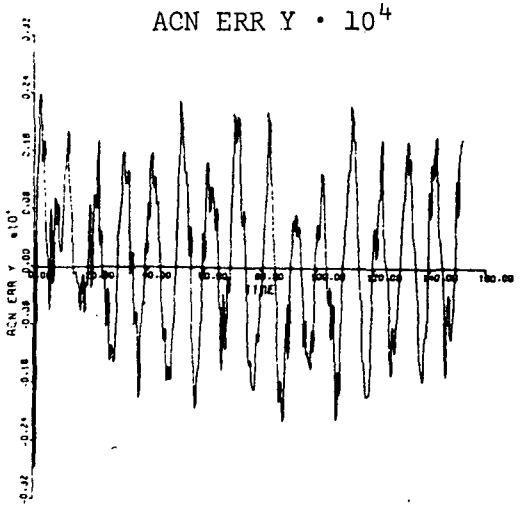

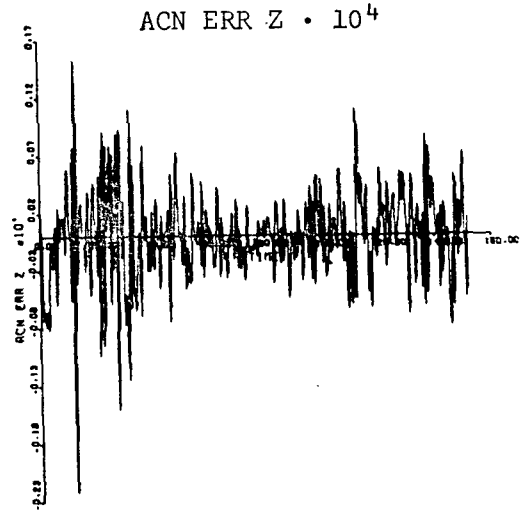

Figure 6c.3 Acceleration Error (m/s^2) vs. Time (days) for Model 2 Acceleration Error Compensation ($1/3\sigma$ Errors)

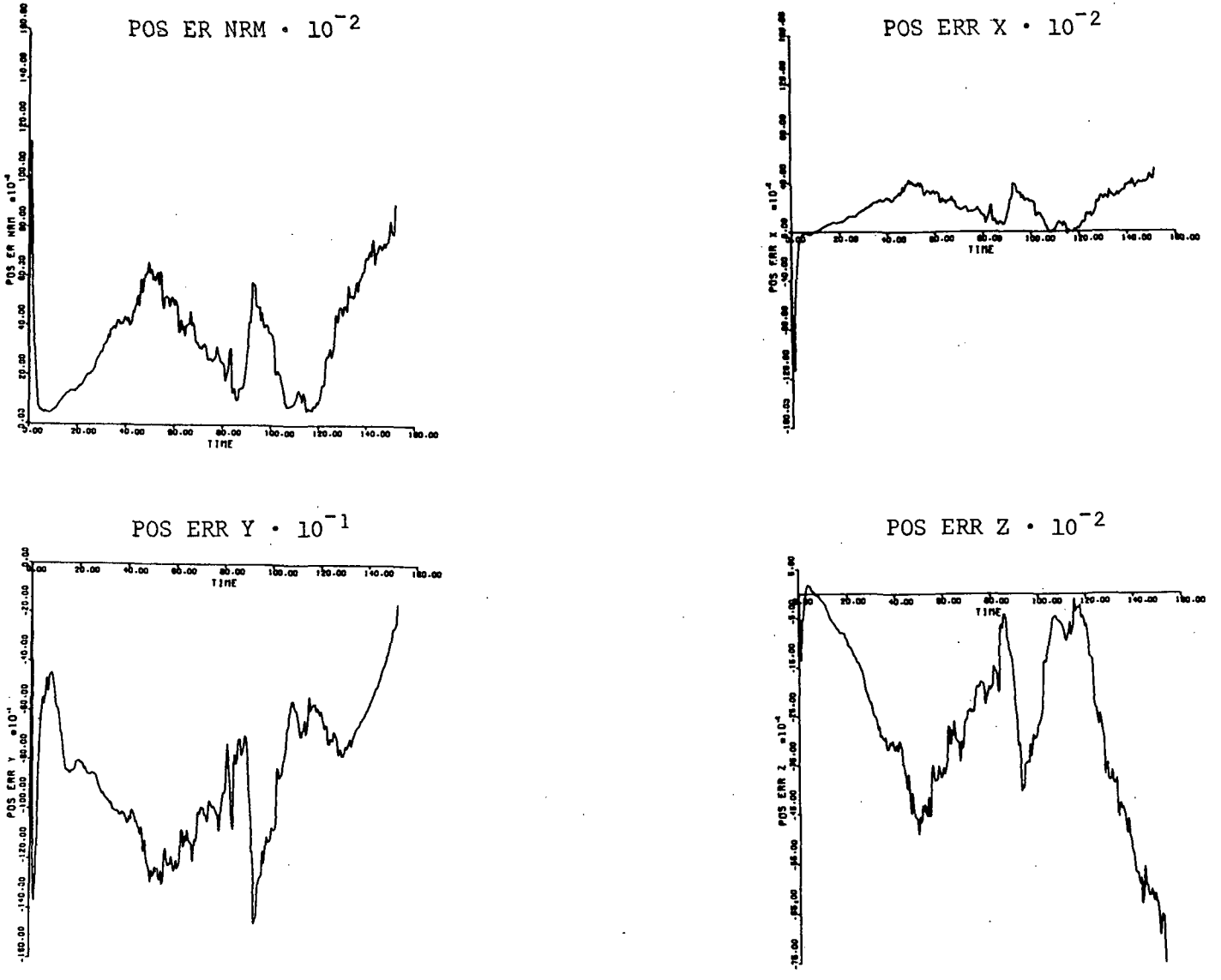

Figure 7a.1 Position Error (km) vs. Time (days) for Model 3 Acceleration Error Compensation (1σ Errors)

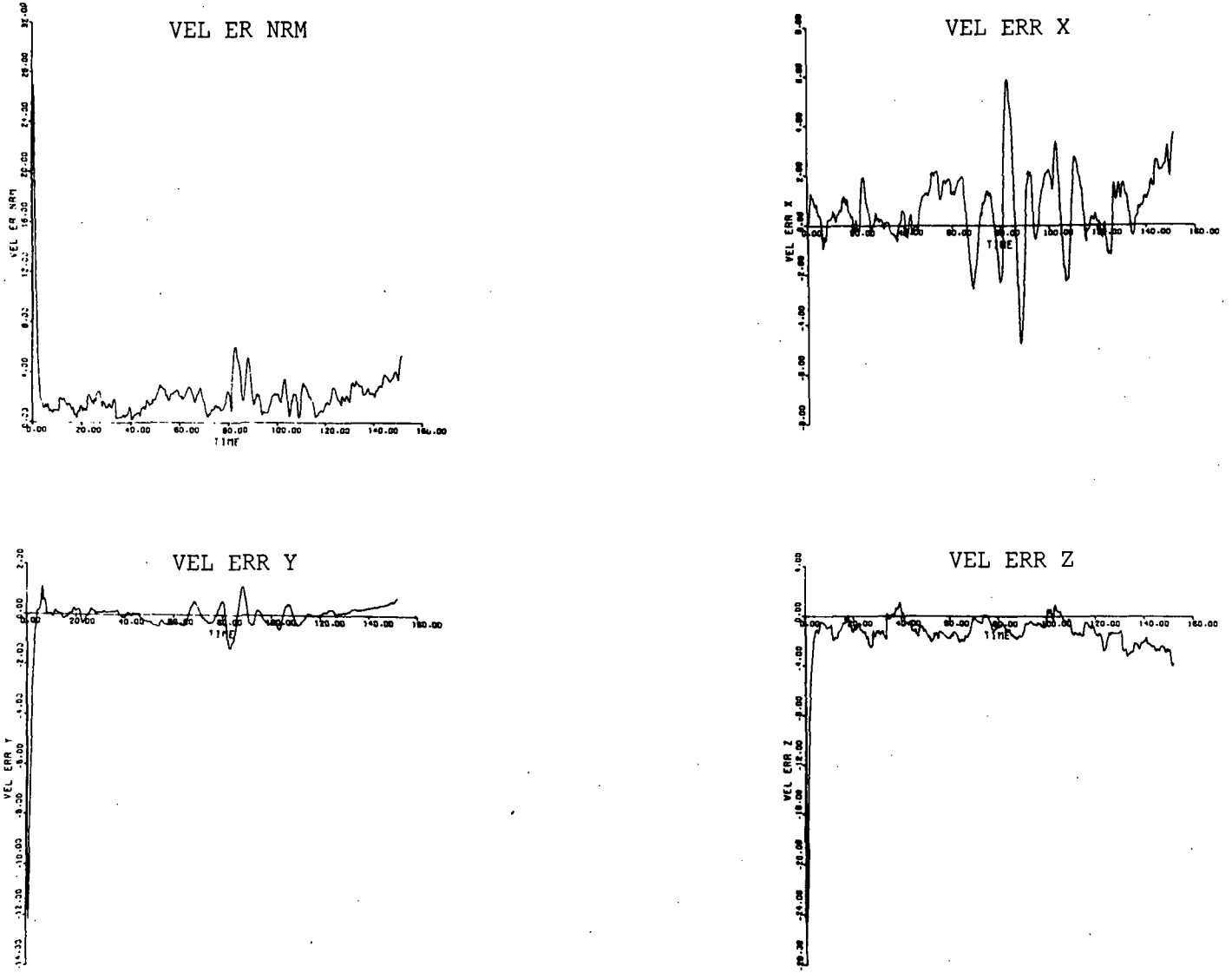

Figure 7a.2 Velocity Error (m/s) vs. Time (days) for Model 3 Acceleration Error Compensation (1σ Errors)

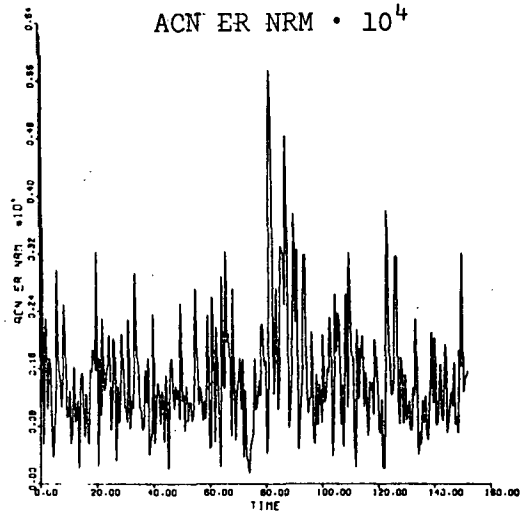

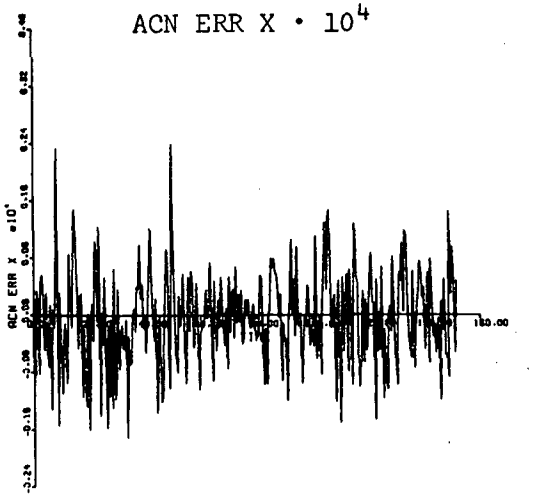

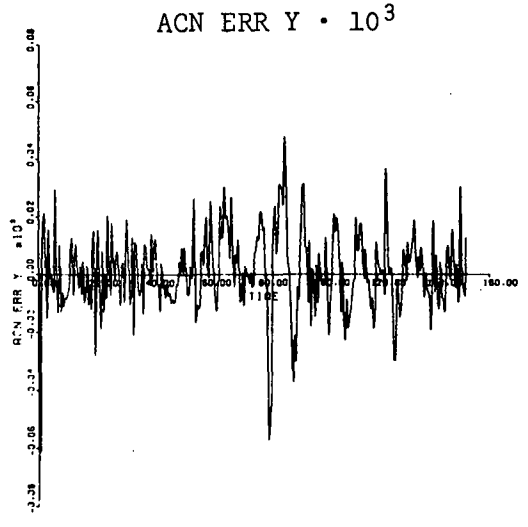

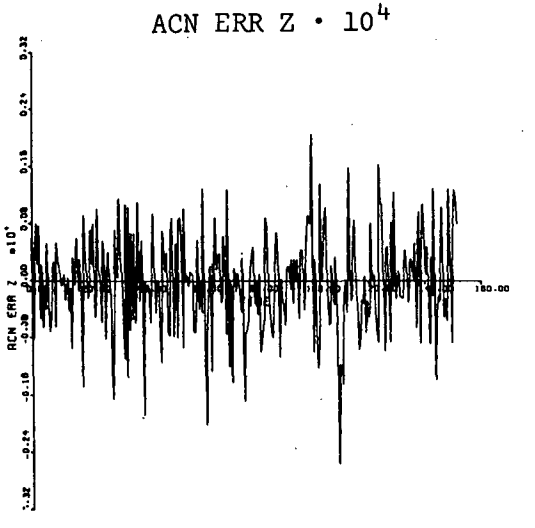

Figure 7a.3 Acceleration Error (m/s^2) vs. Time (days) for Model 3 Acceleration Error Compensation (1σ Errors)

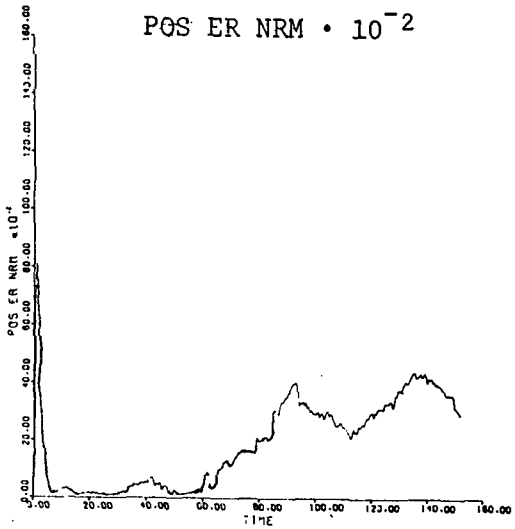

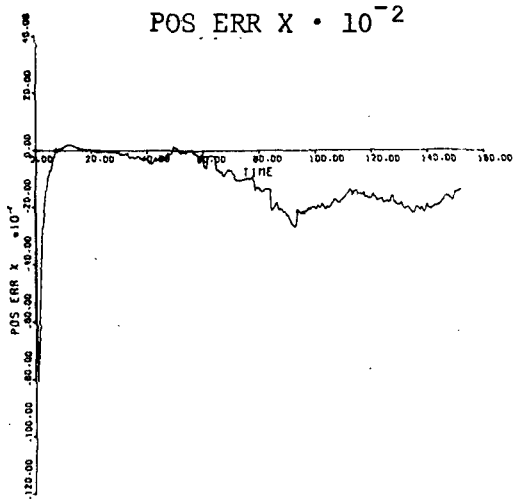

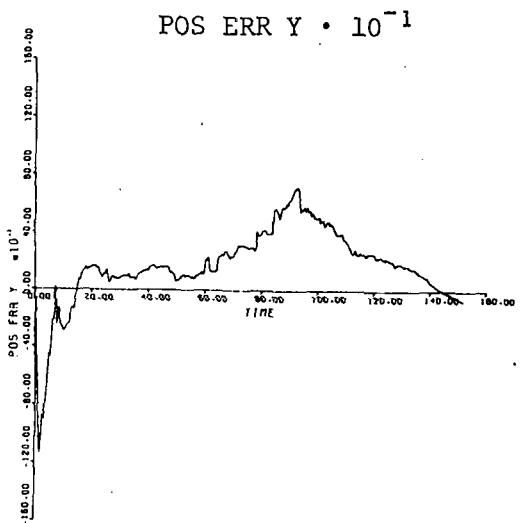

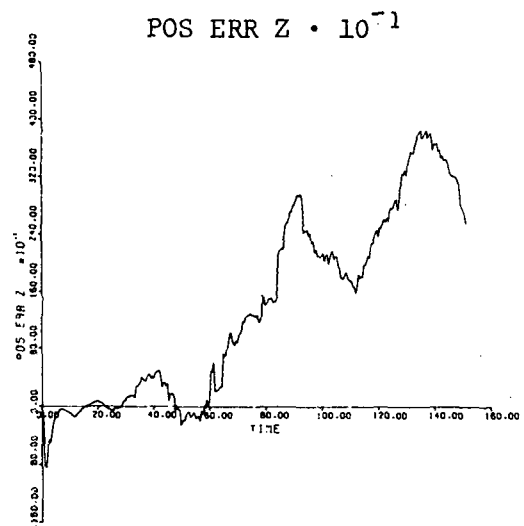

Figure 7b.1 Position Error (km) vs. Time (days) for Model 3 Acceleration Error Compensation (1/3σ Errors)

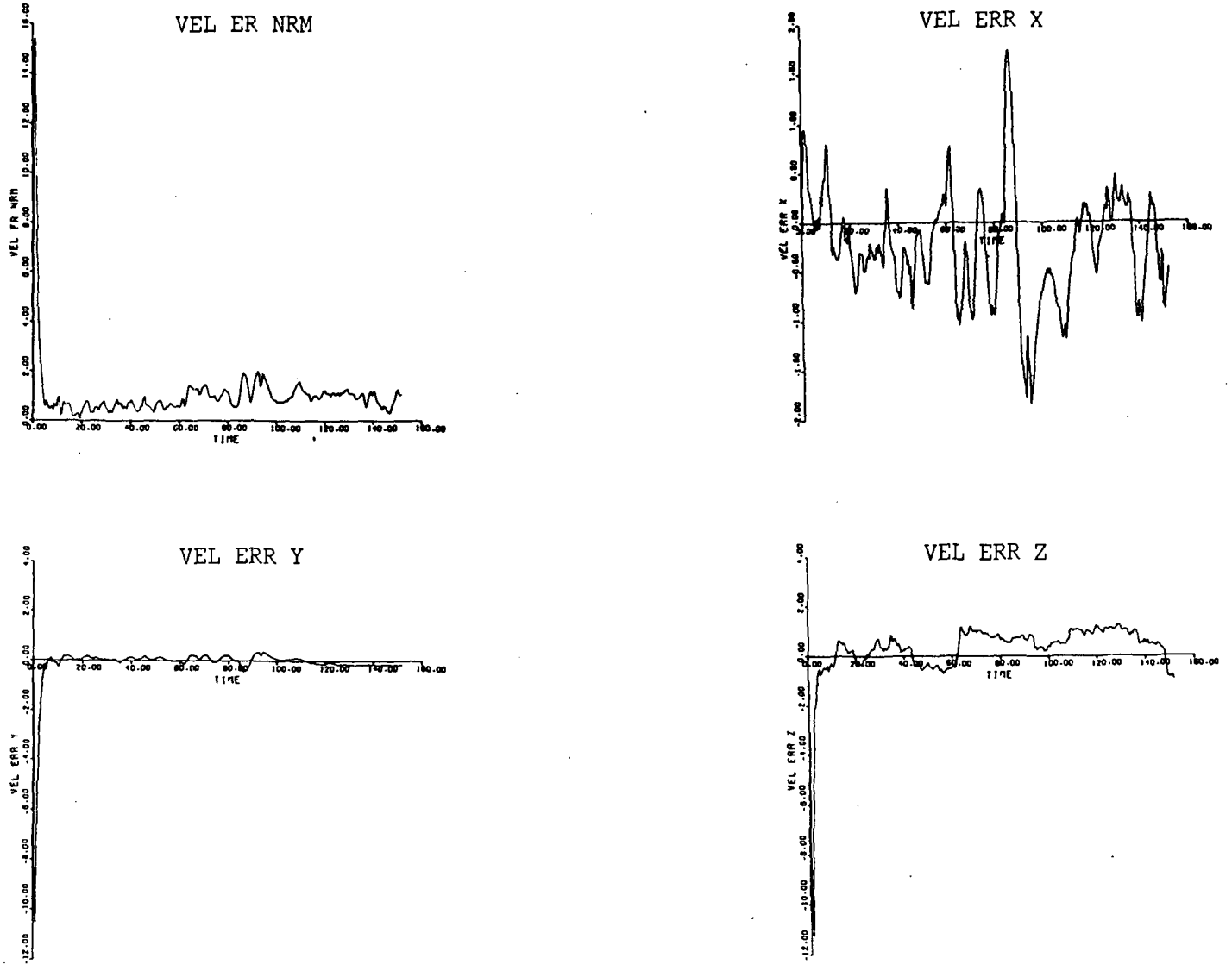

Figure 7b.2 Velocity Error (m/s) vs. Time (days) for Model 3 Acceleration Error Compensation (1/3σ Errors)

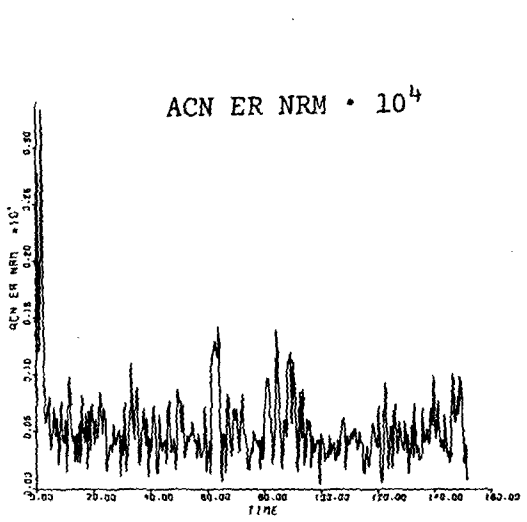

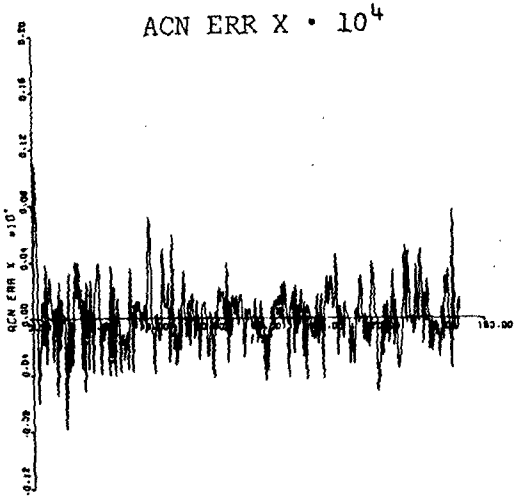

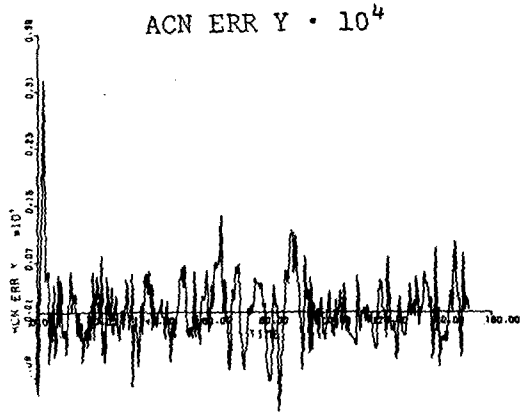

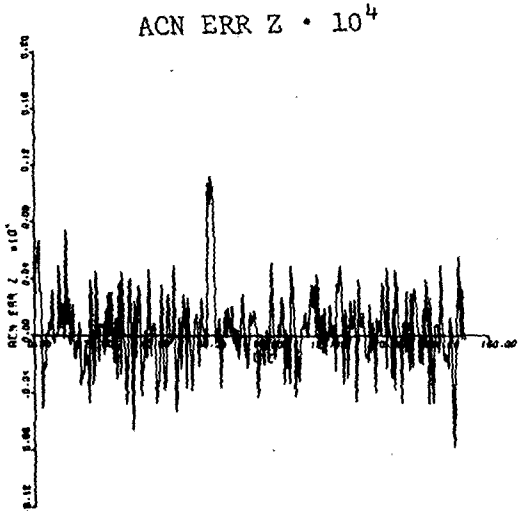

Figure 7b.3 Acceleration Error (m/s^2) vs. Time (days) for Model 3 Acceleration Error Compensation ($1/3\sigma$ Errors)

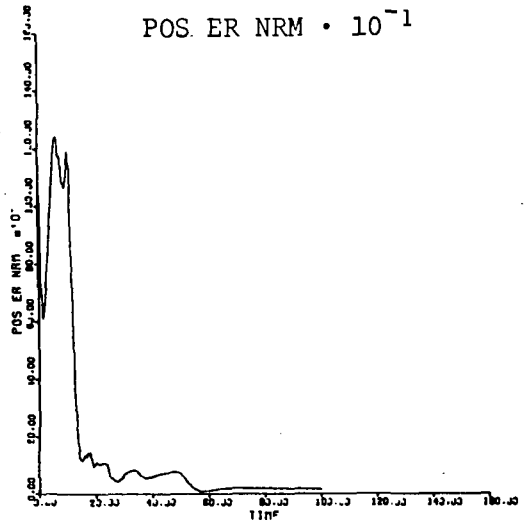

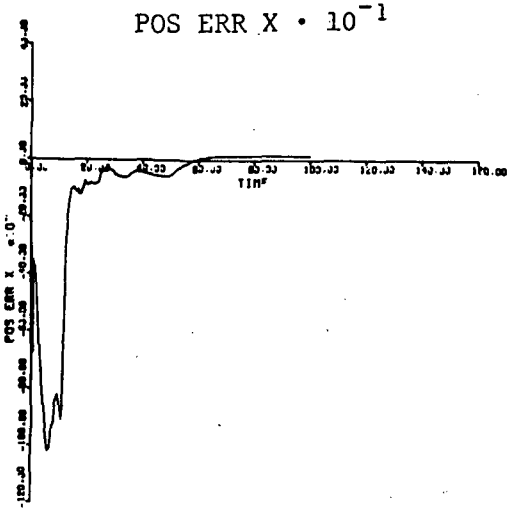

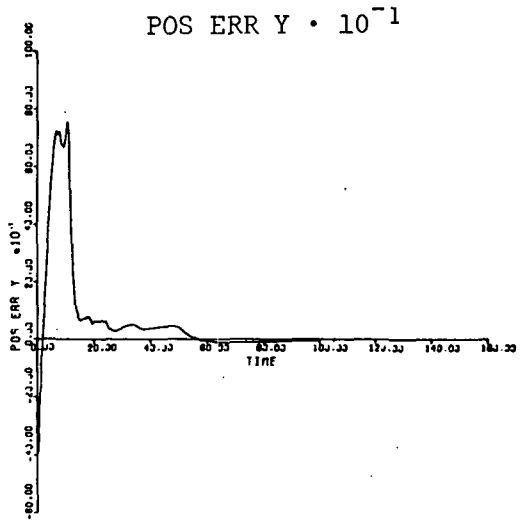

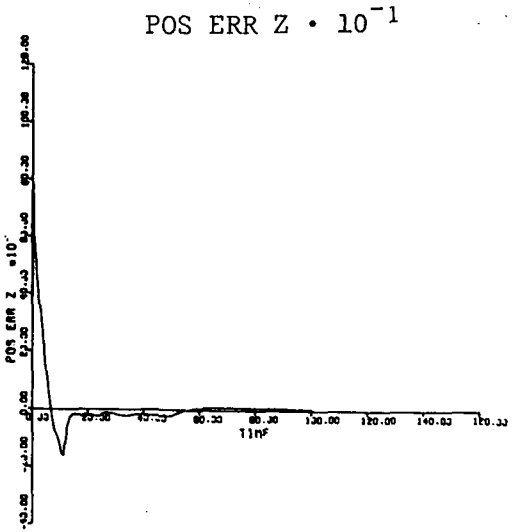

Figure 7c.1 Position Error (km) vs. Time (days) for Model 3 Acceleration Error Compensation (Deterministic Error)

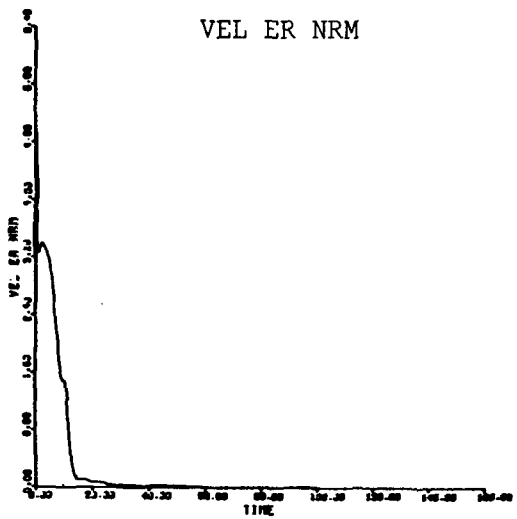

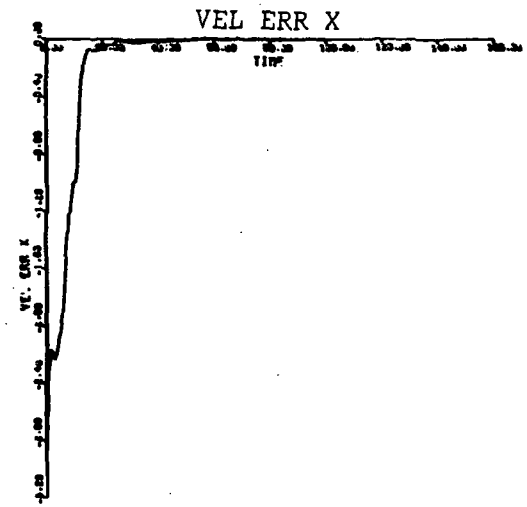

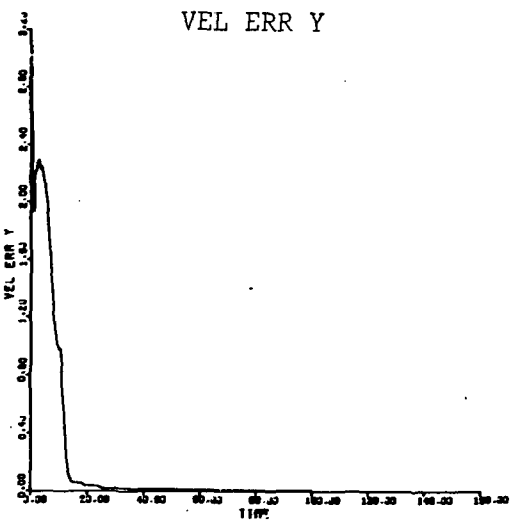

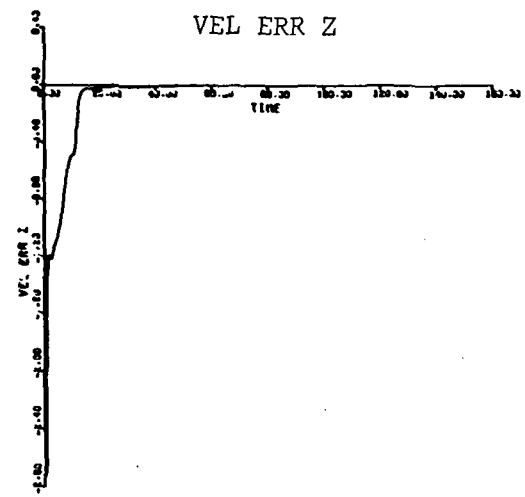

Figure 7c.2 Velocity Error (m/s) vs. Time (days) for Model 3 Acceleration Error Compensation (Deterministic Error)

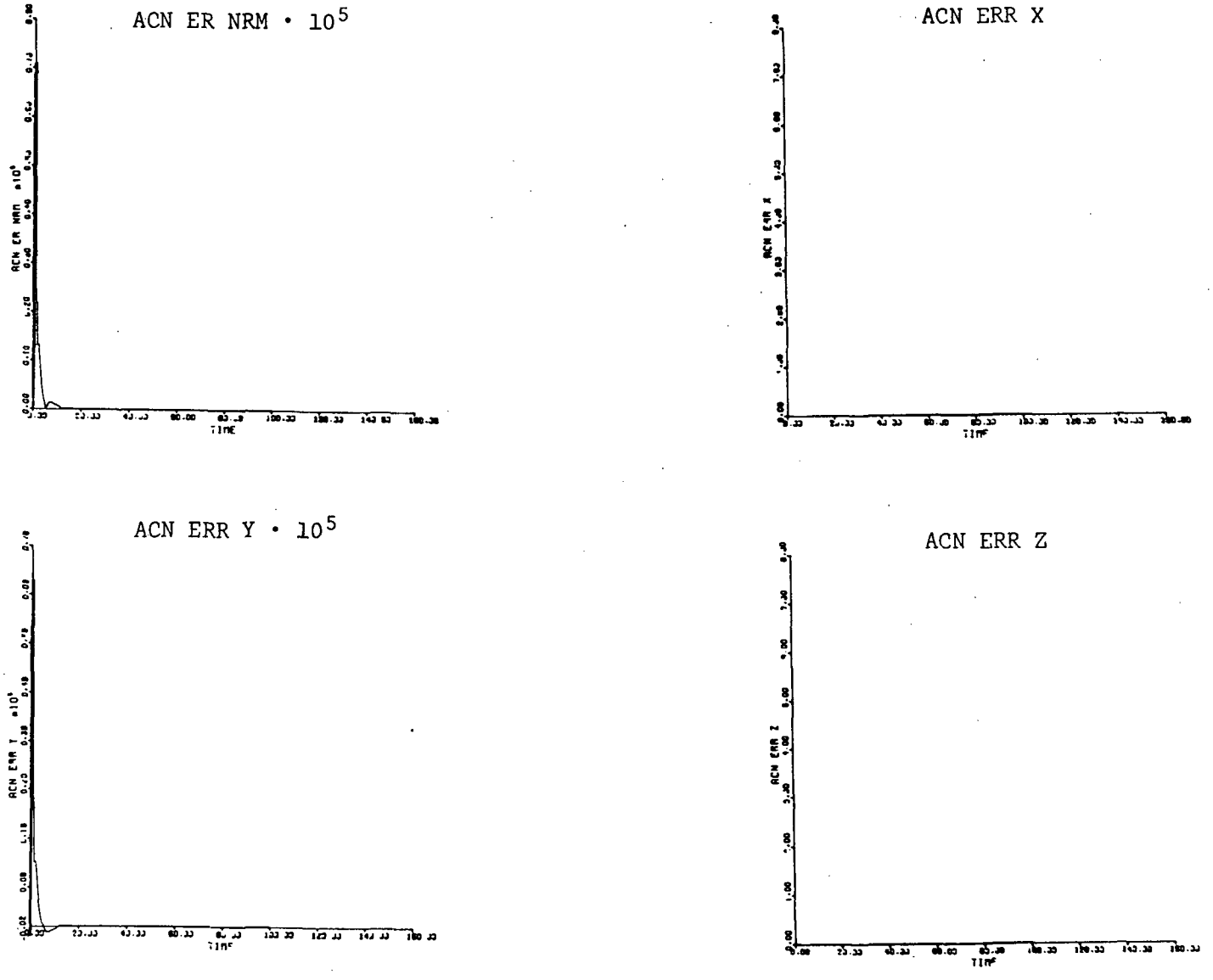

Figure 7c.3 Acceleration Error (m/s^2) vs. Time (days) for Model 3 Acceleration Error Compensation (Deterministic Error)

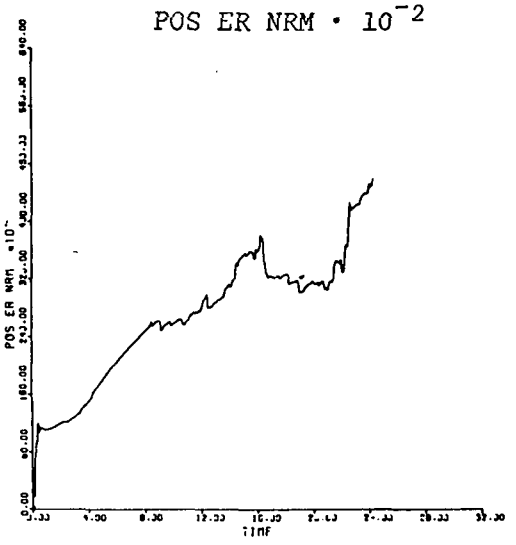

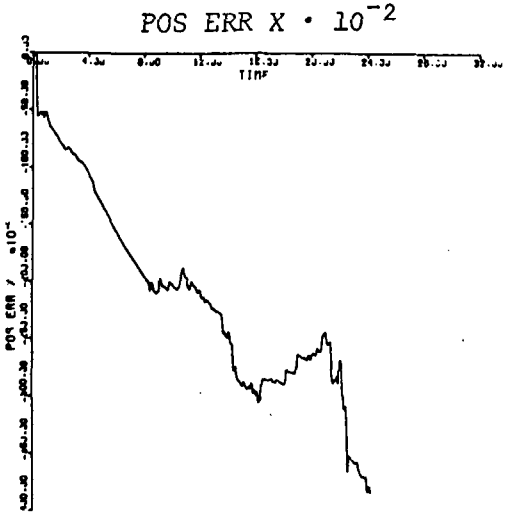

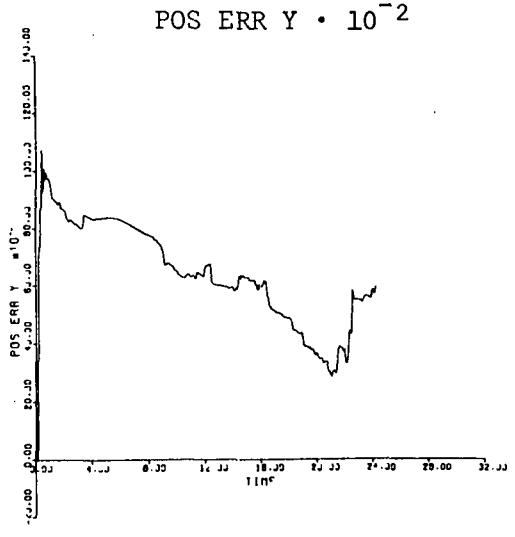

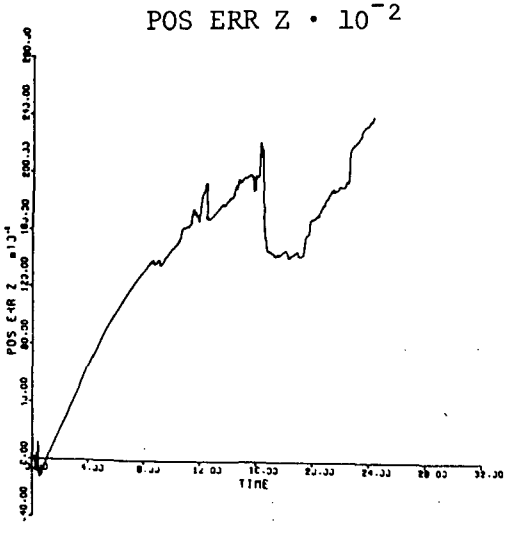

Figure 8a.1 Position Error (km) vs. Time (days) for Model 3, Range-Rate Only at 100-Minute Intervals

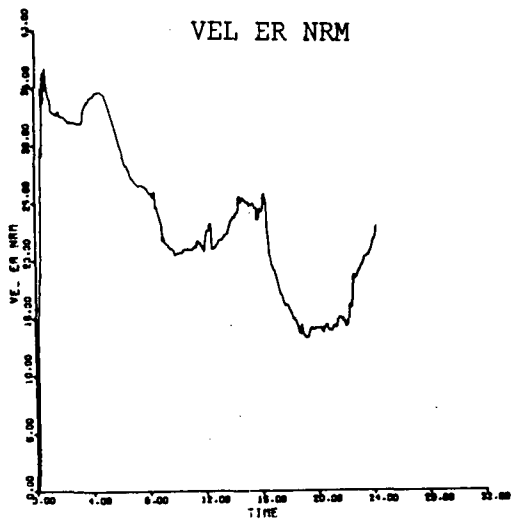

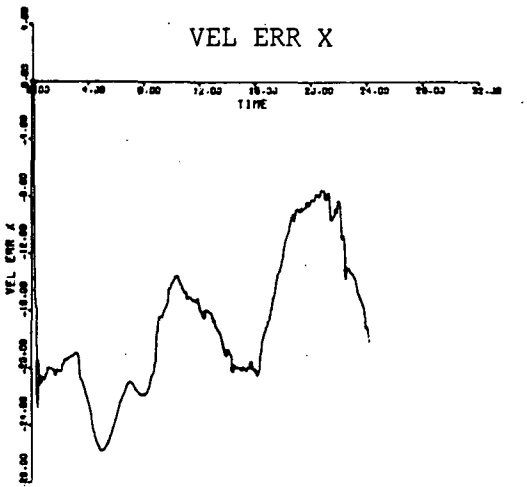

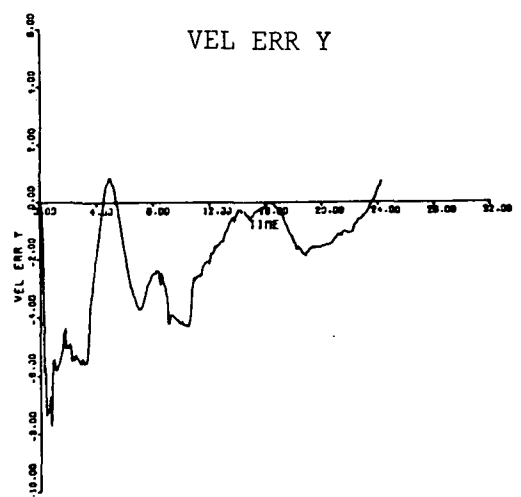

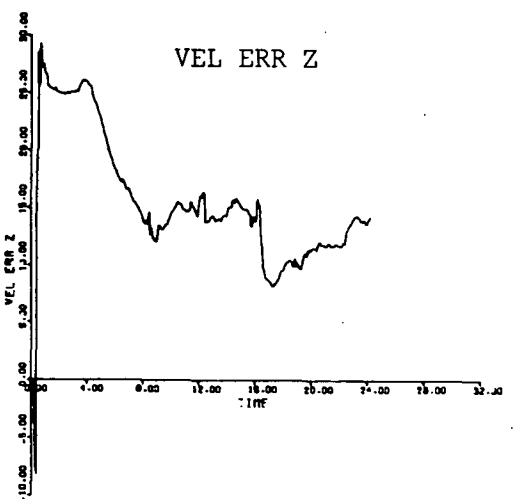

Figure 8a.2 Velocity Error (m/s) vs. Time (days) for Model 3, Range-Rate Only at 100-Minute Intervals

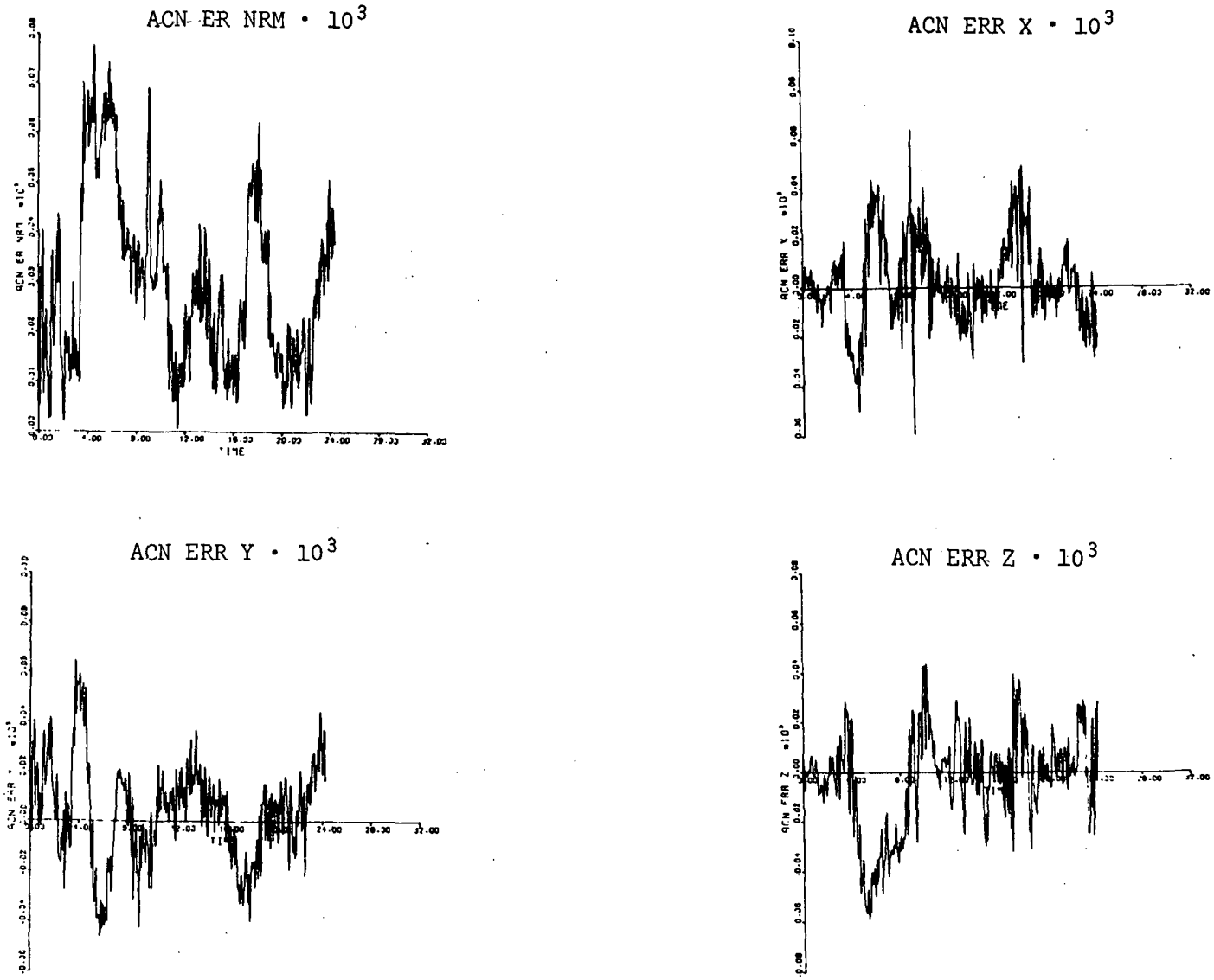

Figure 8a.3 Acceleration Error (m/s^2) vs. Time (days) for Model 3, Range-Rate Only at 100-Minute Intervals

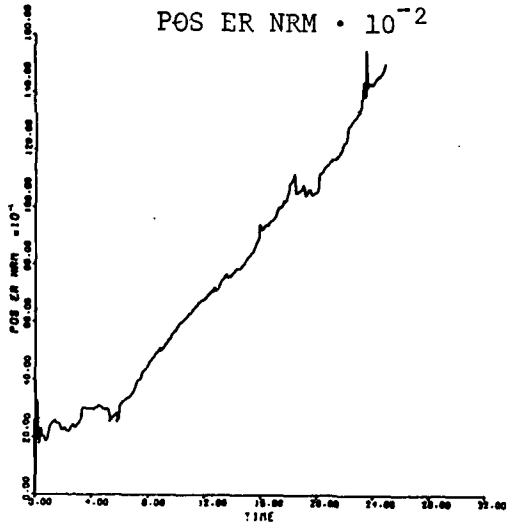

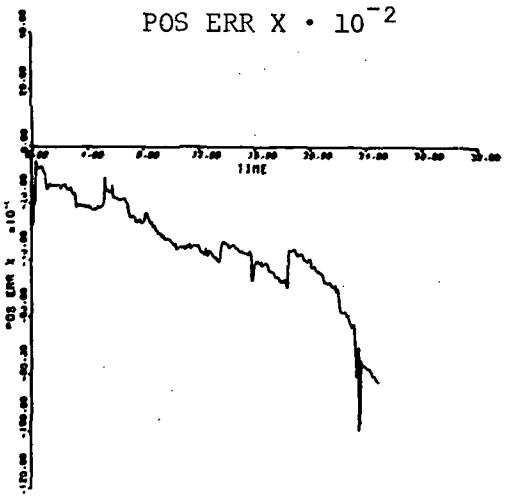

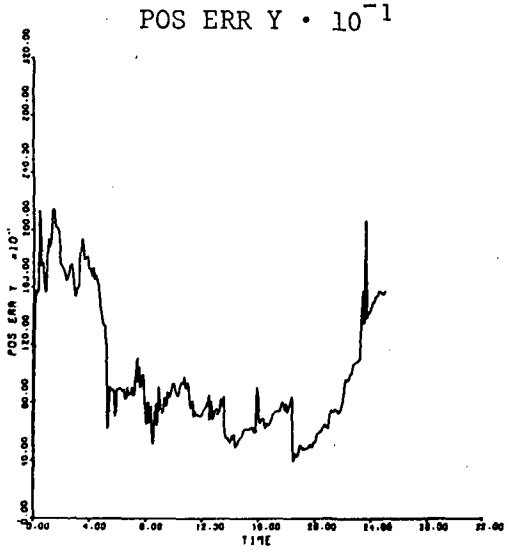

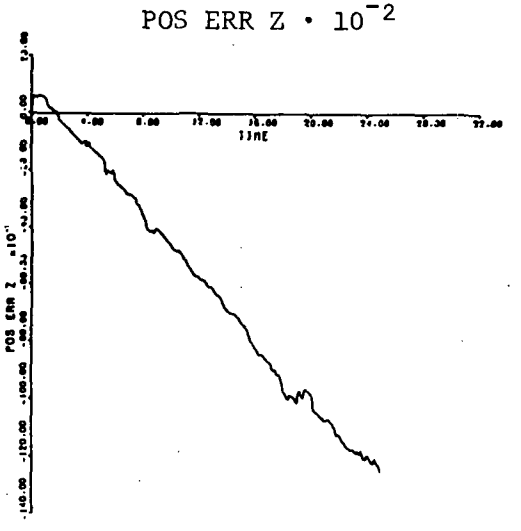

Figure 8b.1 Position Error (km) vs. Time (days) for Model 3, Range-Rate Only at 10-Minute Intervals

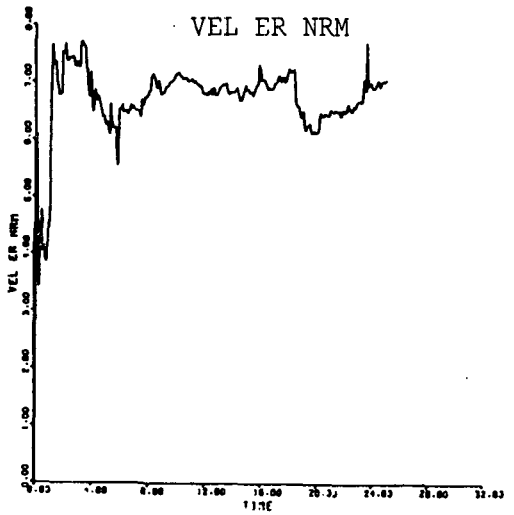

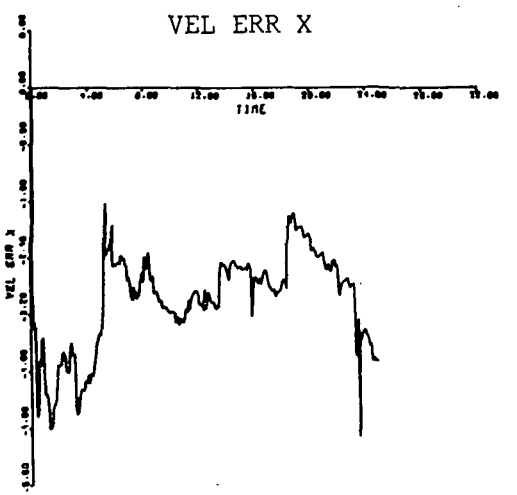

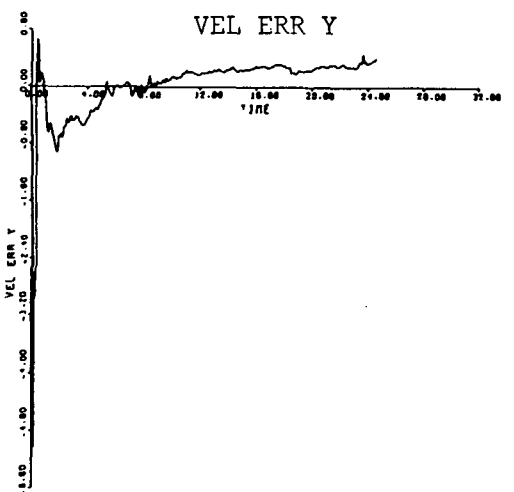

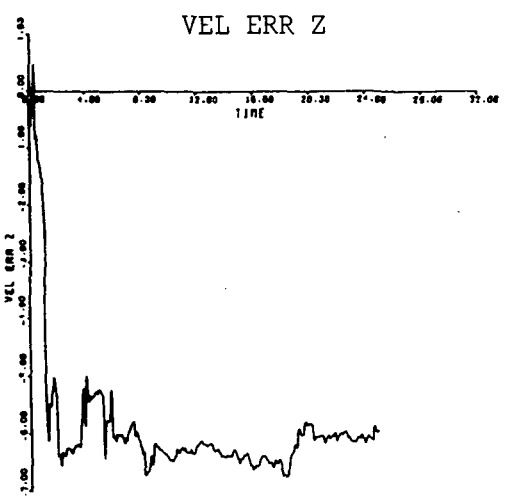

Figure 8b.2 Velocity Error (m/s) vs. Time (days) for Model 3, Range-Rate Only at 10-Minute Intervals

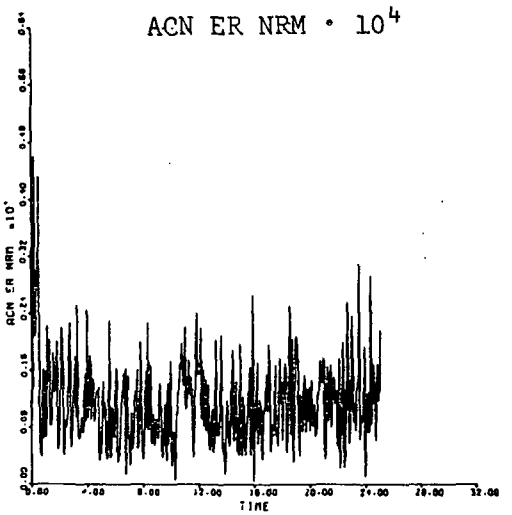

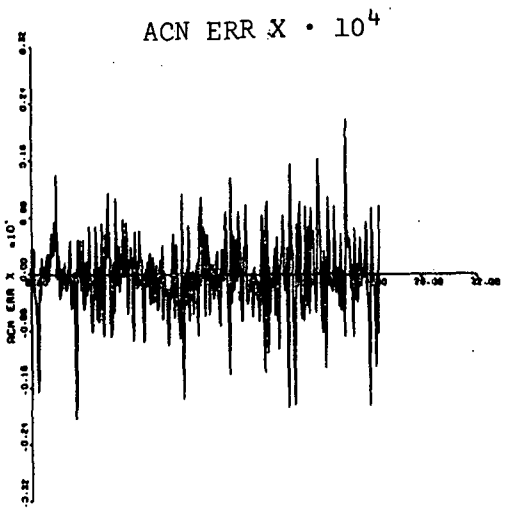

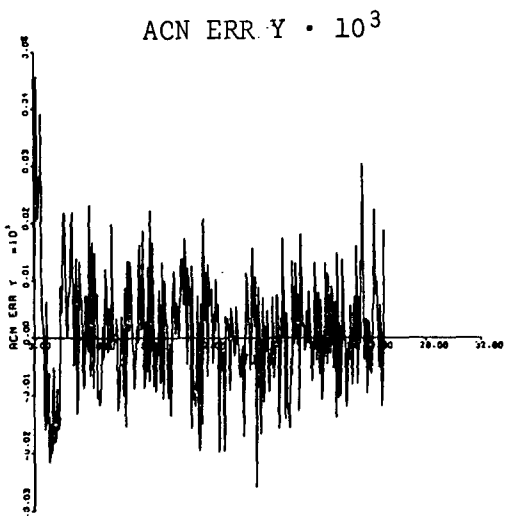

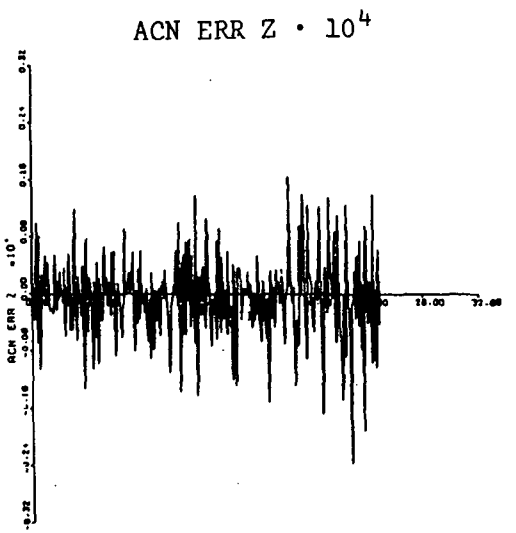

Figure 8b.3 Acceleration Error (m/s^2) vs. Time (days) for Model 3, Range-Rate Only at 10-Minute Intervals

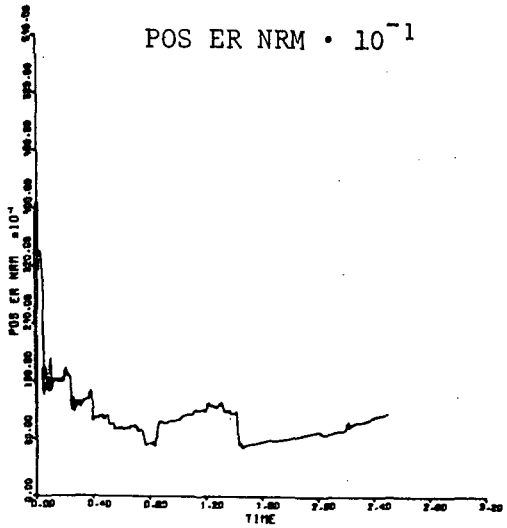

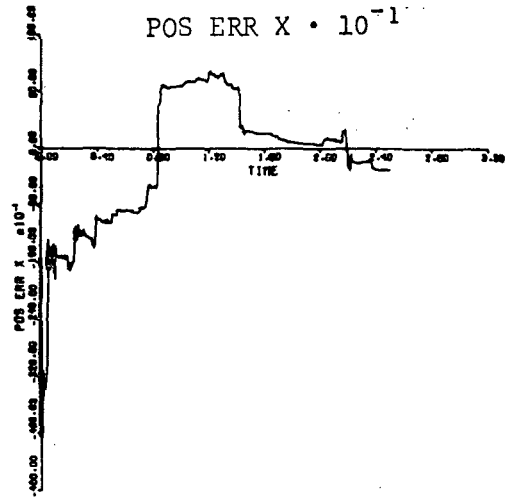

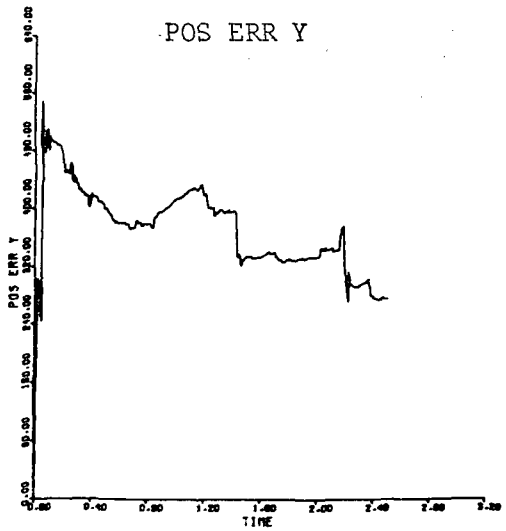

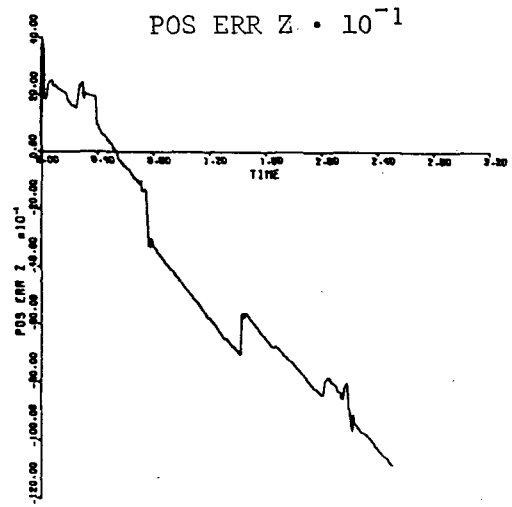

Figure 8c.1 Position Error (km) vs. Time (days) for Model 3, Range-Rate Only at 1-Minute Intervals

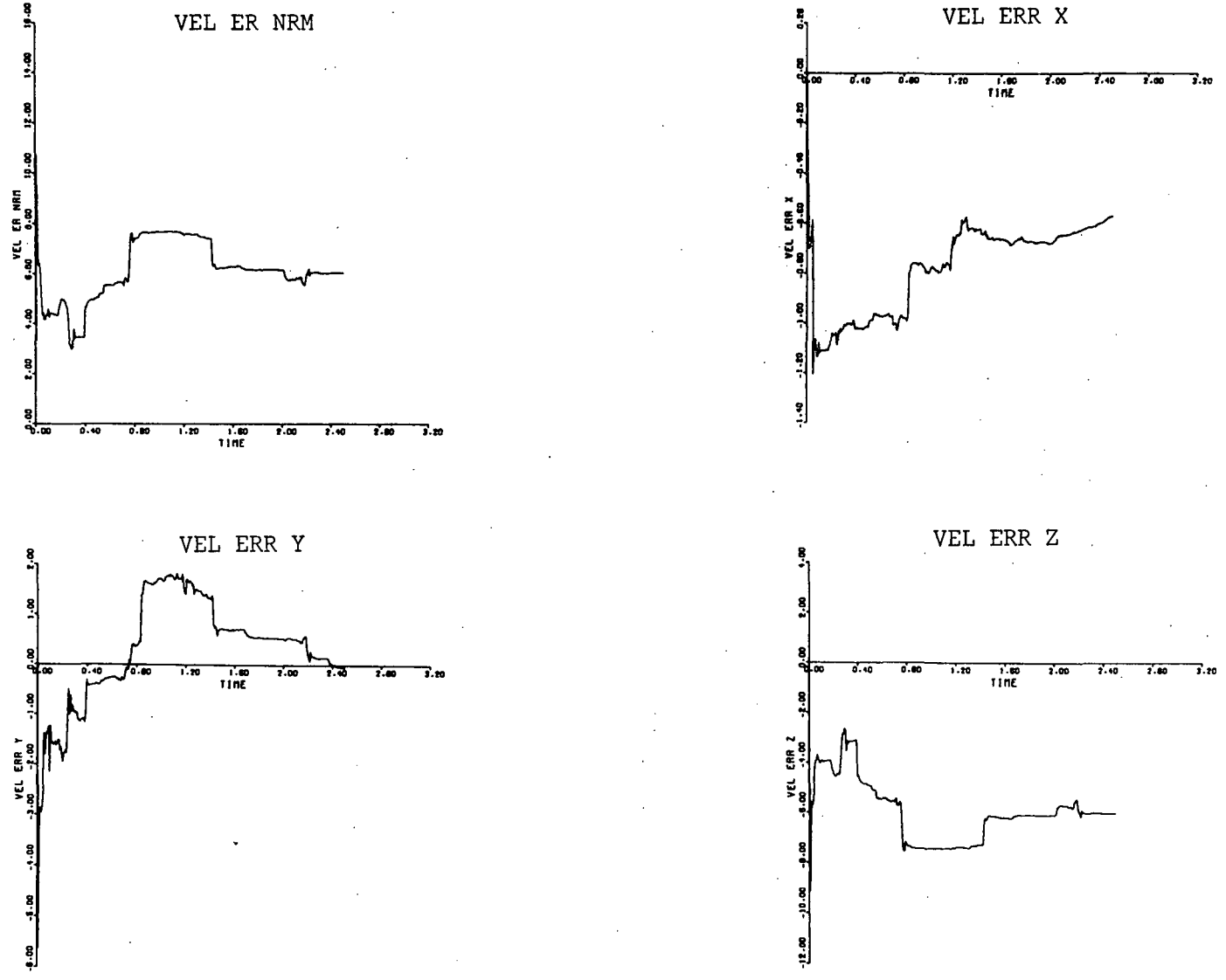

Figure 8c.2 Velocity Error (m/s) vs. Time (days) for Model 3, Range-Rate Only at 1-Minute Intervals

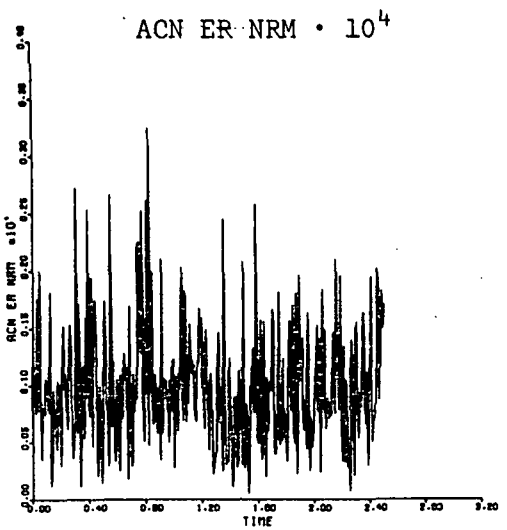

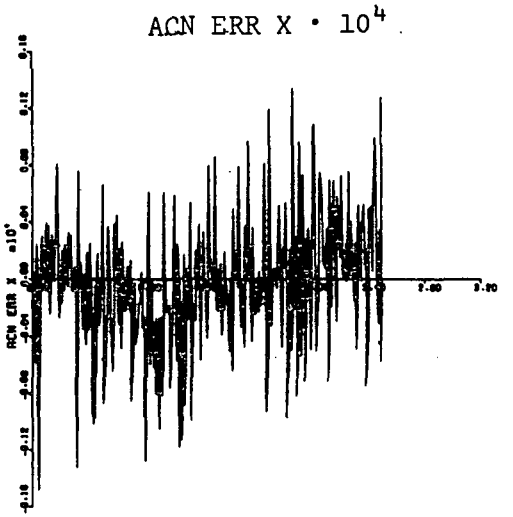

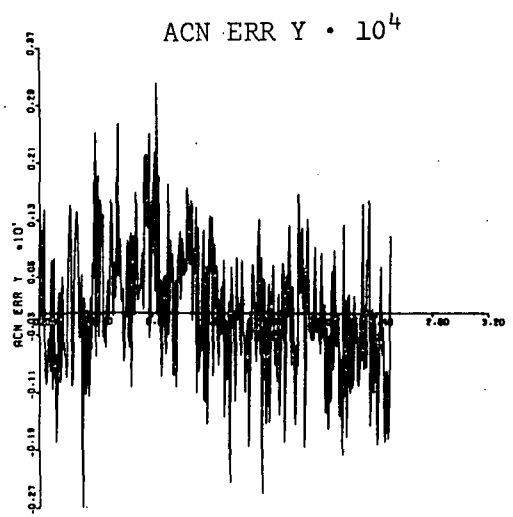

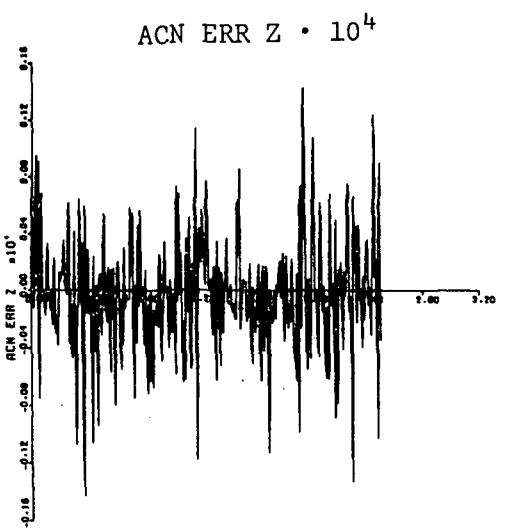

Figure 8c.3 Acceleration Error (m/s^2) vs. Time (days) for Model 3, Range-Rate Only at 1-Minute Intervals

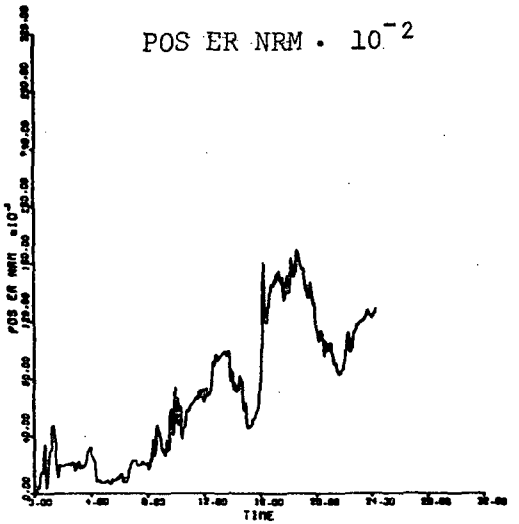

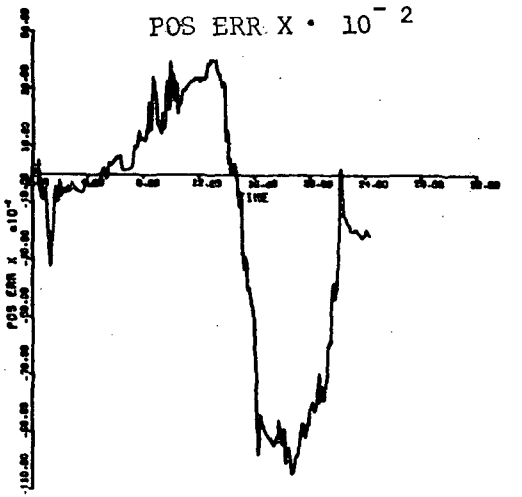

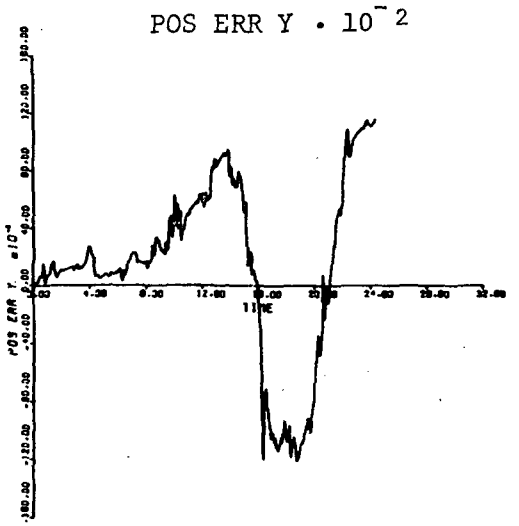

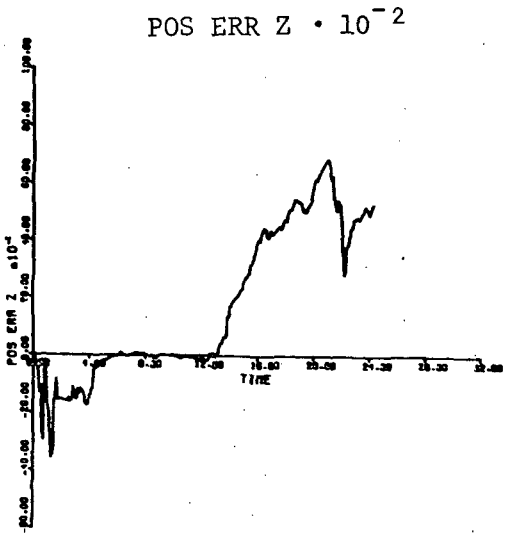

Figure 8d.1 Position Error (km) vs. Time (days) for Model 3, Star-Planet Angle Only at 100-Minute Intervals

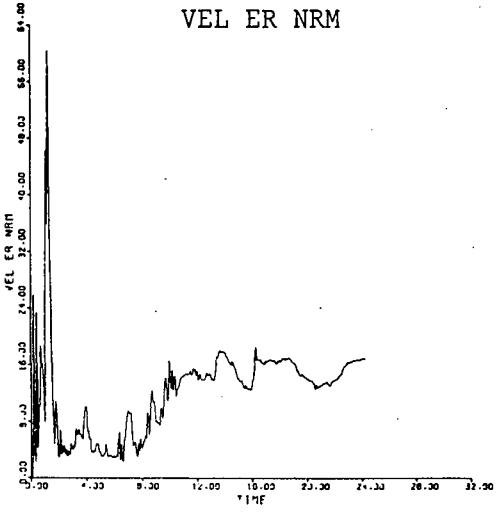

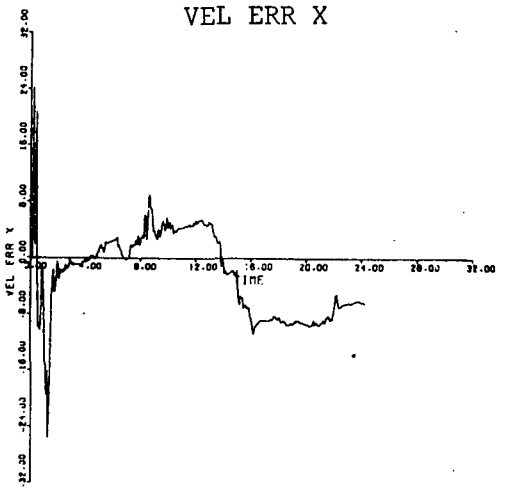

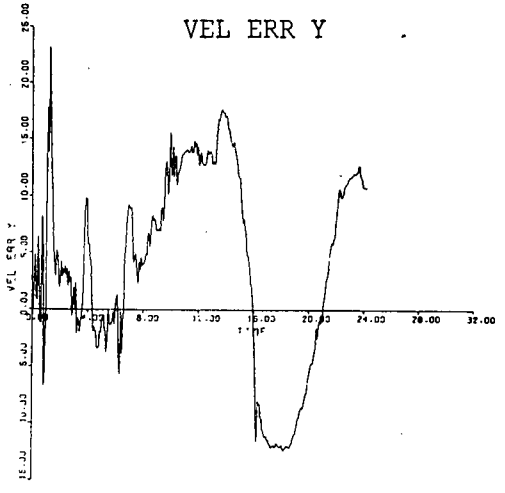

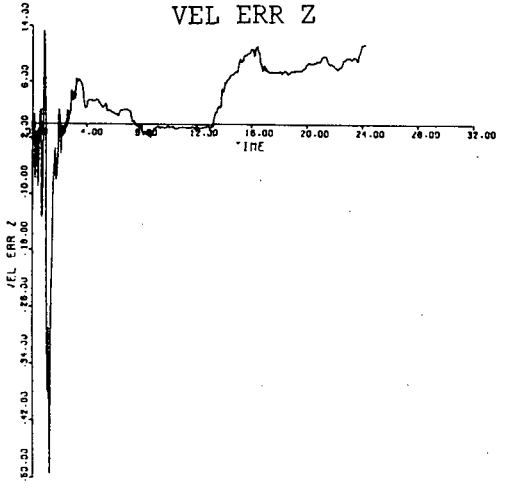

Figure 8d.2 Velocity Error (m/s) vs. Time (days) for Model 3, Star-Planet Angle Only at 100-Minute Intervals

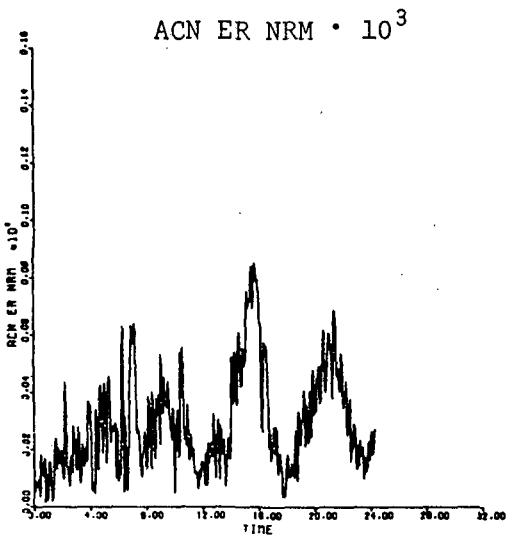

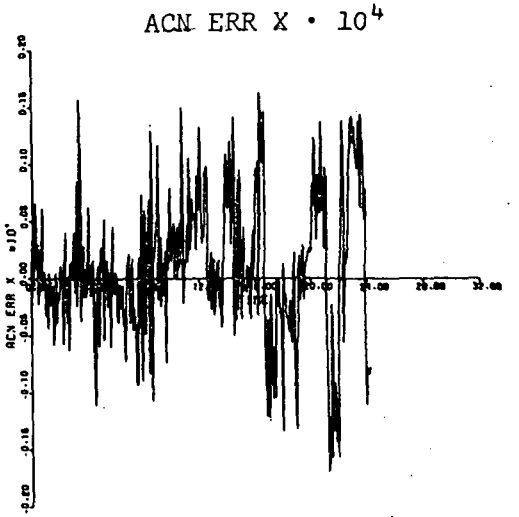

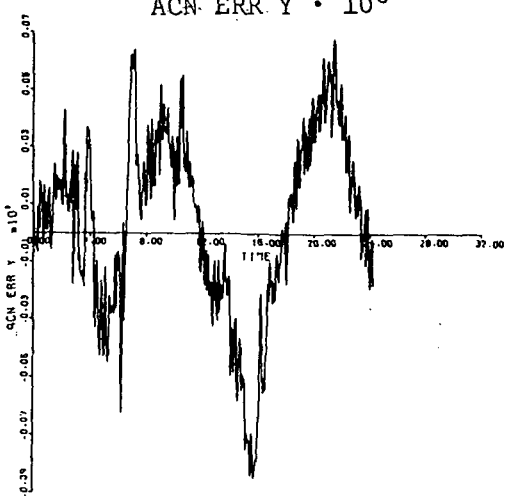

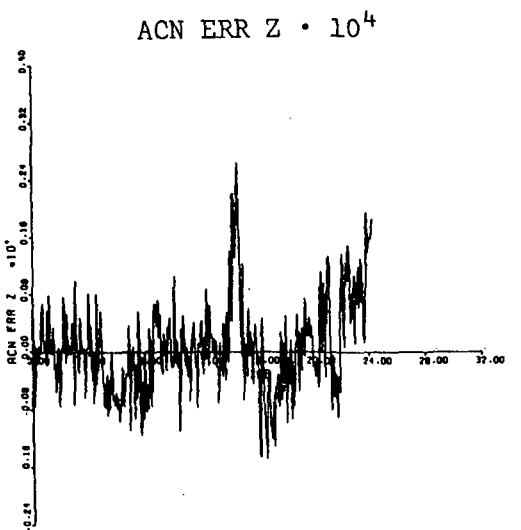

Figure 8d.3 Acceleration Error (m/s^2) vs. Time (days) for Model 3, Star-Planet Angle Only at 100-Minute Intervals

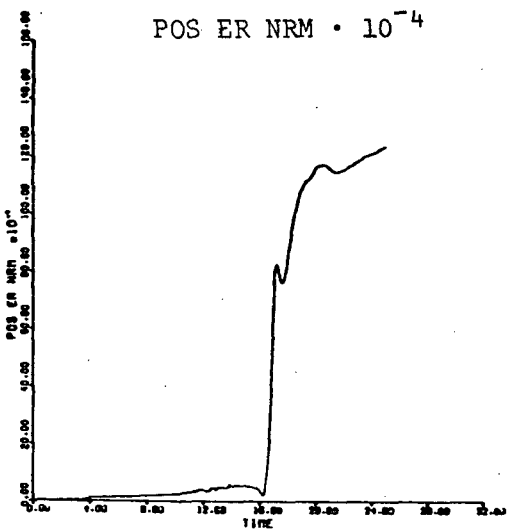

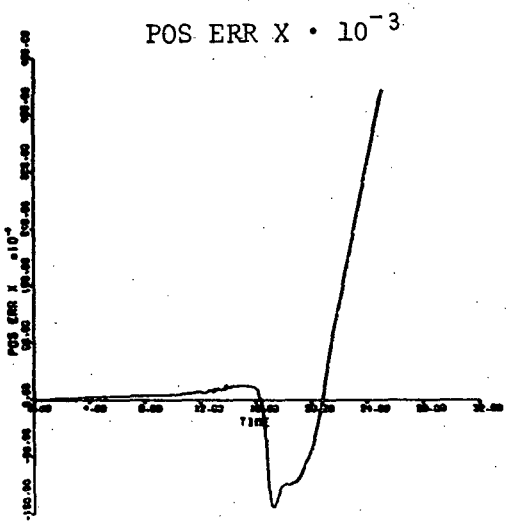

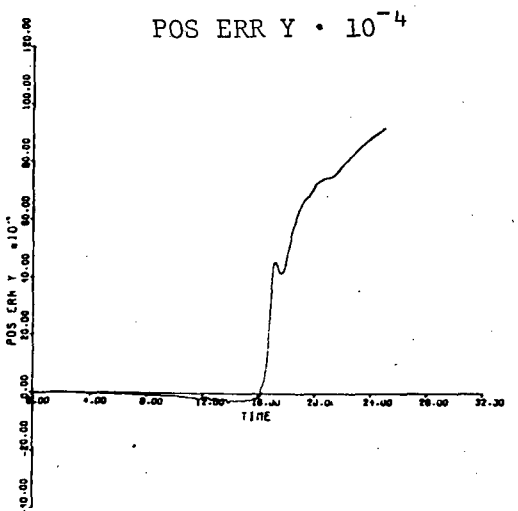

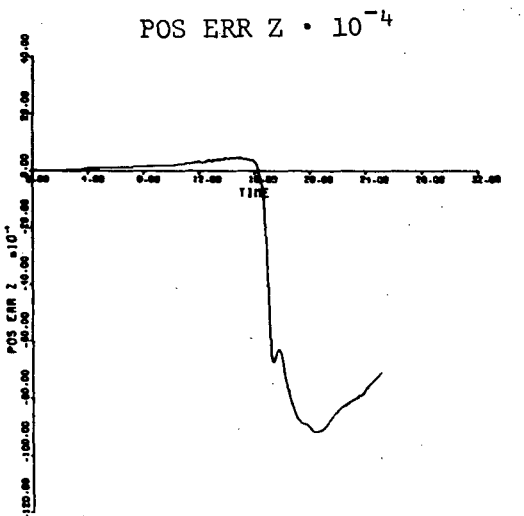

Figure 8e.1 Position Error (km) vs. Time (days) for Model 3, Sun-Star Angle Only at 100-Minute Intervals

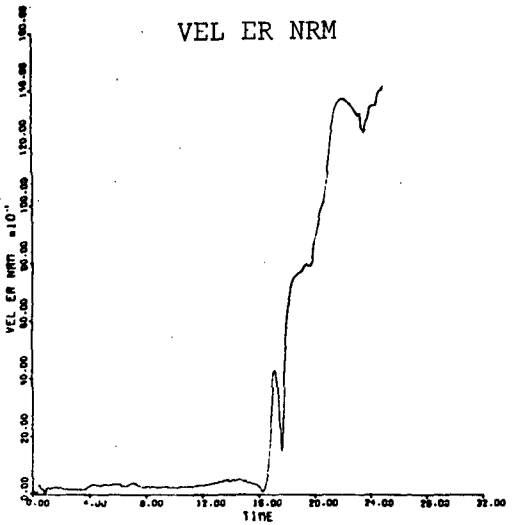

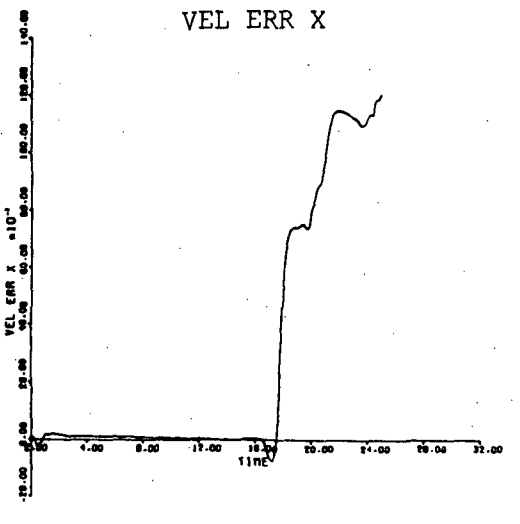

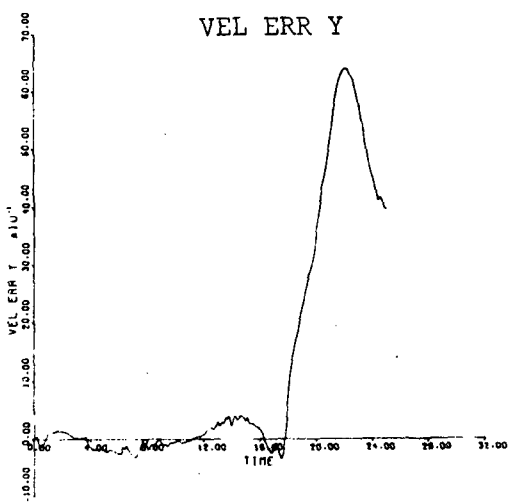

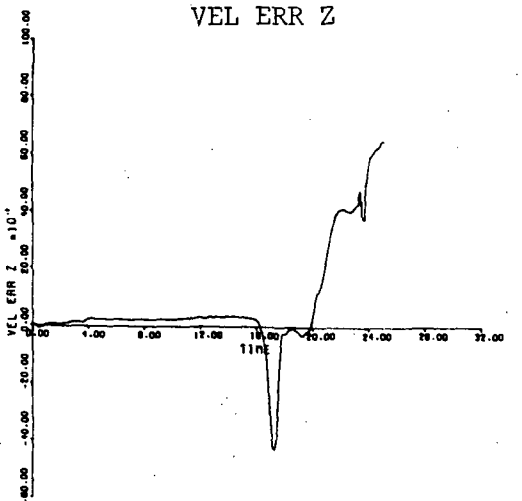

Figure 8e.2 Velocity Error (m/s) vs. Time (days) for Model 3, Sun-Star Angle Only at 100-Minute Intervals

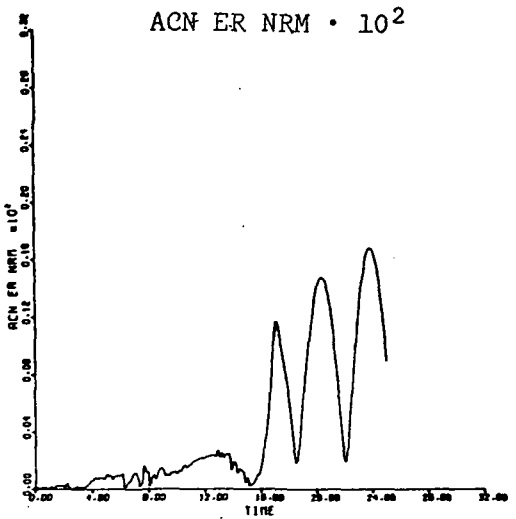

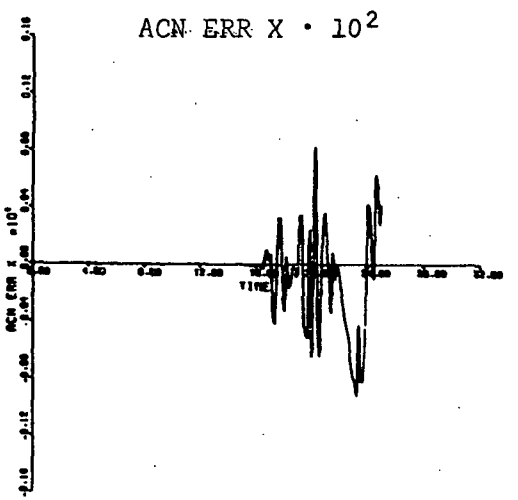

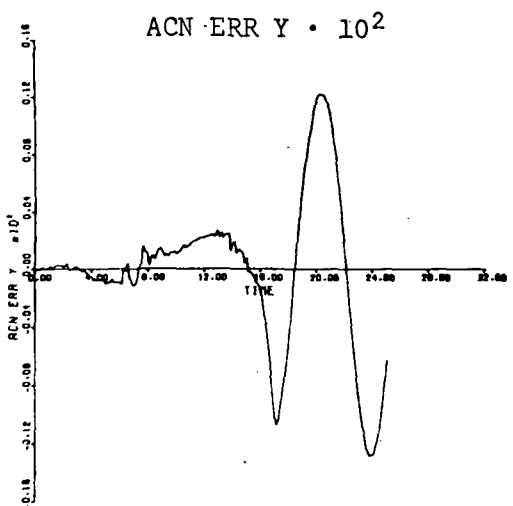

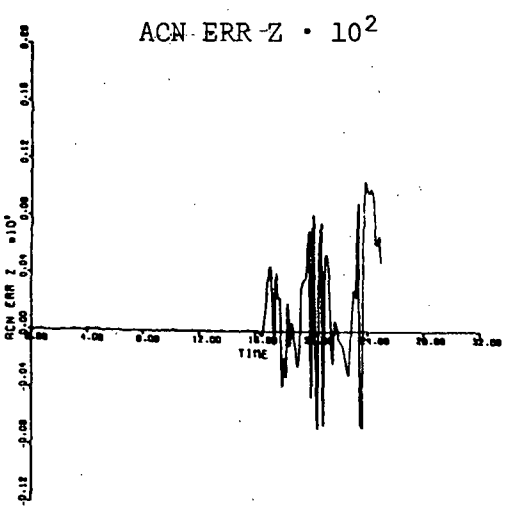

Figure 8e.3 Acceleration Error (m/s^2) vs. Time (days) for Model 3, Sun-Star Angle Only at 100-Minute Intervals

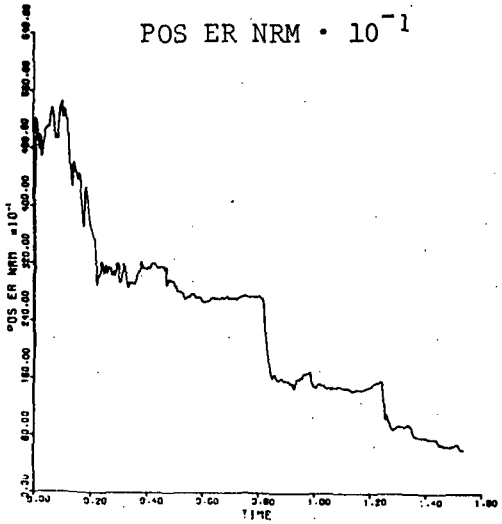

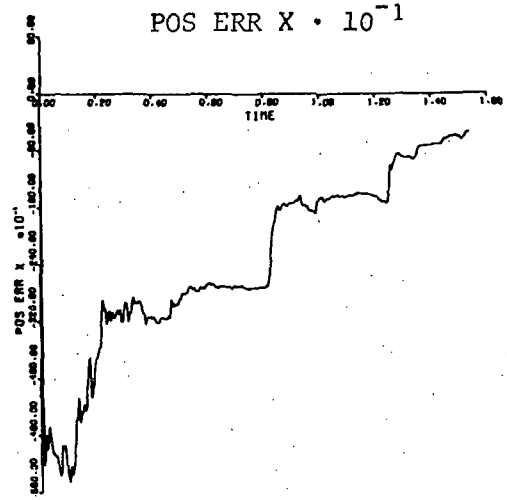

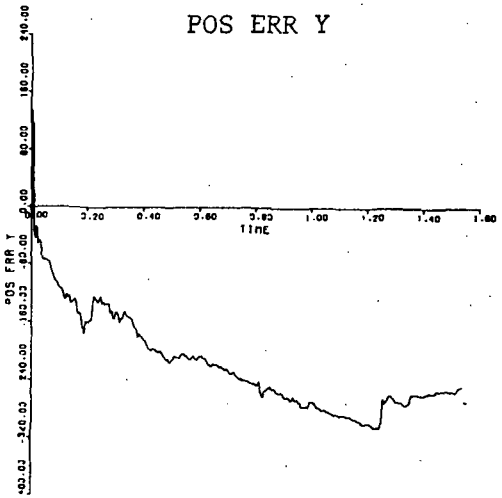

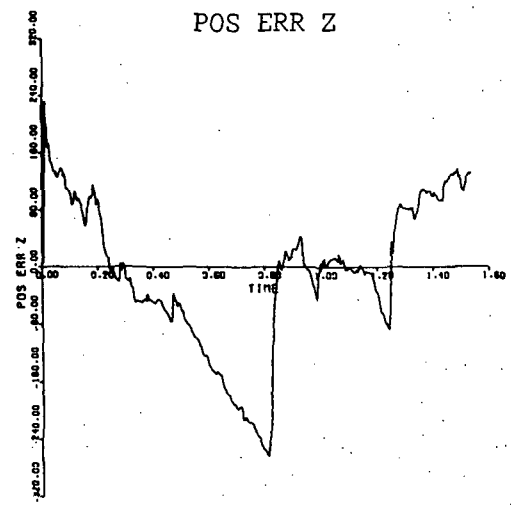

Figure 8f.1 Position Error (km) vs. Time (days) for Model 3, Range-Rate at 1-Minute, Star-Planet at 10-Minute Intervals

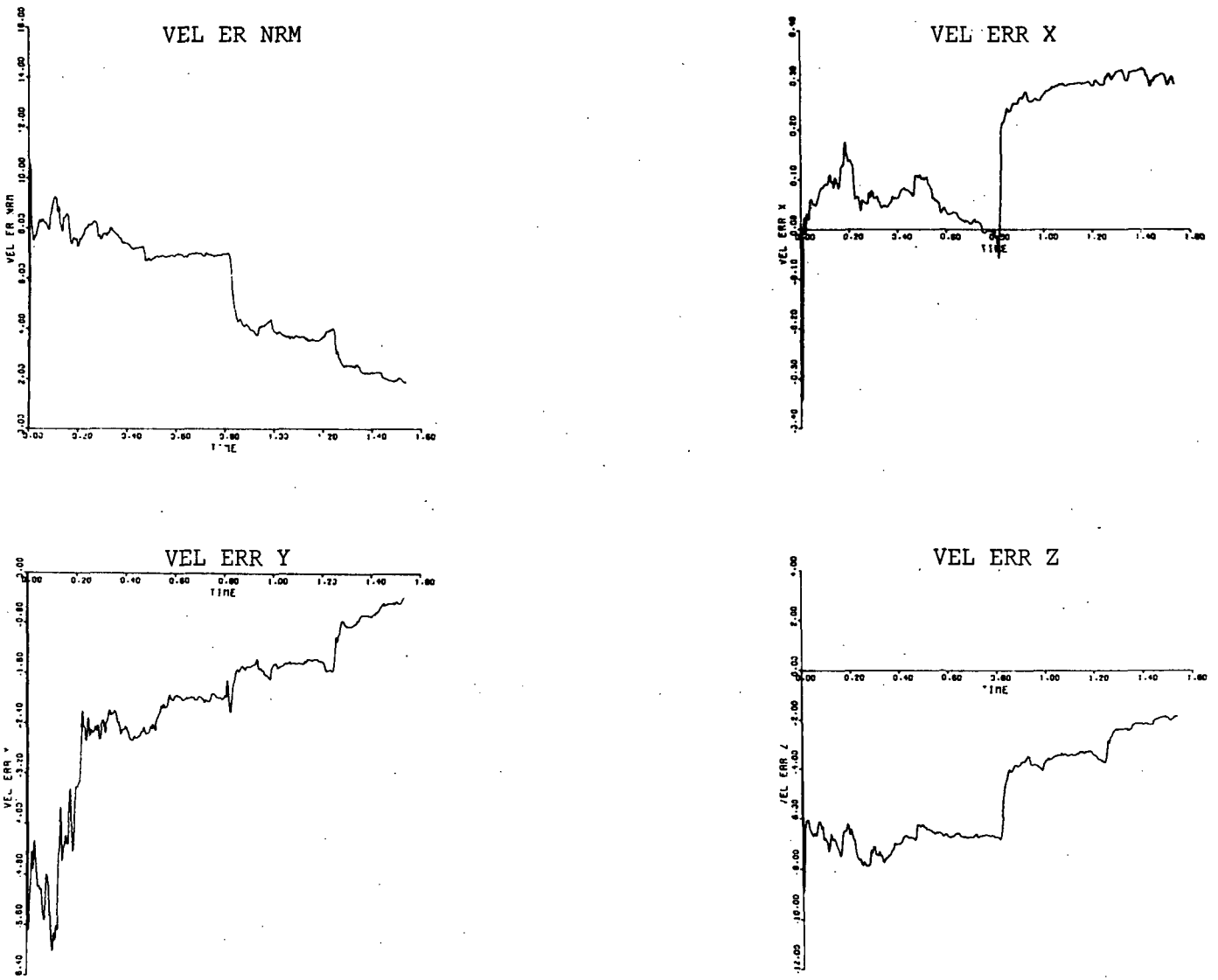

Figure 8f.2 Velocity Error (m/s) vs. Time (days) for Model 3, Range-Rate at 1-Minute, Star-Planet at 10-Minute Intervals

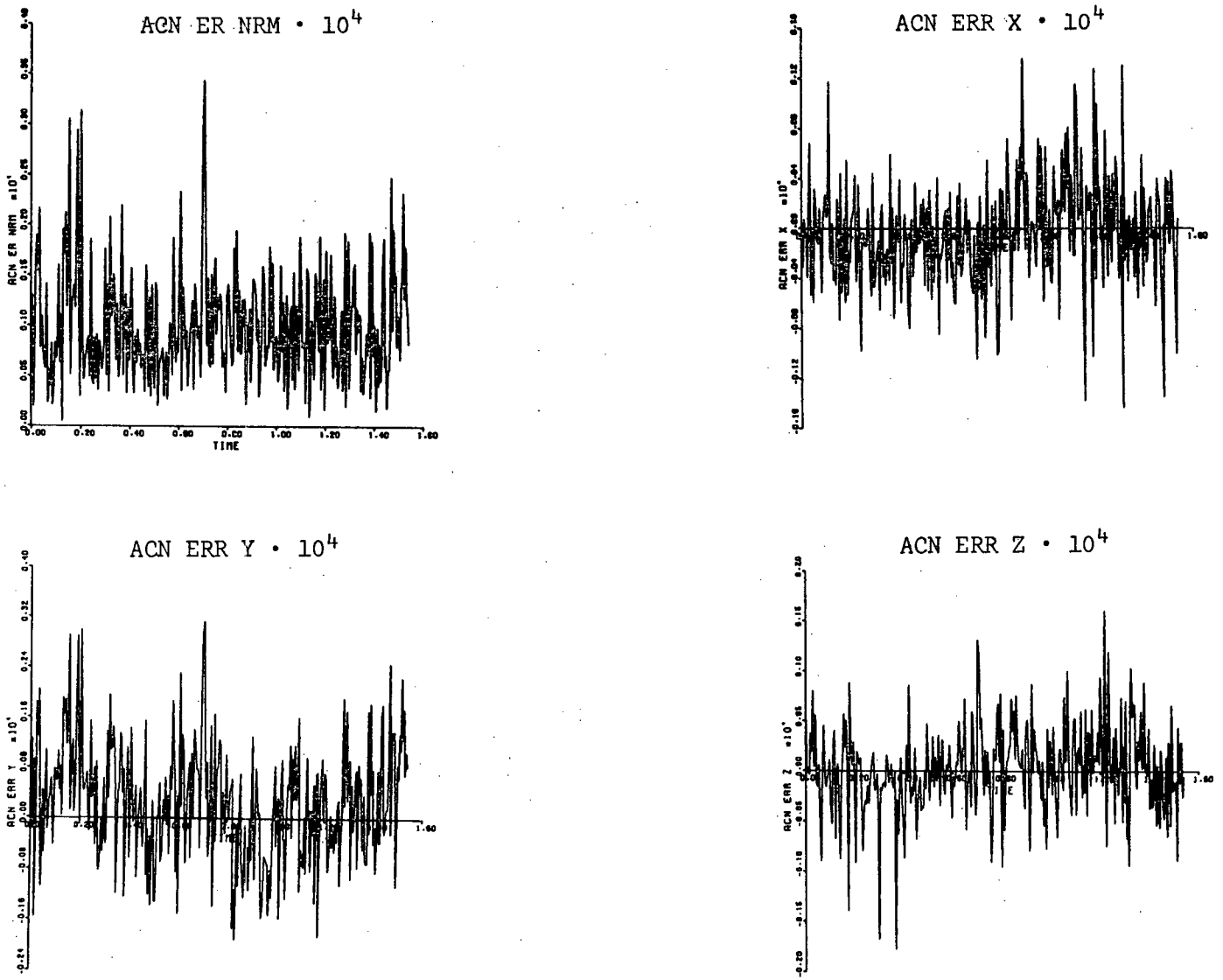

Figure 8f.3 Acceleration Error (m/s^2) vs. Time (days) for Model 3, Range-Rate at 1-Minute, Star-Planet at 10-Minute Intervals

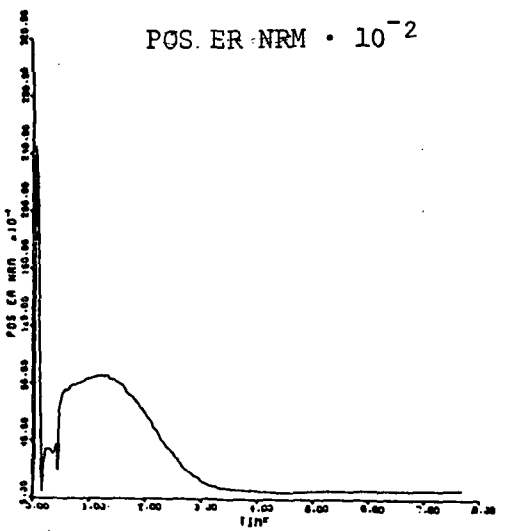

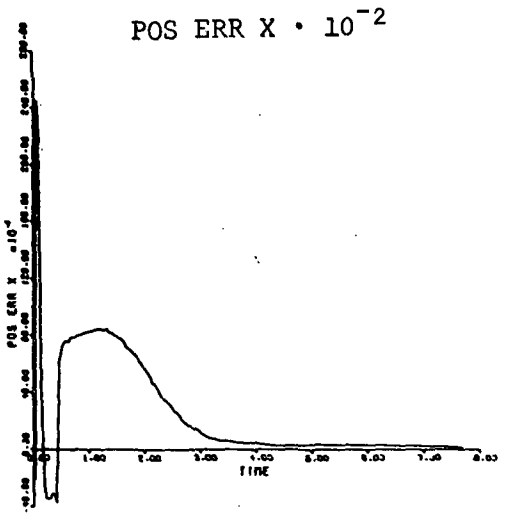

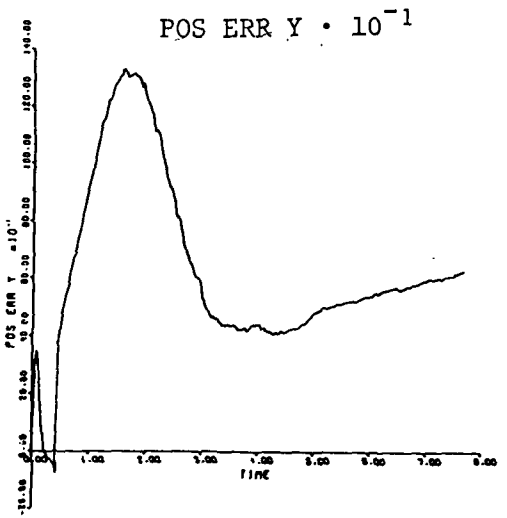

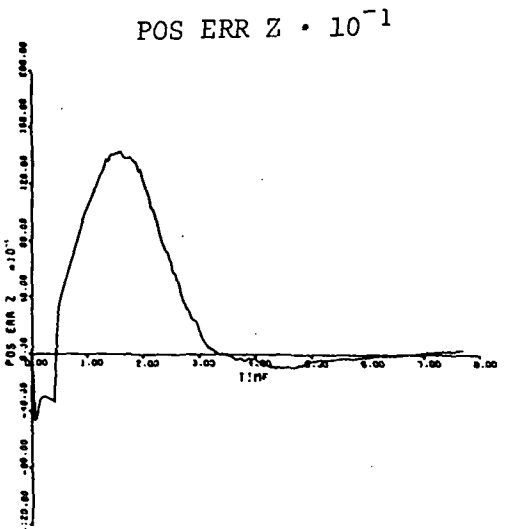

Figure 8g.1 Position Error (km) vs. Time (days) for Model 3, Range-Rate and Star-Planet Angle at 10-Minute Intervals

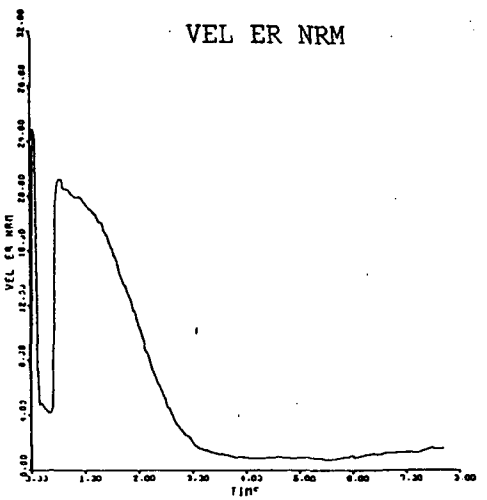

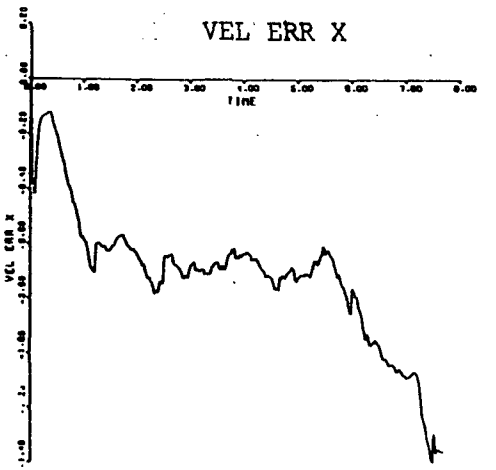

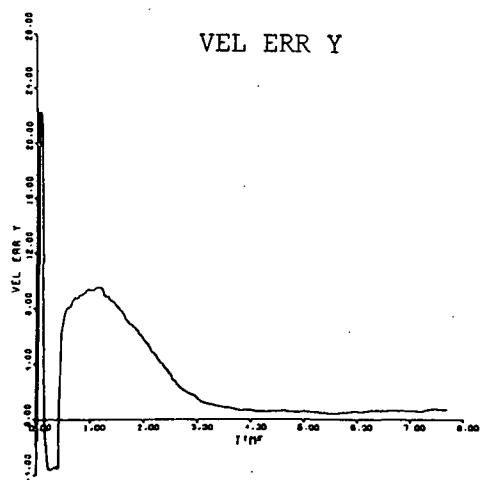

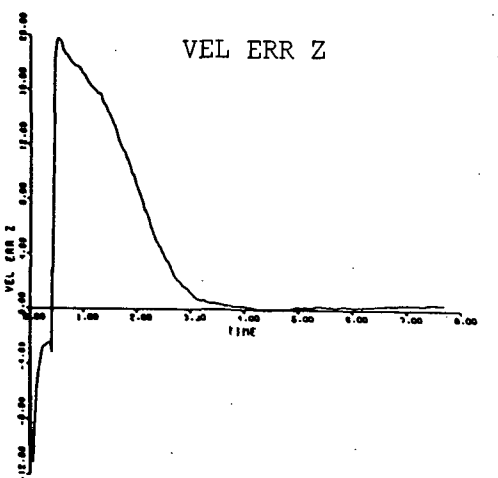

Figure 8g.2 Velocity Error (m/s) vs. Time (days) for Model 3, Range-Rate and Star-Planet Angle at 10-Minute Intervals

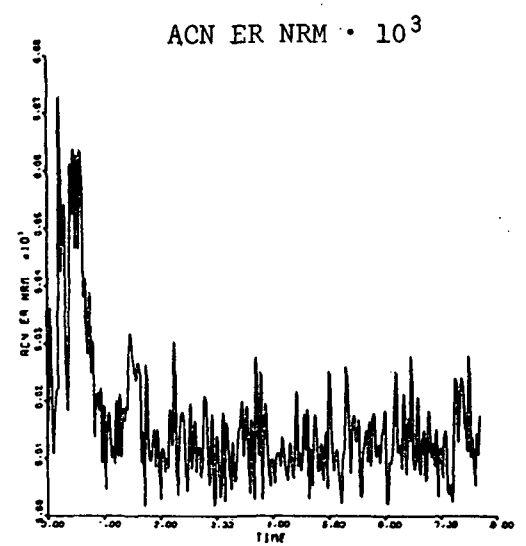

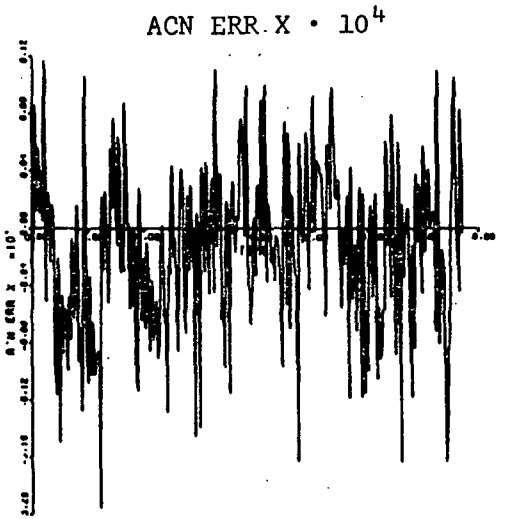

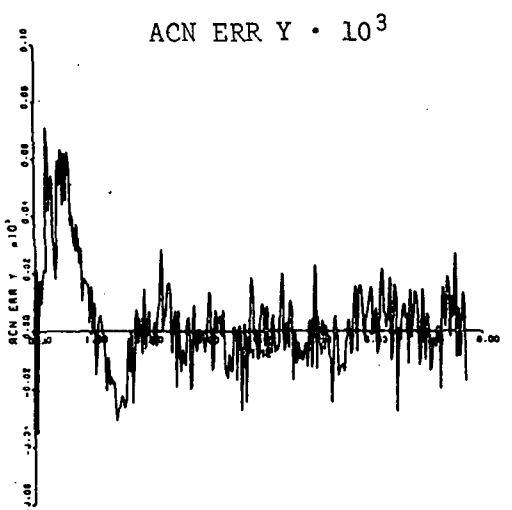

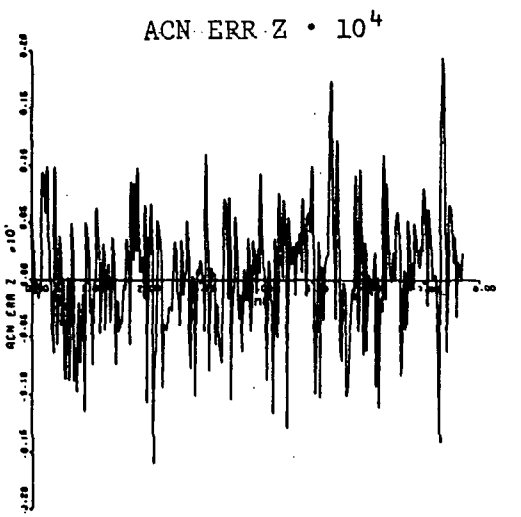

Figure 8g.3 Acceleration Error (m/s^2) vs. Time (days) for Model 3, Range-Rate and Star-Planet Angle at 10-Minute Intervals

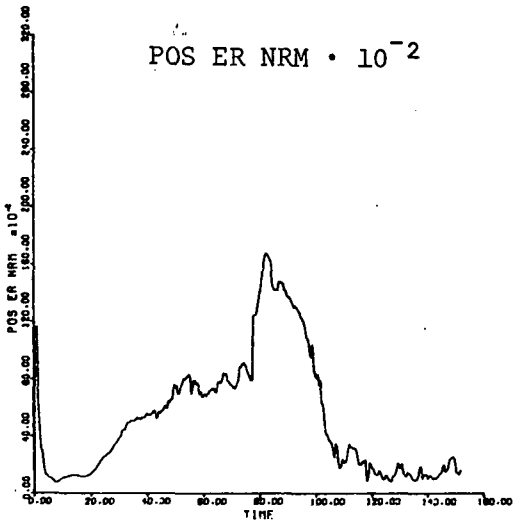

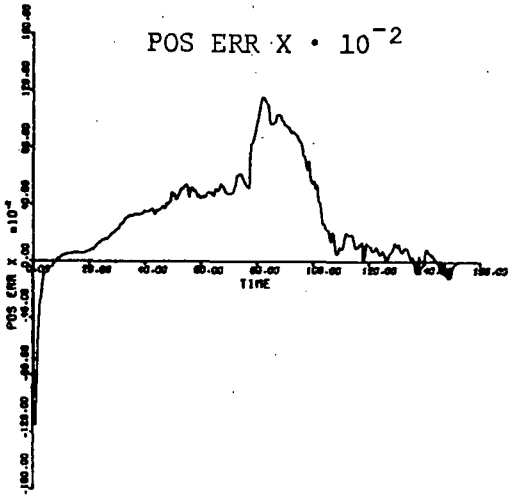

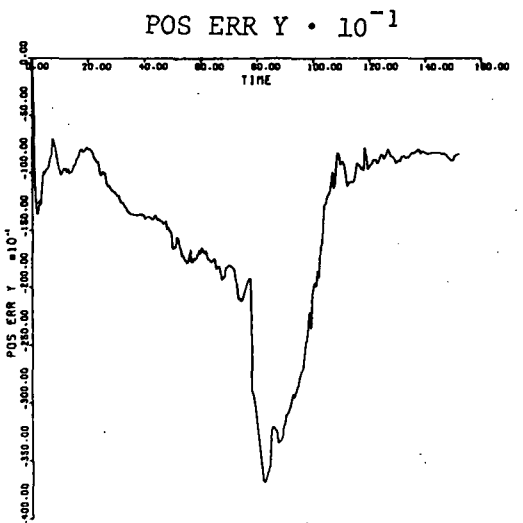

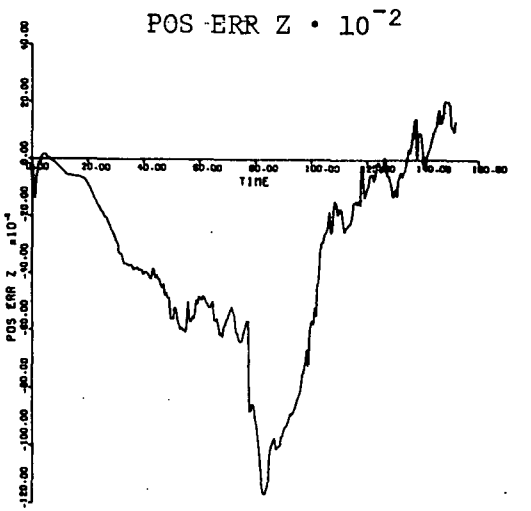

Figure 8h.1 Position Error (km) vs. Time (days) for Model 3, q-Matrix Decreased by 1%

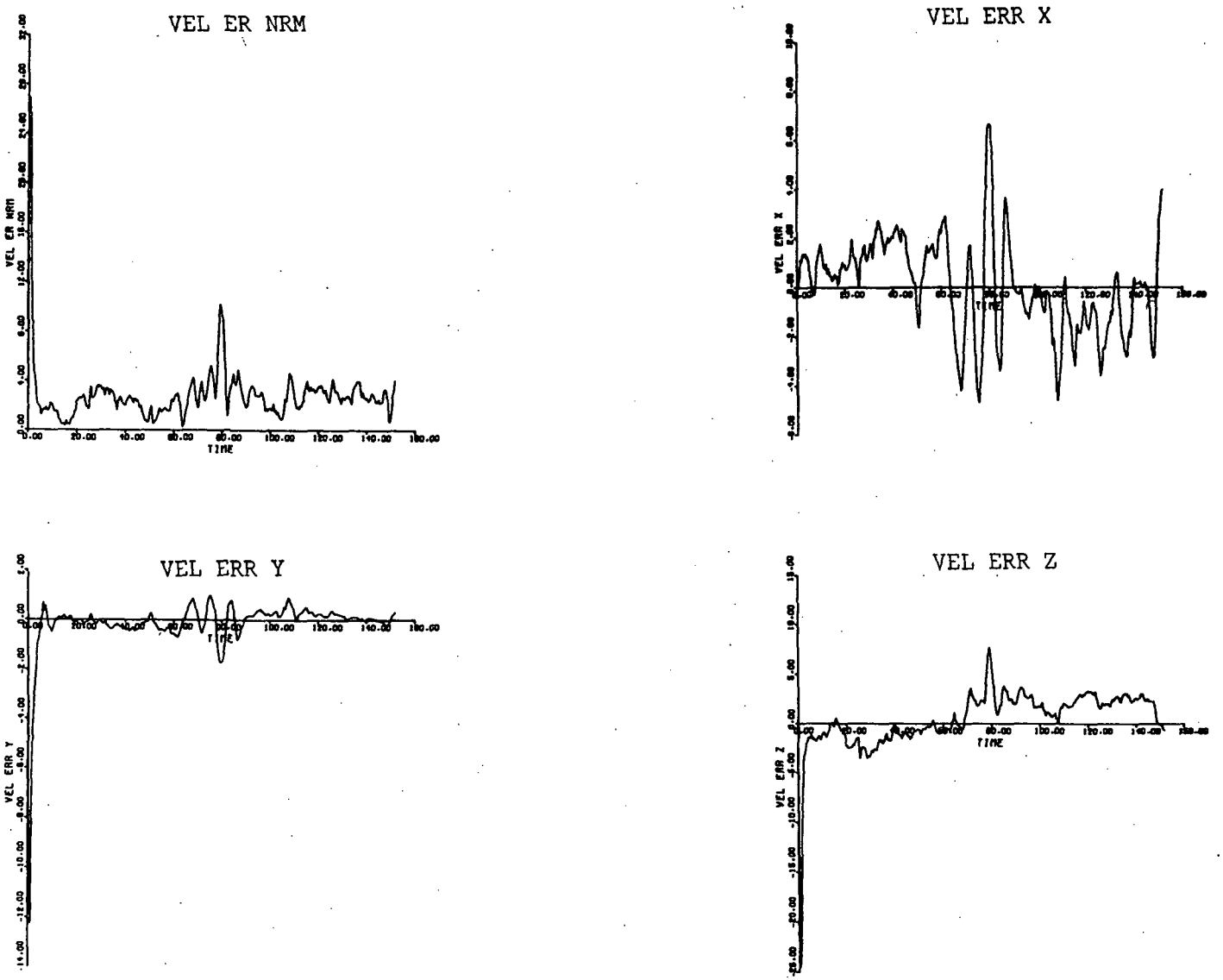

Figure 8h.2 Velocity Error (m/s) vs. Time (days) for Model 3, q-Matrix Decreased by 1%

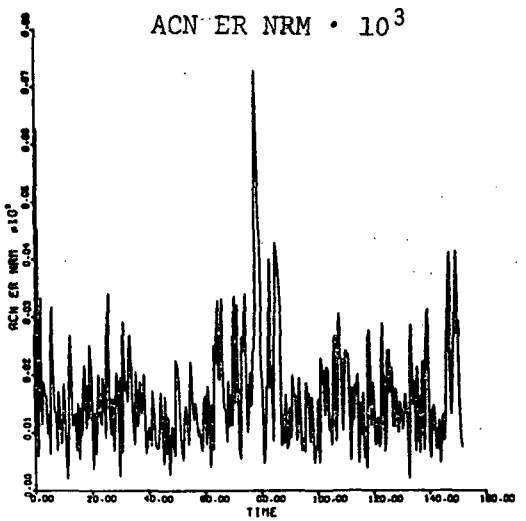

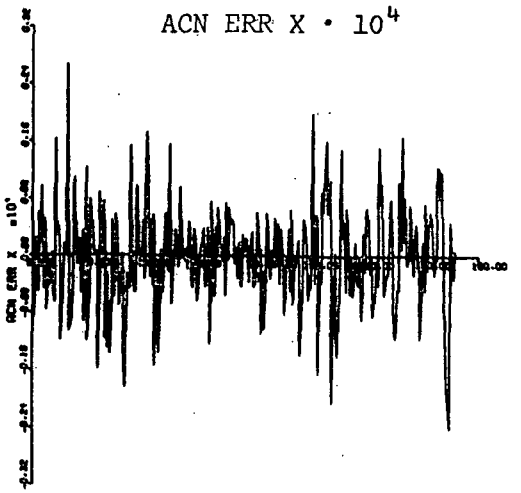

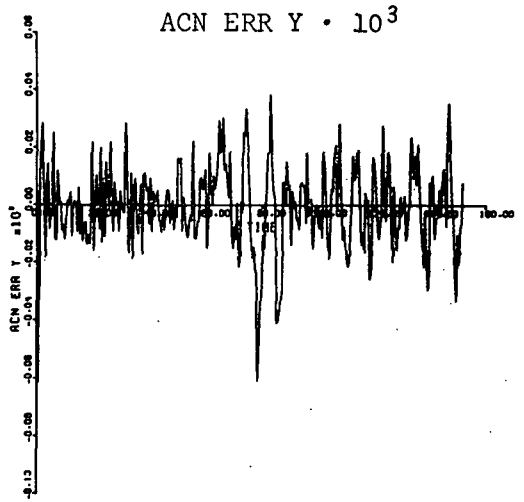

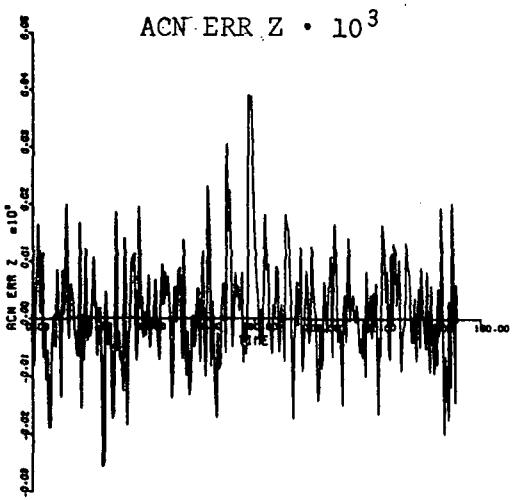

Figure 8h.3 Acceleration Error (m/s^2) vs. Time (days) for Model 3, q-Matrix Decreased by 1%

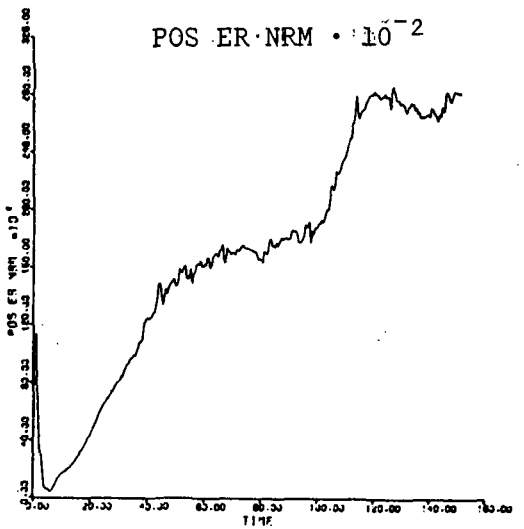

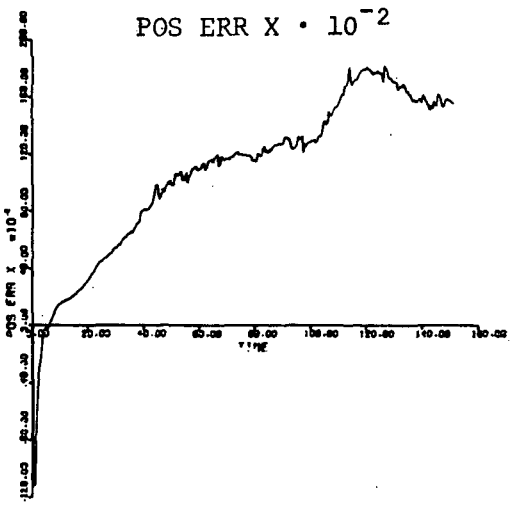

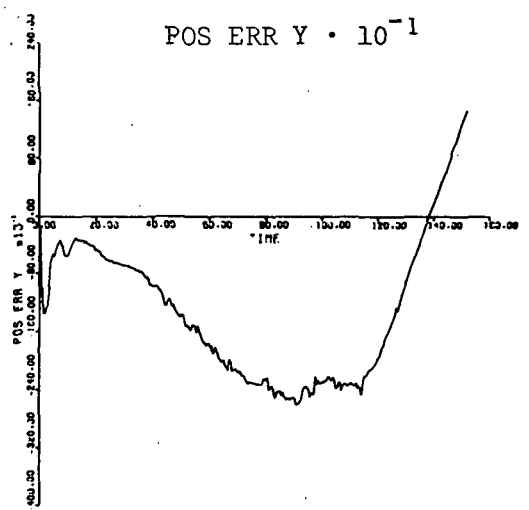

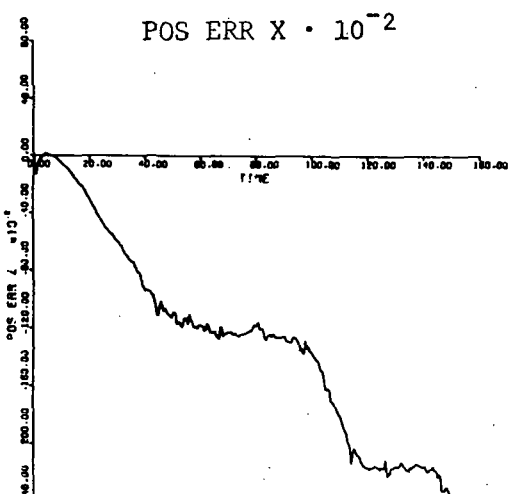

Figure 8i.1 Position Error (km) vs. Time (days) for Model 3, q-Matrix Increased by 1%

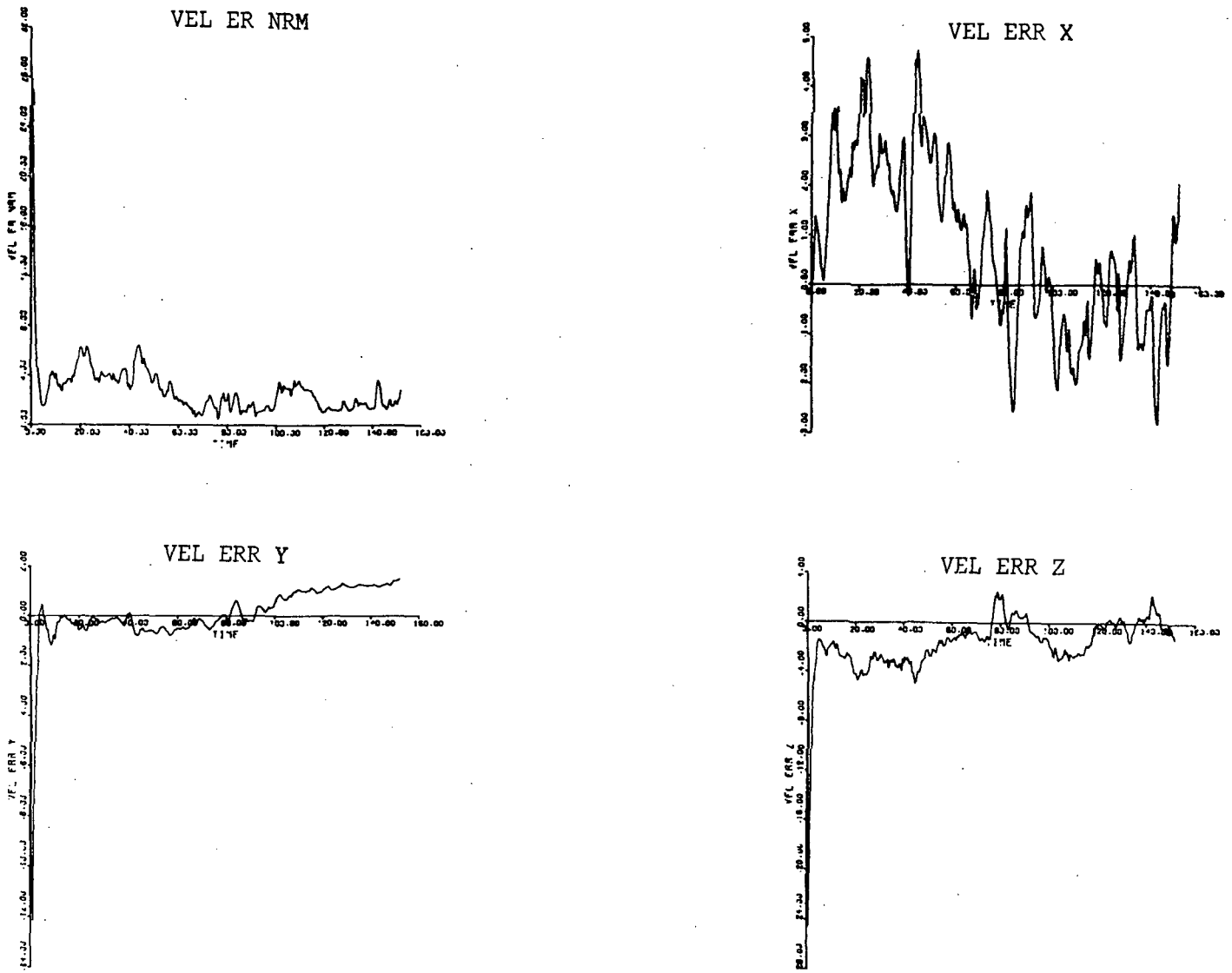

Figure 8i.2 Velocity Error (m/s) vs. Time (days) for Model 3, q-Matrix Increased by 1%

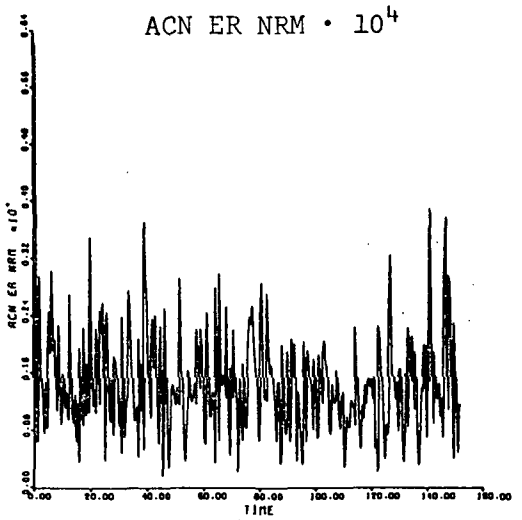

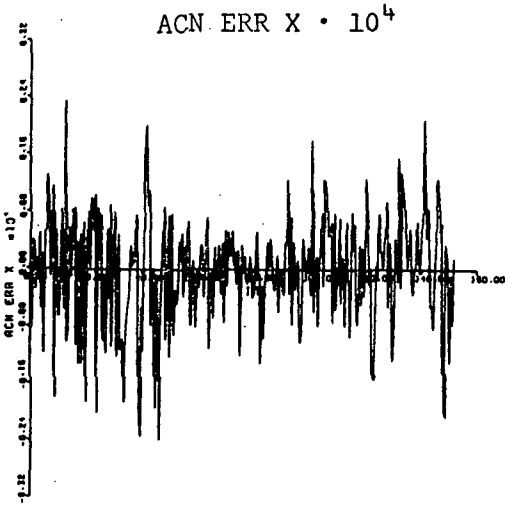

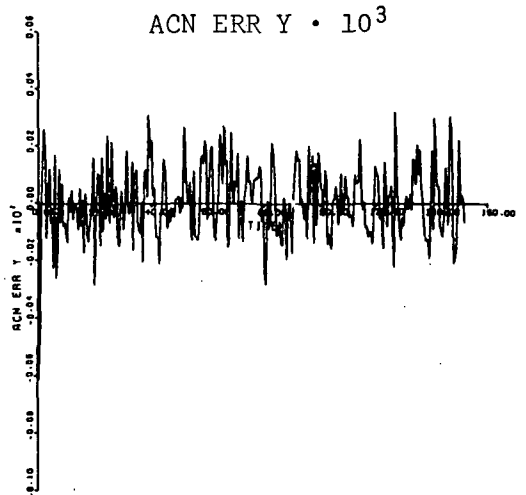

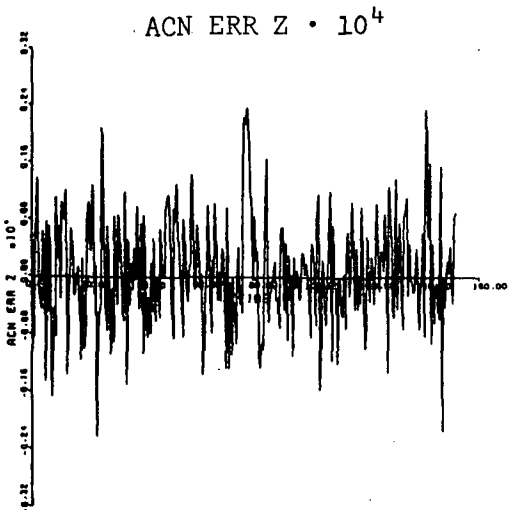

Figure 8i.3 Acceleration Error (m/s^2) vs. Time (days) for Model 3, q-Matrix Increased by 1%

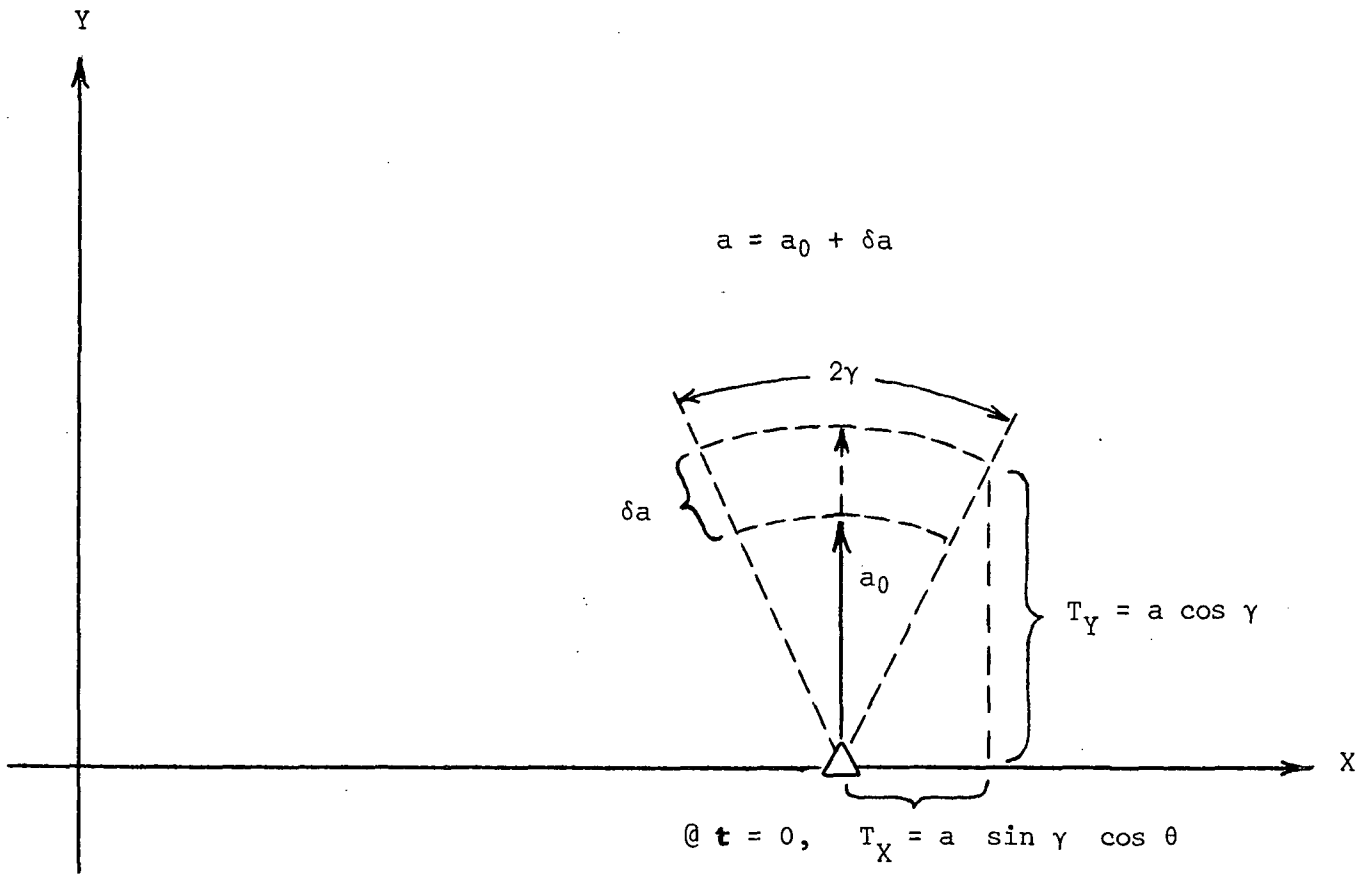

Figure 9 Initial Thrust Acceleration Components, Heliocentric Reference

Figure 10 Estimate of the Frequency Squared